Fall 1-31-2014

Analyses of groundwater contribution to a riverine wetland

Farzad Mahmoodinobar
New Jersey Institute of Technology

Copyright Warning & Restrictions

The copyright law of the United States (Title 17, United States Code) governs the making of photocopies or other reproductions of copyrighted material.

Under certain conditions specified in the law, libraries and archives are authorized to furnish a photocopy or other reproduction. One of these specified conditions is that the photocopy or reproduction is not to be "used for any purpose other than private study, scholarship, or research." If a, user makes a request for, or later uses, a photocopy or reproduction for purposes in excess of "fair use" that user may be liable for copyright infringement,

This institution reserves the right to refuse to accept a copying order if, in its judgment, fulfillment of the order would involve violation of copyright law.

Please Note: The author retains the copyright while the New Jersey Institute of Technology reserves the right to distribute this thesis or dissertation

Printing note: If you do not wish to print this page, then select "Pages from: first page # to: last page #" on the print dialog screen

ABSTRACT

ANALYSES OF GROUNDWATER CONTRIBUTION TO A RIVERINE WETLAND

by
Farzad Mahmoodinobar

Rainfall, runoff, overbank flow and groundwater, all contribute water to wetlands. Each transport element is associated with unique modeling approaches and uncertainties. Transpiration is perhaps the hardest to quantify as it is subject to all the variability of plant growth. Transpiration causes land area to lose moisture and the loss amount depends on precipitation incidence, the temperature and type and extent of vegetation. Plants can intercept virtually all recharge during the growing season and almost none from late fall to early spring in northeastern United States. Thus, an improvement in the transpiration element can contribute considerably to an improved groundwater contribution estimate of the wetland water budget.

The study site is a riverine wetland at Monmouth Battlefield State Park in Manalapan, New Jersey.

Using USGS MODFLOW, a simulation is adapted to the site specific conditions of geology (from in-situ permeability tests), topography (from surveyed elevations and also USGS Topo Map) and vegetation (by assigning different evapotranspiration coefficients to different vegetation covers). Hydrologic factors (i.e. rain data) are reflected in the model. Simulation product is validated using the collected data from monitoring wells. The final product is a wetland hydrologic model for a highly localized prediction of groundwater contribution to a wetland's water budget capable of estimating evapotranspiration. It was concluded that from 1709 millimeters (mm) of precipitation

over modeling period (May 2012 to August 2013), 1000 and 835 mm or a daily average of 2.0 and 1.7 mm/day were lost to the atmosphere through evapotranspiration for forest and farm side of the study area, respectively.

ANALYSES OF GROUNDWATER CONTRIBUTION TO A RIVERINE WETLAND

by
Farzad Mahmoodinobar

A Dissertation
Submitted to the Faculty of
New Jersey Institute of Technology
in Partial Fulfillment of the Requirements for the Degree of
Doctor of Philosophy in Environmental Engineering

Department of Civil and Environmental Engineering

January 2014

APPROVAL PAGE

ANALYSES OF GROUNDWATER CONTRIBUTION TO A RIVERINE WETLAND

Farzad Mahmoodinobar

Dr. Yuan Ding, Dissertation Advisor — Date
Associate Professor of Civil and Environmental Engineering, NJIT

Dr. Robert Dresnack, Committee Member — Date
Professor of Civil and Environmental Engineering, NJIT

Dr. Robert Hazen, Committee Member — Date
Research Scientist, New Jersey Department of Environmental Protection

---

Dr. Taha F. Marhaba, Committee Member — Date
Professor and Chairman of Civil and Environmental Engineering, NJIT

Dr. John R. Schuring, Committee Member — Date
Professor of Civil and Environmental Engineering, NJIT

BIOGRAPHICAL SKETCH

Author: Farzad Mahmoodinobar

Degree: Doctor of Philosophy

Date: January 2014

Undergraduate and Graduate Education:

- Doctor of Philosophy in Environmental Engineering,
  New Jersey Institute of Technology, Newark, NJ, USA, 2014

- Master of Science in Civil Engineering
  Sharif University of Technology, Tehran, Iran, 2009

- Bachelor of Science in Civil Engineering
  Isfahan University of Technology, Isfahan, Iran, 2007

Major: Environmental Engineering

Presentations and Publications:

Mahmoodinobar F., Ding Y and Hazen R, "Analyses of Groundwater Contribution to a Riverine Wetland," presented at The Ninth Annual Graduate Student Research Day, Newark, NJ, October 2013.

To My Family

ACKNOWLEDGMENT

I wish to express my deepest gratitude to my advisor, Professor Yuan Ding, for her invaluable encouragement and guidance throughout the course of this research and dissertation. I am also grateful to the members of dissertation committee, Dr. Robert Hazen, Professor Robert Dresnack, Professor Taha Marhaba and Professor John Schuring for their helpful evaluations and suggestions.

I would also like to thank Mr. Emmanuel Charles from U.S. Geological Survey, Dr. Thomas Atherholt from State of New Jersey Department of Environmental Protection, Mr. Jason Nolan from National Weather Service Middle Atlantic River Forecast Center and my dear friend Dr. Yazdan Majdi for their tremendous support and help.

Finally, I would like to deeply thank my parents, Laleh and Behzad, and my brother, Farbod for their continuous support, encouragements and understanding during all these years.

TABLE OF CONTENTS

TABLE OF CONTENTS
(Continued)

Chapter **Page**

TABLE OF CONTENTS
(Continued)

LIST OF TABLES

LIST OF FIGURES

LIST OF FIGURES
(Continued)

LIST OF FIGURES
(Continued)

LIST OF FIGURES
(Continued)

Figure **Page**

CHAPTER 1

LITERATURE REVIEW

1.1 Introduction

In Chapter 1, water cycle will be reviewed then the significance of wetlands in the water cycle will be discussed. Evapotranspiration, as the hardest element of the water cycle to quantify, will be reviewed. Select studies on evapotranspiration in wetlands will be presented followed by previous efforts in quantifying the evapotranspiration in the state of New Jersey.

In Chapter 2, Monmouth Battlefield State Park will be introduced as the Study Area. Methodology for field investigations in the Study Area, including land surveying, setting up monitoring wells and measuring water levels at the wells, soil classification and soil hydraulic conductivity tests will be discussed and the results will be presented.

Chapter 3 focuses on the introduction of USGS MODFLOW and its graphical user interface, ModelMuse.

In Chapter 4, modeling efforts using ModelMuse will be described and the results of the simulation will be presented and compared to the Field Investigation data.

Finally, Chapter 5 will present the results discussion and conclusion and applications of the present study. At the end, a few suggestions for further studies will be presented.

Objective of this study is to develop a wetland hydrologic model for a highly localized prediction of groundwater contribution to a wetland's water budget capable of estimating evapotranspiration.

1.2 The Water Cycle

The continuous movement of water on, above and below the surface of earth creates the water cycle. Water cycle has been subject to vast modeling efforts in order to have a better understanding of the transport elements associated with it. The water cycle, shown in **Figure 1.1**, is defined as the continuous movement of water from one reservoir to another, such as from river to ocean, or from the ocean to atmosphere, by the physical processes of evaporation, condensation, precipitation, infiltration, runoff, and subsurface flow going through different phases: liquid, solid (ice), and gas (vapor) (Wikimedia Foundation, Inc., 2013).

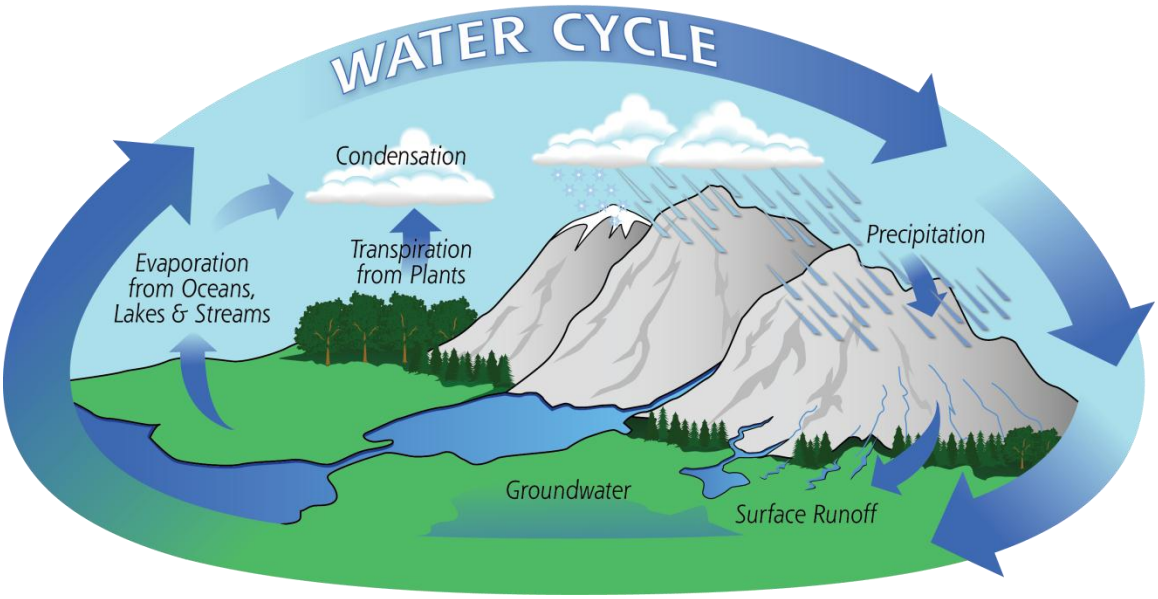

Figure 1.1 Water cycle (The National Aeronautics and Space Administration, 2013).

The sun, which drives the water cycle, heats water in the oceans. Some of it evaporates as vapor into the air. Ice and snow can sublimate directly into water vapor. Rising air currents take the vapor up into the atmosphere, along with water from

evapotranspiration, which is water transpired from plants and evaporated from the soil. The vapor rises into the air where cooler temperatures cause it to condense into clouds.

Air currents move clouds around the globe; cloud particles collide, grow, and fall out of the sky as precipitation. Some precipitation falls as snow and can accumulate as ice caps and glaciers, which can store frozen water for thousands of years. Snowpacks in warmer climates often thaw and melt when spring arrives, and the melted water flows overland as snowmelt.

Most precipitation falls back into the oceans or onto land, where, due to gravity, the precipitation flows over the ground as surface runoff. A portion of runoff enters rivers in valleys in the landscape, with streamflow moving water towards the oceans. Runoff, and ground-water seepage, accumulate and are stored as freshwater in lakes. Not all runoff flows into rivers, though. Much of it soaks into the ground as infiltration. Some water infiltrates deep into the ground and replenishes aquifers (saturated subsurface rock), which store huge amounts of freshwater for long periods of time.

Some infiltration stays close to the land surface and can seep back into surface-water bodies (and the ocean) as groundwater discharge, and some groundwater finds openings in the land surface and emerges as freshwater springs. Over time, though, all of this water keeps moving, some to re-enter the ocean, where the water cycle completes (U.S. Geological Survey, 2013).

Due to increasing interest in the wetlands hydrology over the past years, wetlands and water cycle as a part of wetlands hydrology will be further discussed in this chapter.

1.3 Wetlands

Over recent decades, wetlands have been recognized increasingly for their high biodiversity and for the important hydrological functions many wetlands perform, including flood alleviation, low-flow support, nutrient cycling and groundwater recharge. Wetland hydrology is a primary driving force influencing wetland ecology, its development and persistence (Mitsch & Gosselink, 1993).

A wetland is a land area that is saturated with water, either permanently or seasonally, such that it takes on the characteristics of a distinct ecosystem. Water saturation (hydrology) largely determines how the soil develops and the types of plant and animal communities living in and on the soil. Wetlands may support both aquatic and terrestrial species. The prolonged presence of water creates conditions that favor the growth of specially adapted plants (hydrophytes) and promote the development of characteristic wetland (hydric) soils (US Environmental Protection Agency, 2012).

Figure 1.2 shows how wetlands can form from fresh water.

Figure 1.2 What makes a freshwater, a wetland? (Murphy, 2008)

1.3.1 Significance of Wetlands in the Water Cycle

Wetlands play a number of roles in the environment, principally water purification, flood control, and shoreline stability. Wetlands are also considered the most biologically diverse of all ecosystems, serving as home to a wide range of plant and animal life.

Wetlands can provide habitats or even modulate water flow and consequently influence water quality (Hemond & Benoit, 1988). Recognizing the importance of wetlands to wildlife and to water quality has caused an increasing interest in researching the role of hydrology as a driving force for wetland processes. Wetland's hydraulic fluxes often include surface inflow and outflow, precipitation, transpiration and exchange between groundwater and surface water. **Figure 1.3** shows a typical wetland's hydraulic fluxes.

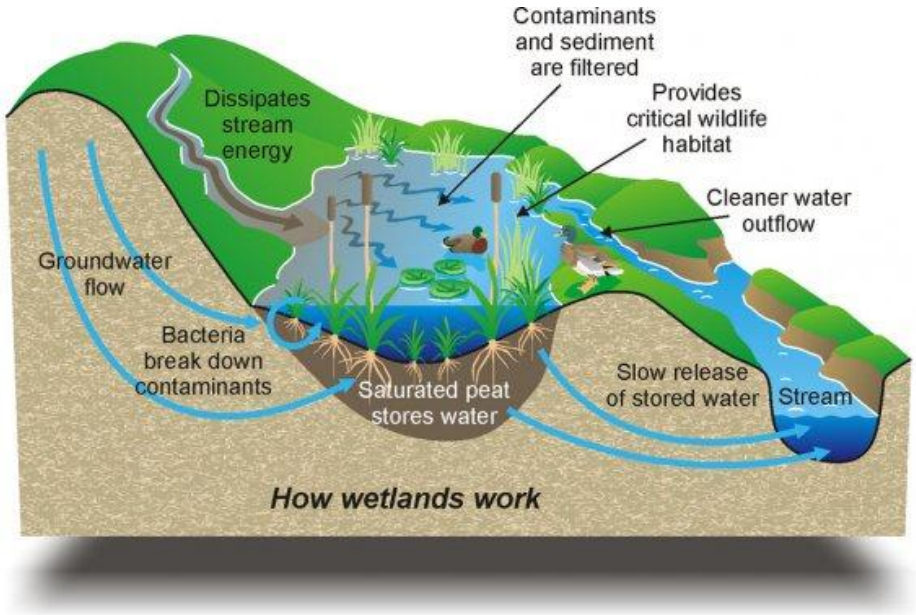

Figure 1.3 A typical wetland (Wordpress, 2011).

developing a more thorough understanding of water budgets in wetlands depend in part on our ability to quantify time-varying interactions between groundwater and surface water (Choi & Harvey, 2000) and by extension, the water cycle.

Progress in quantifying the water balance of lake systems provided useful guidance for wetland research (Crowe (1985) and Stauffer (1985)).

Hydrologic fluxes in lakes and wetlands often include surface inflow and outflow, precipitation, evapotranspiration, and exchange between surface water and ground water. For most wetlands, evapotranspiration is the major component of water loss (Sun & Song, 2008).

Each transport element is associated with unique modeling approaches and uncertainties. Evapotranspiration is perhaps the hardest to quantify as it is subject to all the variability of plant growth.

1.4 Evapotranspiration

Evapotranspiration has been the subject of many reports for almost a century (Pereira, 2004). In general, evapotranspiration is the sum of evaporation and transpiration (see **Figure 1.4**). U.S. Geological Survey (2013) defines evapotranspiration as the water lost to the atmosphere from the ground surface, evaporation from the capillary fringe of the groundwater table, and the transpiration of groundwater by plants whose roots tap the capillary fringe of the groundwater table.

The transpiration aspect of evapotranspiration is essentially evaporation of water from plant leaves. Studies have revealed that transpiration accounts for about 10 percent of the moisture in the atmosphere, with oceans, seas, and other bodies of water (lakes,

rivers, streams) providing nearly 90 percent, and a tiny amount coming from sublimation. Evapotranspiration is shown in **Figure 1.4**.

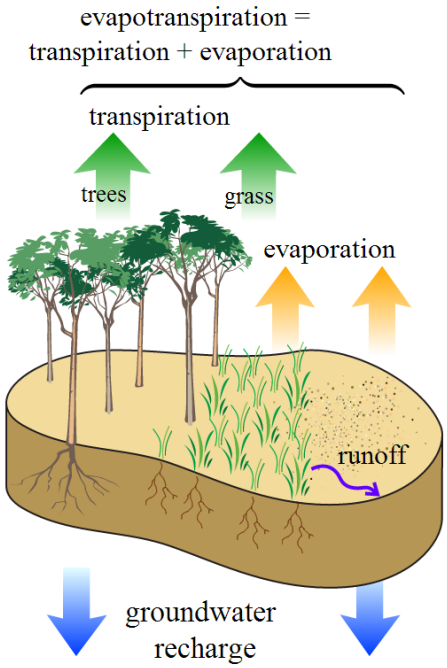

Figure 1.4 Evapotranspiration as a sum of transpiration and evaporation (Wikimedia Foundation, Inc., 2013).

During a growing season, a leaf will transpire many times more water than its own weight. An acre of corn gives off about 3,000-4,000 gallons of water each day, and a large oak tree can transpire 40,000 gallons per year.

The amount of water that plants transpire varies greatly geographically and over time. There are a number of factors that determine transpiration rates:

- **Temperature:** Transpiration rates go up as the temperature goes up, especially during the growing season, when the air is warmer due to stronger sunlight and warmer air masses. Higher temperatures cause the plant cells which control the stoma where water is released to the atmosphere to open, whereas colder temperatures cause the openings to close.

- **Relative humidity:** As the relative humidity of the air surrounding the plant rises the transpiration rate falls. It is easier for water to evaporate into dryer air than into more saturated air.

- **Wind and air movement:** Increased movement of the air around a plant will result in a higher transpiration rate. This is somewhat related to the relative humidity of the air, in that as water transpires from a leaf, the water saturates the air surrounding the leaf. If there is no wind, the air around the leaf may not move very much, raising the humidity of the air around the leaf. Wind will move the air around, with the result that the more saturated air close to the leaf is replaced by drier air.

- **Soil-moisture availability:** When moisture is lacking, plants can begin to senesce (premature ageing, which can result in leaf loss) and transpire less water.

- **Type of plant:** Plants transpire water at different rates. Some plants which grow in arid regions, such as cacti and succulents, conserve precious water by transpiring less water than other plants (U.S. Geological Survey, 2013).

Evapotranspiration estimates are needed in a wide range of problems in hydrology, agronomy, forestry and land management, and water resources planning, such as water balance computation, irrigation management, river flow forecasting, investigation of lake chemistry, ecosystem modeling, etc. (C.-Y. Xu, 2005). Reliable estimates of evapotranspiration are also essential for the improvement of atmospheric circulation models (Yates, 1997).

1.5 Quantifying Evapotranspiration

Several methods have been proposed in the literature for calculating actual evapotranspiration. Monteith (1963) and (1965) introduced resistance terms into the well-known method of Penman (1948) and derived at an equation for evapotranspiration from surfaces with either optimal or limited water supply. This method, often referred to as Penman–Monteith method, has been successfully used to estimate evapotranspiration from different land covers. They tried to predict relative rates of evaporation from leaves with wet and dry surfaces and to investigate the dependence of transpiration rate on wind speed and surface roughness. In order to have reliable estimates of evapotranspiration, the method proved to require data on aerodynamic resistance and surface resistance which are not readily available, so that the Penman–Monteith method for estimating actual evapotranspiration has been limited in practical use (C.-Y. Xu, 2005).

Using replicated, whole plant lysimeters, Pauliukonis and Schneider (2001) quantified and compared the daily evapotranspiration and temporal evapotranspiration patterns of three plant species common in wetlands of the northeastern US: weeping willow (Salix babylonica L.), red maple (Acer rubrum L.), and cattail (Typha latifolia L.). The results suggest that these common wetland plant species have inherently different evapotranspiration rates – see **Figure 1.5** – and therefore wetland plant composition can have an important influence on the amount of water contributed to local and regional evapotranspiration budgets. Due to the small size of the trees used in this experiment, the amount by which evapotranspiration rates of mature trees exceed rates of other plants was underestimated.

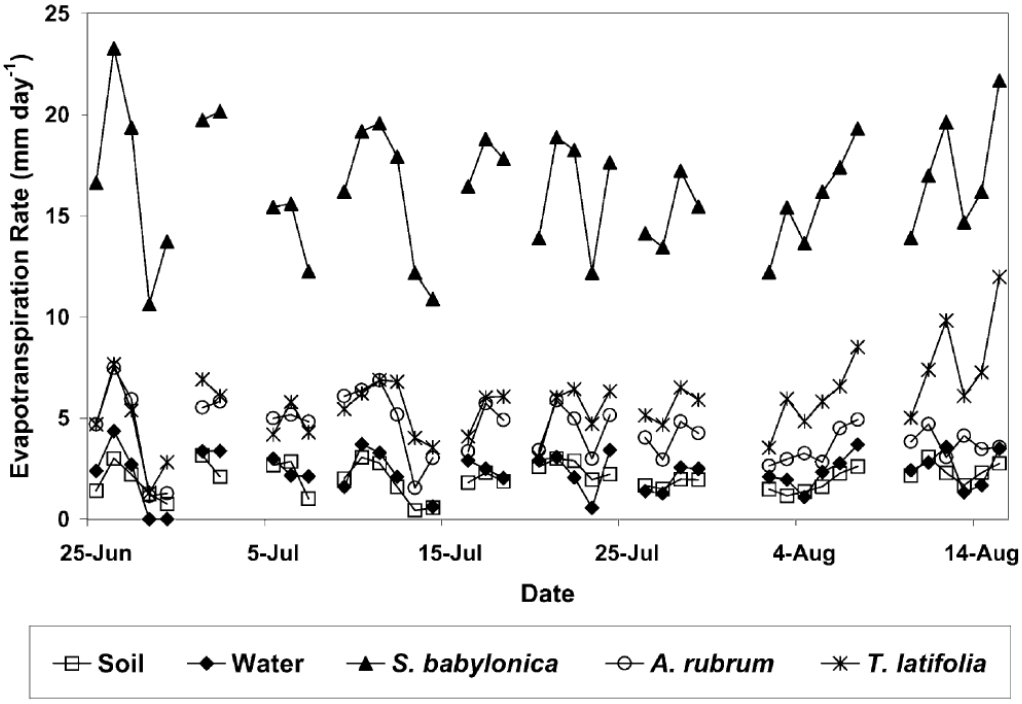

Figure 1.5 Average evapotranspiration rates (mm per day) for all treatments. Missing data points indicate days in which data were not collected due to rain (Pauliukonis & Schneider, 2001).

C.-Y. Xu (2005) evaluated and compared three evapotranspiration models using the complementary relationship approach for estimating areal actual evapotranspiration in three study regions representing a large geographic and climatic diversity. These regions consist of NOPEX region in Central Sweden (cool temperate, humid), Baixi catchment in Eastern China (subtropical, humid), and the Potamos tou Pyrgou River catchment in Northwestern Cyprus (semiarid to arid). The models were the CRAE model of Morton, the Advection– Aridity (AA) model of Brutsaert and Stricker, and the GG model proposed by Granger and Gray using the concept of relative evapotranspiration (the ratio of actual to potential evapotranspiration). The calculation was made on a daily basis and comparison was made on monthly and annual bases. The study was performed in two steps: First, the three evapotranspiration models with their original parameter values were

applied to the three regions in order to test their general applicability. Second, the parameter values were locally calibrated based on the water balance study.

The results showed that using the original parameter values all three complementary relationship models worked reasonably well for the temperate humid region, while the predictive power decreases in moving toward regions of increased soil moisture control, i.e. increased aridity. In such regions, the parameters need to be calibrated. They also concluded that using the locally calibrated parameter values all three models produced the annual values correctly.

This study was used to show the importance of locally calibrated parameter values. Comparison of the mean monthly actual evapotranspiration calculated by the water balance model and the three complementary relationship evapotranspiration models using the locally tuned parameter values for the three study regions are shown in **Figure 1.6**.

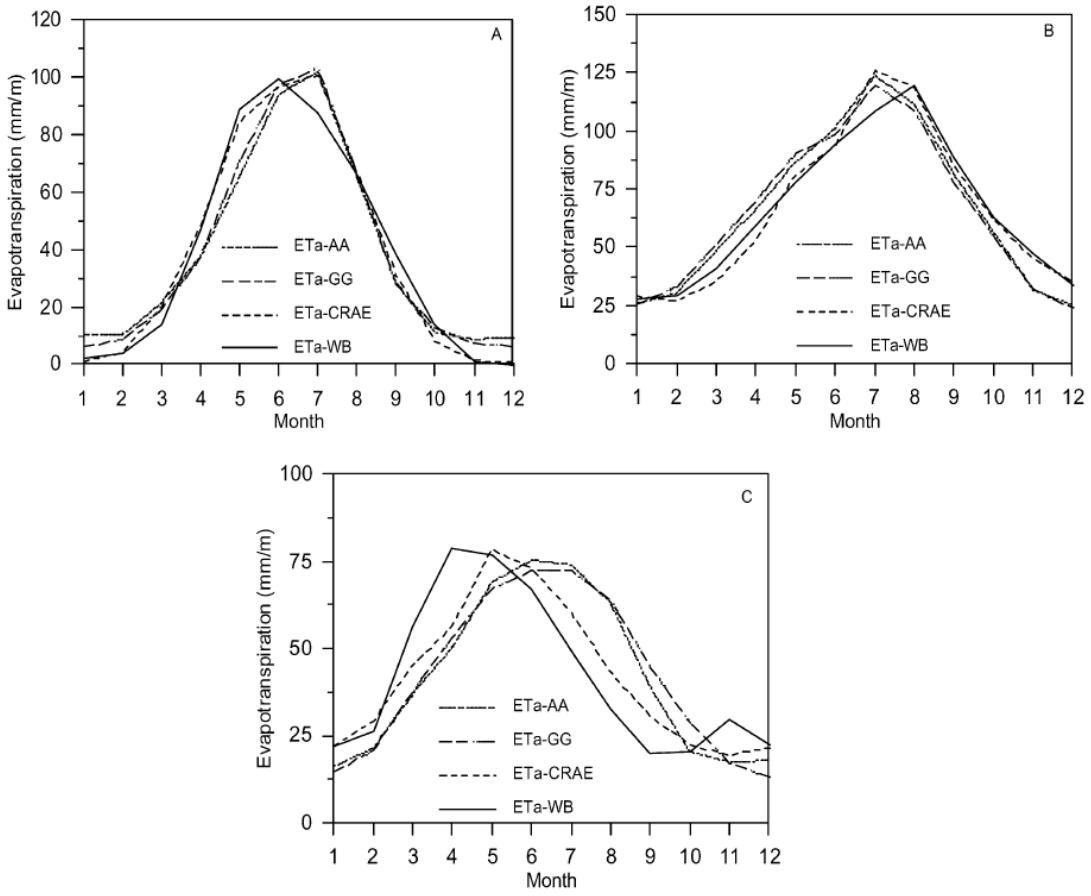

Figure 1.6 Comparison of the mean monthly actual evapotranspiration calculated by the water balance model and the three complementary relationship evapotranspiration models using the locally tuned parameter values for the three study regions (C.-Y. Xu, 2005).

Observed daily evapotranspiration at 18 sites were analyzed by Douglas, et al. (2009). They measured daily evapotranspiration and ancillary climate data and then used these data to compare the performance of three common methods for estimating the potential evapotranspiration. Three methods they used are: the Turc method (Tc), the Priestley-Taylor method (PT) and the Perman-Monteith method (PM). The sites were distributed throughout the State of Florida and represent a variety of land cover types: three in open water, four in marshlands, four in grasslands/pastures, and five in citrus and forest areas. They reported the highest daily evapotranspiration values to occur in the

open water sites, ranging from an average of 3.3 $mm\ d^{-1}$ in the winter to 5.3 $mm\ d^{-1}$ in the spring. Daily evapotranspiration at the marsh sites was also high, ranging from 2.7 $mm\ d^{-1}$ in winter to 4.4 $mm\ d^{-1}$ in summer. The lowest daily evapotranspiration occurred in the winter and fall seasons at the grass sites - with the values of 1.3 $mm\ d^{-1}$ and 2.0 $mm\ d^{-1}$, respectively – and at the forested sites – with the values of 1.8 $mm\ d^{-1}$ and 2.3 $mm\ d^{-1}$, respectively.

1.6 Evapotranspiration in Wetlands

A number of studies have been carried out on wetland evapotranspiration; however, due to the different wetland conditions and the methods used, the results have differed greatly (Herbst and Kappen (1999), Burba, et al. (1999), Pauliukonis and Schneider (2001) and Acreman, et al. (2003)).

Acknowledging the evapotranspiration as a principle component of the hydrological cycle in wetlands, Sun and Song (2008) measured evapotranspiration from a Carex lasiocarpa dominated marsh in the Sanjiang Plain, northeast China, during the growing season (May to September) of 2005. The Sanjiang Plain is the largest concentrative distribution area of freshwater marshes in China. The study station is located at Sanjiang Mire Wetland Experimental Station, Chinese Academy of Sciences in Northern China. Covered continuously by a clay layer, this plain has a slope grade of about 1:5000 to 1:10,000, which is favorable for wetland formation. Generally, freshwater sedge marshes are the major form of wetland in this plain.

The climate is a temperate continental monsoon type with annul mean temperature 1.9 ºC and -21 ºC, respectively. Water and soil in marshes are completely

frozen from late October to the following April and begin to melt in late April. The annual mean precipitation is about 600 mm, concentrated in July and August, accounting for more than 60% of the annual precipitation. Precipitation is the main water source in freshwater marshes.

The seasonal variation of daily evapotranspiration rates and the main environmental factors influencing evapotranspiration were analyzed. Penman, Penman–Monteith (PM) and Priestley–Taylor (PT) models were then used for simulating daily evapotranspiration and a comparison between the estimates of the three models and the measured evapotranspiration was done.

The results showed that daily evapotranspiration rates ranged from 0.58–4.80 $mm.d^{-1}$ with an average of 2.31 $mm.d^{-1}$ during the measurement period. Daily ET increased from early May, reaching the maximum of 4.80 $mm.d^{-1}$ at June 29, and then declined till early August and then declined till the end of the growing season.

From May to September, the monthly average daily ET was 1.41, 3.07, 2.68, 2.49 and 1.73 $mm.d^{-1}$, respectively The low ET rate in May was mainly due to the fact that the leaves had not fully matured, as evidenced by the low Leaf Area Index values, which results in low transpiration rate. In September, the low ET rate was caused by the senescence of leaves and the low radiation. As mentioned, about 70% of the growing-season precipitation concentrated in July and August, thus the radiation in July and August was less than that of June. Accordingly the ET rates in July and August were lower than that of June. Measured evapotranspiration is shown in **Figure 1.7**.

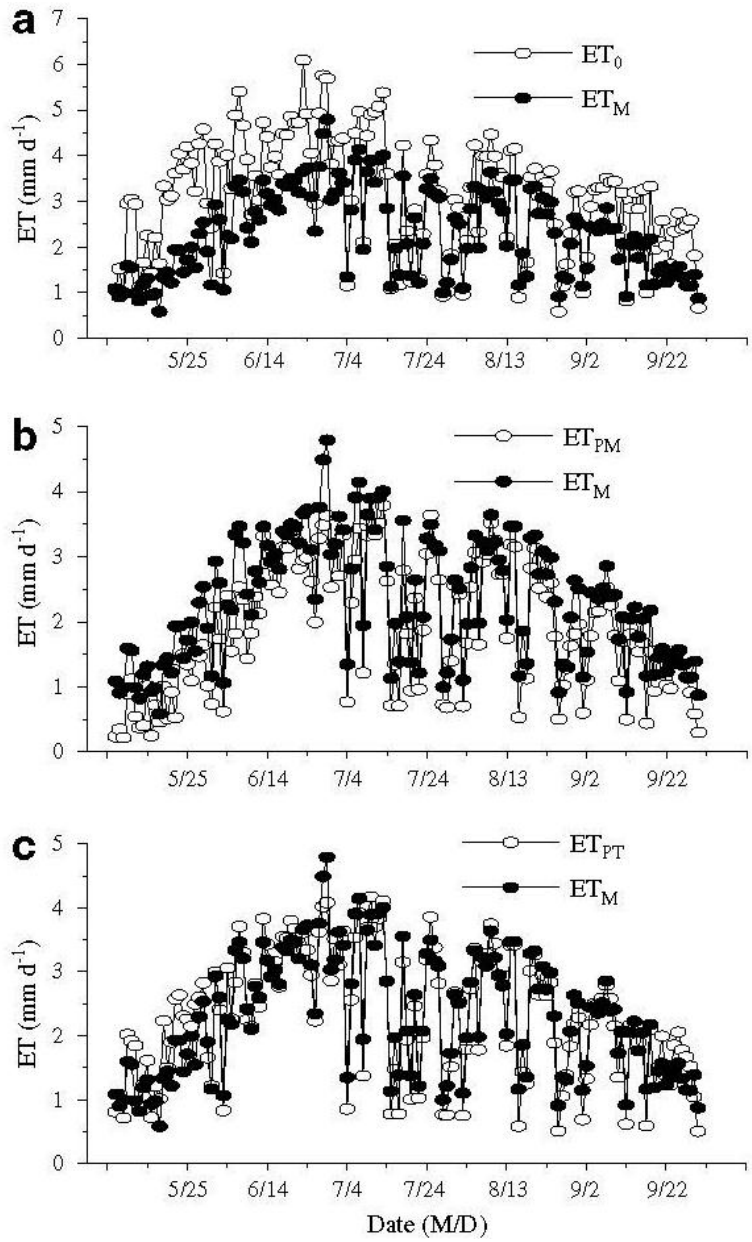

Figure 1.7 Evapotranspiration measured with eddy covariance method (ET_M) and those estimated with different models: (a) Penman(ET_0); (b) Penman-Monteith(ET_{PM}) and (c) Priestley-Taylor(ET_{PT}) (Sun & Song, 2008).

Previous plot-scale investigations have indicated a substantial difference in evapotranspiration between wetlands and uplands. This difference is shown in **Figure 1.8**. Evapotranspiration is expected to be greater in wetlands than in uplands areas

because wetland soils are wetter and water is more readily available for evapotranspiration (Ballard and Buell (1975) and Ballard (1979)).

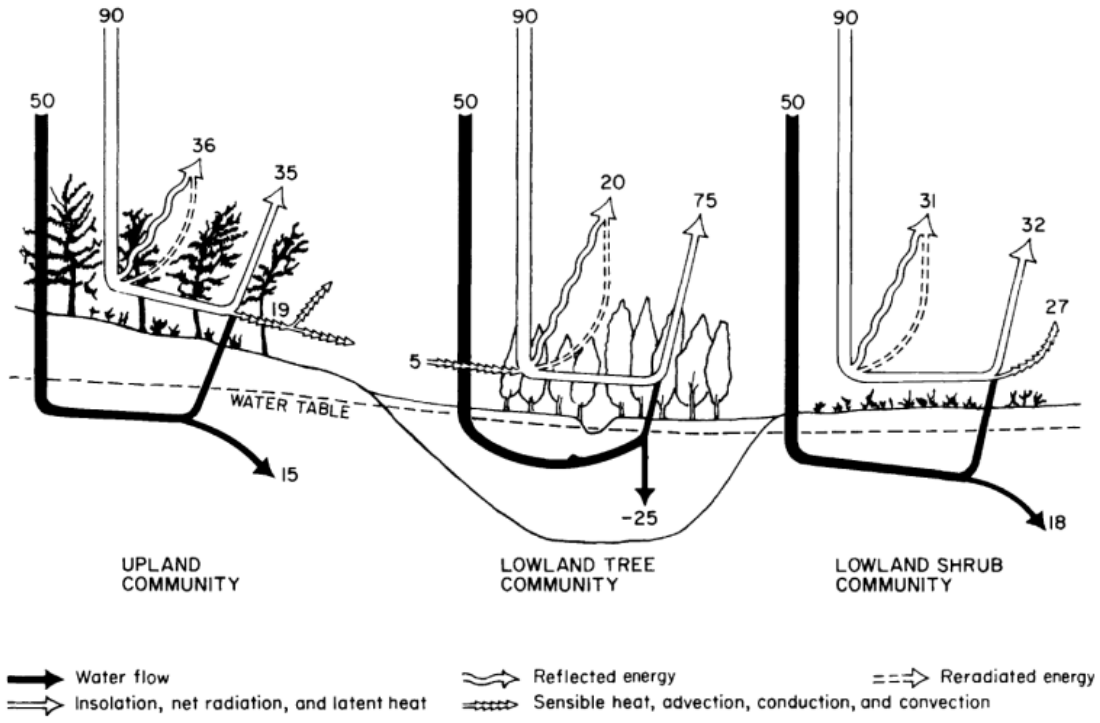

Figure 1.8 Typical summer water and energy budgets for three Pine Barrens ecosystem types. Values are expressed in centimeters of water per unit area (Ballard, 1979).

Evaluation of this difference over larger areas was made possible by comparing evapotranspiration measurements collected at the wetland station with those collected at nearby upland stations operated by the U.S. Forest Service (USFS) (Sumner, Nicholson, & Clark, 2012). Previous investigations by USFS determined that when averaged across all upland sites for all years of measurement (2005-09), annual upland evapotranspiration was 606 $mm.yr^{-1}$. The average annual evapotranspiration measured at the wetland site during 2005-06 (801 $mm.yr^{-1}$) is about 32 percent higher than the average of that at the upland sites. The average annual evapotranspiration at the wetland site is about 17

percent higher than evapotranspiration at the upland sites when averaged over years without disturbance at a particular stand. Factors contributing to differences in evapotranspiration rates among different sites and among different years included water availability, dominant plant species, and leaf area. Interannual variability of wetlands evapotranspiration may be less than that of uplands evapotranspiration because the upland sites are more susceptible to periodic drought conditions, disturbance by fire, and insect defoliation.

1.7 Evapotranspiration in the State of New Jersey

Water budgets are fundamental to the understanding of hydrologic systems. If the various components of the water budget can be quantified, including inflows, outflows, and changes in stored water, then a more complete understanding and evaluation of a hydrologic system becomes possible.

Determination of evapotranspiration played a key role in early water-supply planning in the state of New Jersey. Vermuele (1894) approximated monthly and annual evapotranspiration for southern New Jersey watersheds on the basis of calculations made using empirical relations between precipitation and runoff in other East Coast watersheds. These calculations were used to estimate the safe yield for Joseph Wharton's 1891 proposal to divert flow from more than 1,191 square kilometers of "the great pine belt" of southern New Jersey and deliver it to the cities of Camden and Philadelphia (City of Philadelphia, 1892). Wood (1937) quantified interception (the amount of rain or snow stored on leaves and branches and eventually evaporated back to the atmosphere), an important component of the hydrologic cycle that contributes to evapotranspiration, in an oak-pine forest in the Pinelands. After statistical analysis of the data, they concluded that

there was a significant difference between the rain gauge readings made in the woods and those in the open which shows the interception by the plants.

A number of studies were conducted during the 1950s and 1960s to understand the effects of forest management practices on water resources (Buell, 1955); related research continued into the 1970s. Lull and Axley (1958) studied evapotranspiration in different upland vegetative communities by measuring soil moisture changes, but significant differences were not found among the communities. Barksdale (1958) concluded that evapotranspiration in the lower Delaware River Basin accounted for about 50 percent of precipitation. Rhodehamel (1970) found reasonable agreement between this evapotranspiration rate and estimated evapotranspiration rates from other investigations in the Pinelands and vicinity. Summer evapotranspiration rates in hardwood-dominated and cedar-dominated wetlands in the Pinelands were estimated from water-table fluctuations, and no differences in the evapotranspiration rates of these communities were detected (Ballard (1971); Buell and Ballard (1972)). Evapotranspiration rates in lowland shrub communities were found to be lower than those of lowland tree communities. Evapotranspiration rates were shown to be greater in lowland (wetland) areas of the Pinelands, where water is more available to plants, than in upland areas (Ballard & Buell, 1975). Ballard (1979) examined these differences in an energy flux context and concluded that in wetland tree areas, the net summer loss of groundwater discharge through evapotranspiration was 250 millimeters (mm).

Evapotranspiration has been estimated as part of water-supply and availability studies in the New Jersey Coastal Plain. Mean evapotranspiration rates in the major drainage areas of the New Jersey Coastal Plain were estimated by Vowinkel and Foster

(1981) as the long-term difference between mean precipitation and mean runoff. Estimates of evapotranspiration (presented as "water loss") for basins partly within the Pinelands ranged from 414 to 653 mm/yr. More detailed examination of water budgets that included evapotranspiration in selected drainage areas that are within the New Jersey Coastal Plain and at least partly within the Pinelands are presented in a series of reports by Watt and Johnson (1992), Johnsson and Barringer (1993), Watt, et al. (1994), Johnson and Watt (1996), Watt, et al. (2003), and Gordon (2004). Although the methods used to estimated evapotranspiration in these studies vary somewhat, the evapotranspiration estimates were all based on the concept of water-budget closure and are, therefore, consistent with estimates of other water-budget components. The evapotranspiration estimates from the previously mentioned series of reports range from 563 to 658 mm/yr.

Other recent investigations have examined the physiological responses of variety of shrub and tree species to hydrologic stress, fire, and insect defoliation. As part of their research on carbon and fire dynamics in the Pinelands, Clark, et al. (2010) and (2011), measured evapotranspiration flux using an eddy covariance method at an oak-dominated upland site and two pine-dominated upland sites. They observed that evapotranspiration at the oak-dominated upland site was slightly greater in summer and lower in winter than evapotranspiration at the pitch pine-dominated upland site and the evapotranspiration averaged 51 to 62 percent of annual precipitation at the sites when they were undisturbed. Additional flux monitoring demonstrated the effects of the fire and insect defoliation in evapotranspiration and water-use efficiency at the three sites; annual evapotranspiration at one of the defoliated sites was as low as 419 mm/yr, 37 percent of incident precipitation (Clark, Skowronski, Gallagher, Schafer, & Renninger, 2011). When all

years were considered, maximum seasonal leaf area index at these sites explained 82 and 80 percent of the variation in daily evapotranspiration during the summer at the oak-and pine-dominated sites, respectively. Schafer (2011) examined changes in stomatal conductance in response to drought, defoliation, and morality in an upland oak/pine forest in the Pinelands. Drought caused reductions in canopy-level conductance and corresponding reductions in evapotranspiration, with the magnitude of the effect varying by species.

CHAPTER 2

FIELD INVESTIGATIONS

2.1 Introduction

To further study the water cycle and also to be able to compare the modeling results to actual values, field investigations were conducted. In this chapter Monmouth Battlefield State Park will be introduced. After presenting a brief history of the park, the unique feature of the site, which is the reason behind choosing this specific park as the Study Area, will be described.

Methodology of collecting data during the site visits will be presented. A description of the monitoring wells installation, performed land survey and the tests at the site (e.g., soil classification, permeability test, etc.) and the reason behind them will be discussed. Finally, the results of the field investigations will be presented.

Water levels, elevations, soil classification and hydraulic conductivity results will be implemented in the developed model.

Water level readings at the monitoring wells and also at the Stream will be utilized to validate the developed model which will be discussed further in the next chapter.

2.2 Monmouth Battlefield State Park

2.2.1 History

Monmouth Battlefield State Park is a 2,979-acre New Jersey state park located on the border of Manalapan and Freehold Township, in Monmouth County, New Jersey, United States. This park preserves the historical battlefield on which the American Revolutionary War's Battle of Monmouth was waged. **Figure 2.1** shows the location of the park (NJDEP, 2013).

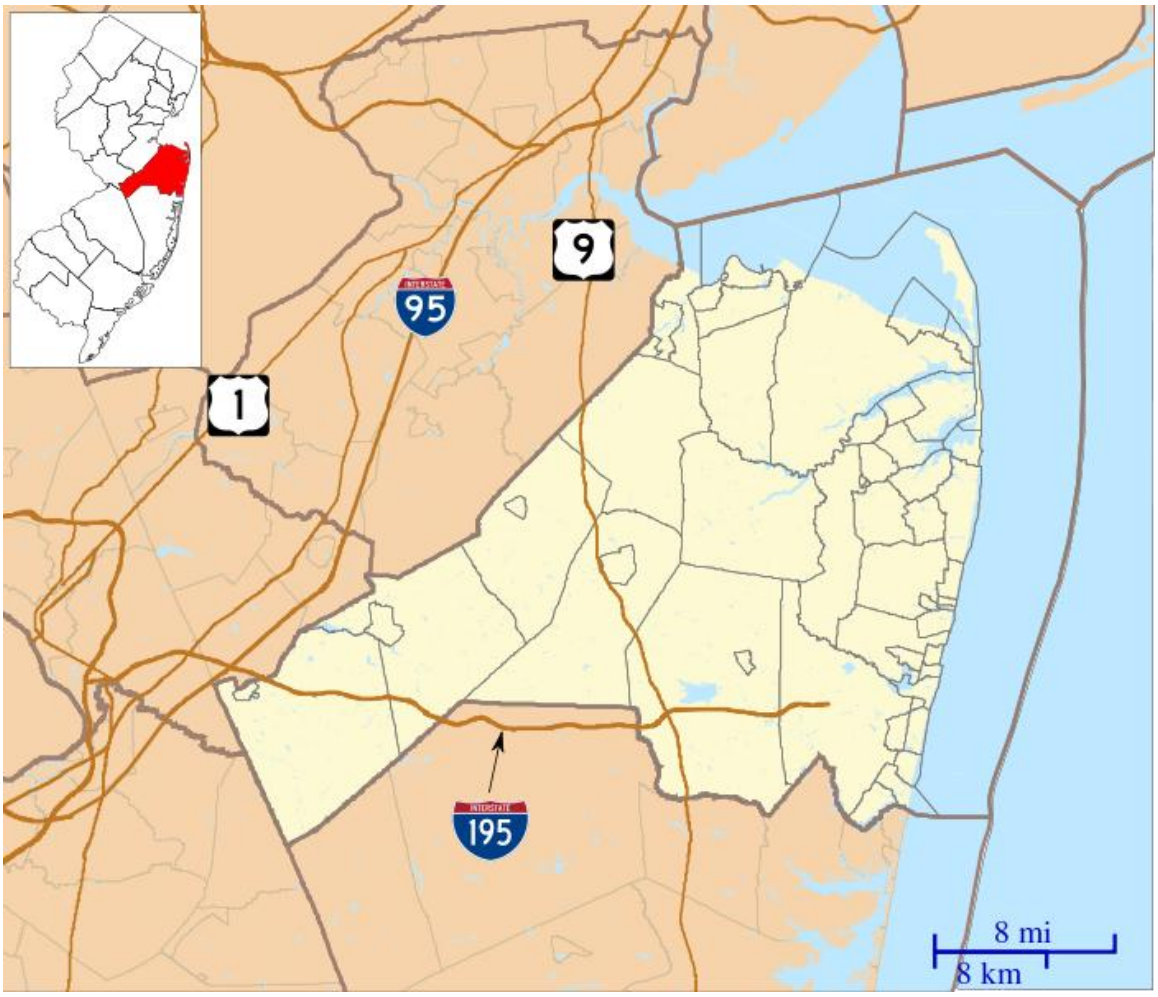

Figure 2.1 Location of the Monmouth Battlefield State Park (Wikimedia Foundation, Inc., 2013).

The Battle of Monmouth was an American Revolutionary War (or American War of Independence) battle fought on June 28, 1778 in Monmouth County, New Jersey. The Continental Army under General George Washington attacked the rear of the British Army column commanded by Lieutenant General Sir Henry Clinton as they left Monmouth Court House (modern Freehold Borough). It is known as the Battle of Monmouth Courthouse.

Unsteady handling of lead Continental elements by Major General Charles Lee had allowed British rearguard commander Lieutenant General Charles Cornwallis to seize the initiative but Washington's timely arrival on the battlefield rallied the Americans along a hilltop hedgerow. Sensing the opportunity to smash the Continentals, Cornwallis pressed his attack and captured the hedgerow in stifling heat. Washington consolidated his troops in a new line on heights behind marshy ground, used his artillery to fix the British in their positions, and then brought up a four gun battery under Major General Nathanael Greene on nearby Combs Hill to enfilade the British line, requiring Cornwallis to withdraw. Finally, Washington tried to hit the exhausted British rear guard on both flanks, but darkness forced the end of the engagement. Both armies held the field, but the British commanding General Clinton withdrew undetected at midnight to resume his army's march to New York City.

While Cornwallis protected the main British column from any further American attack, Washington had fought his opponent to a standstill after a pitched and prolonged engagement; the first time that Washington's army had achieved such a result. The battle demonstrated the growing effectiveness of the Continental Army after its six month encampment at Valley Forge, where constant drilling under officers such as Major

General Friedrich Wilhelm von Steuben and Major General Gilbert du Motier, Marquis de Lafayette greatly improved army discipline and morale. The battle improved the military reputations of Washington, Lafayette and Anthony Wayne but ended the career of Charles Lee, who would face court martial at Englishtown for his failures on the day. According to some accounts, an American soldier's wife, Mary Hays, brought water to thirsty soldiers in the June heat, and became one of several women associated with the legend of Molly Pitcher.

According to one story, she was the wife of an American artilleryman who came to battle with her husband, bringing water for swabbing the cannons and for the thirsty crews, and took a soldier's place after he fell, and fought beside her husband. There is a common misconception that her husband was the soldier that fell, but research by the society that preserves the battlefield has proven this to be incorrect. The story is based on a true incident but has become embellished over the years. Two places on the battlefield are marked as sites of the "Molly Pitcher Spring".

Although never accorded formal preservation, the Monmouth Battlefield is one of the best preserved of the Revolutionary War battlefields. Each year, during the last weekend in June, the Battle of Monmouth is reenacted at Monmouth Battlefield State Park in modern Freehold Township and Manalapan (Wikimedia Foundation, Inc., 2013).

2.2.2 Geologic Setting

Geologic materials in Monmouth County include surficial deposits and Coastal Plain bedrock formations. Surficial deposits are sediments laid down within the past 10 million years. they overlie the bedrock formations and include river sediments laid down in terraces and floodplains in valleys; older river deposits that form upland gravels, the

Pensauken Formation, and the Beacon Hill Gravel; modern estuary, wetland and beach sediments; older estuarine and beach sediments that form the Cape May Formation; and hillslope deposits. Surficial deposits are generally less than 25 feet thick, except in estuaries and on Sandy Hook, where they are as much as 240 feet thick.

Coastal Plain bedrock formations are layered, unconsolidated sand, clay, and silt laid down in marine and coastal settings in the Cretaceous and Tertiary periods between 90 and 10 million years ago. The layers dip to the southeast and crop out as belts running northeast-southwest border of the county. Their total thickness ranges from about 500 feet along the northwest border of the county to about 1500 feet in the southeast corner. (Stanford, Pristas, & Hall, 2009)

United States Department of Agriculture reports a Type B soil for this area in the Natural Resources Conservation Service (USDA, 2013).

2.2.3 Study Area

Study Area is a riverine wetland and surrounding hillsides in the Monmouth Battlefield State Park. The site has a unique feature because there are two very different vegetative covers on the two sides of the wetland. A stream flows from northwest to southeast. Approaching the wetland from southwest side, there is a forested area which turns into shrubs and grass on the northeast side of the Stream. This unique feature presents the opportunity to compare the effects of evapotranspiration element which influences the amount of the recharge that reaches the water table throughout the year. This feature can be viewed in **Figure 2.2**.

2.2.4 Study Corridor

Study Corridor is an imaginary corridor defined within the site in order to perform tests, take samples and collect data from various features of the site.

The southwest side of the Corridor starts at the Forest Side of the Study Area runs over the Stream and ends at the northeast side at the Farm Side. The Study Corridor is shown in **Figure 2.2**.

Figure 2.2 Aerial view of the Study Corridor within the Study Area.

2.3 Methodology

2.3.1 Groundwater Levels

In order to observe and record the groundwater levels, monitoring wells were installed over time along the Study Corridor.

At the designated locations, a hand auger (see **Figure 2.3**) was used to bore the soil to the depth of ten (10) feet below ground level or one (1) foot below the water interface, whichever happened first.

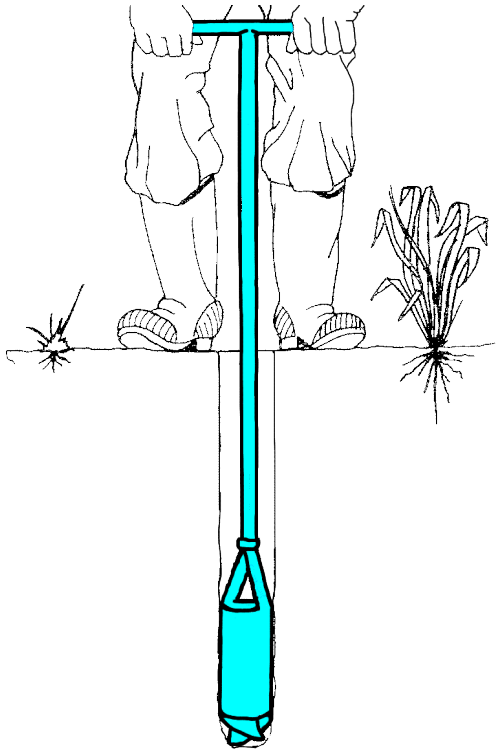

Figure 2.3 Using a hand auger to bore the soil.

Ten (10) foot long, perforated PVC pipes with a diameter of four (4) inches (see **Figure 2.4**) were covered with black filter socks (see **Figure 2.5**) and were installed in the bored locations. Perforated pipes help the groundwater to enter/leave the pipe at ease

and black filter sock prevents the pipes to be filled in by the soil that can be washed in to the pipes by the flow of the groundwater.

Figure 2.4 Perforated PVC pipes used in the monitoring wells.

Figure 2.5 Perforated four (4) inch pipe covered by black filter sock.

Using a tape measure (see **Figure 2.6**) or a metered floating stick (see **Figure 2.7**), water levels at the monitoring wells were determined and then recorded in a field book with a half inch measurement accuracy.

Figure 2.6 Reading water level from a monitoring well using a tape measure.

Figure 2.7 Reading water level from a monitoring well using a metered floating stick.

2.3.2 Land Survey

In order to better establish the topography of the Study Corridor, a land survey was conducted along the Corridor. Stream level was used as the benchmark (BM). A theodolite was fastened to a tripod with the fastening screws in a location where could clearly see the BM and the area in which the other locations elevations were to be determined. Then the theodolite was leveled using the fine leveling screws. The leveling rod was held vertically on the BM. The rod was sighted with the theodolite and the reading was recorded in the field book. Then the rod was moved to the other points where the elevations were to be determined. The rod, while held vertically, was sighted with the

theodolite and the readings were recorded in the field book. By subtracting these readings from the BM reading, the relative elevation of each location was determined.

As a result of this land survey, monitoring wells relative elevations to the Stream were established.

2.3.3 Soil Classification

A further understanding of the texture and grain size of the soil will result in a more accurate modeling experience and will expedite model validation process.

In order to classify the soil, soil samples will be collected along the Study Corridor using a hand auger in accordance with "ASTM D1452-09 Standard Practice for Soil Exploration and Sampling by Auger Borings" (ASTM International, 2013). This practice covers equipment and procedures for the use of (hand) augers in shallow depth geotechnical exploration.

Collected samples are to be classified according to "ASTM D2487-11 Standard Practice for Classification of Soils for Engineering Purposes (Unified Soil Classification System)" (ASTM International, 2013). This standard classifies soils from any geographic location into categories representing the results of prescribed laboratory tests to determine the particle-size characteristics. Sieve analysis will be performed to assess the particle size distribution of the collected soil samples.

2.3.4 Soil Hydraulic Conductivity

Soil hydraulic conductivity describes the ease with which water can move through pore spaces or fractures of soil. It depends on the intrinsic permeability of the material and on the degree of saturation. Implementing a more precise hydraulic conductivity in the model will result in a more accurate simulation.

In order to determine the hydraulic conductivity of the soil in the Study Corridor, the auger-hole method was utilized in various locations along the Corridor.

The auger-hole method is a rapid, simple and reliable method for measuring hydraulic conductivity of soil below a water table. It is mostly used in connection with the design of drainage systems in waterlogged land and in canal seepage investigations. The method originated by Diserens (1934), was improved by Hooghoudt (1936) and later by Kirkham (1945), Kirkham and Van Bavel (1948), Ernst (1950), Johnson, Frevert and Evans (1952) and Kirkham (1955).

The general principle is that a hole is bored into the soil to a certain depth below the water table. When equilibrium is reached with the surrounding groundwater, a part of the water in the hole is removed. The water seeps into the hole again, and the rate of which the water rises in the hole is measured and then converted by a suitable formula to the hydraulic conductivity (k) for the soil.

The auger-hole method gives the average permeability of the soil layers extending from the water table to a small distance (a few decimeters) below the bottom of the hole. If there is an impermeable layer at the bottom of the hole, the value of k is governed by the soil layers above this impermeable layer. The radius of the column of soil of which the permeability is measured is about 1-2 feet.

In measuring hydraulic conductivity in the field, four phases can be distinguished:

1. The drilling of the holes – This has to be done with the minimum disturbance to the soil.

2. The removal of the water from the holes – This can start when equilibrium with the surrounding groundwater is attained and the depth of the water table has been recorded.

3. The measurement of the rate of rise – The measurement consists of the rate at which the water rises in the hole. The observations are made either

with a constant time interval (Δt) or with fixed intervals for the rise of the water (Δy), depending on the equipment available.

4. The computation of the hydraulic conductivity from the measurement data. – The Equation (2.1) has been obtained for homogeneous soil (Ernst & Westerhof, 1950)

$$k = \frac{4000 * r * \Delta y}{\left(\frac{H}{r} + 20\right)\left(2 - \frac{y}{H}\right) * y * \Delta t} \tag{2.1}$$

Where:

$k =$ Hydraulic conductivity $(\frac{m}{day})$

$H =$ Depth (cm) of hole below the groundwater table.

$y =$ Distance (cm) between groundwater level and the average level of the water in the hole for the time interval Δt (s).

$r =$ Radius of the auger-hole(cm).

$S =$ Depth (cm) of the impermeable layer below the bottom of the hole or the layer, which has a permeability of about one tenth or less of the permeability of the layers above.

For a graphical representation, please see **Figure 2.8**.

Please note that Equation (2.1) represents an empirically derived approximate expression of the results of a number of relaxation constructions. Hence this equation does not show the exact relationship that should theoretically exist between the different quantities, although the value of k will be within a maximum error of 20%.

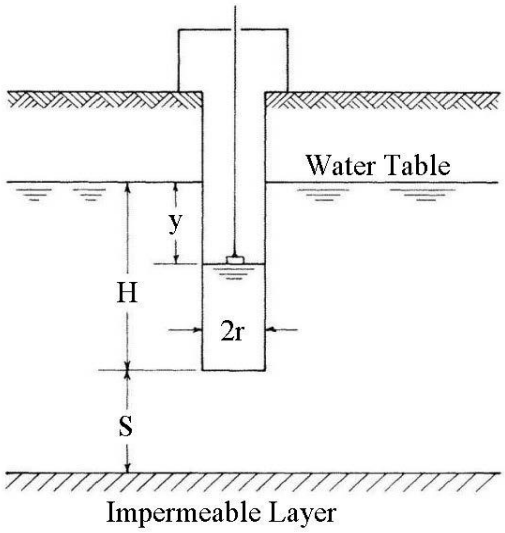

Figure 2.8 Schematic of auger-hole method in determining the hydraulic conductivity of the soil under groundwater level (Van Beers, 1983).

2.4 Results

2.4.1 Groundwater Levels

Fourteen (14) monitoring wells were installed along the Study Corridor, seven (7) on the Forest Side of the Stream and the remaining seven (7) on the Farm Side. Out of the fourteen (14) locations, seven (7) are in a straight line (MW 1, 2, 4 and 5 on the Forest Side of the Stream and, 6, 7 and 8 on the Farm Side of the Stream). The readings from those 7 locations and also the readings from the Stream water levels will be used to validate the developed model by comparing the simulated water levels to the observed ones.

Monitoring wells locations are presented in **Figure 2.9**.

Water levels were recorded from May 3, 2011 to July 28, 2013 during the site visits. Water level readings are shown in **Figure 2.10** (for the seven monitoring wells in the straight line) and in **Table 2.1** (for all the monitoring wells).

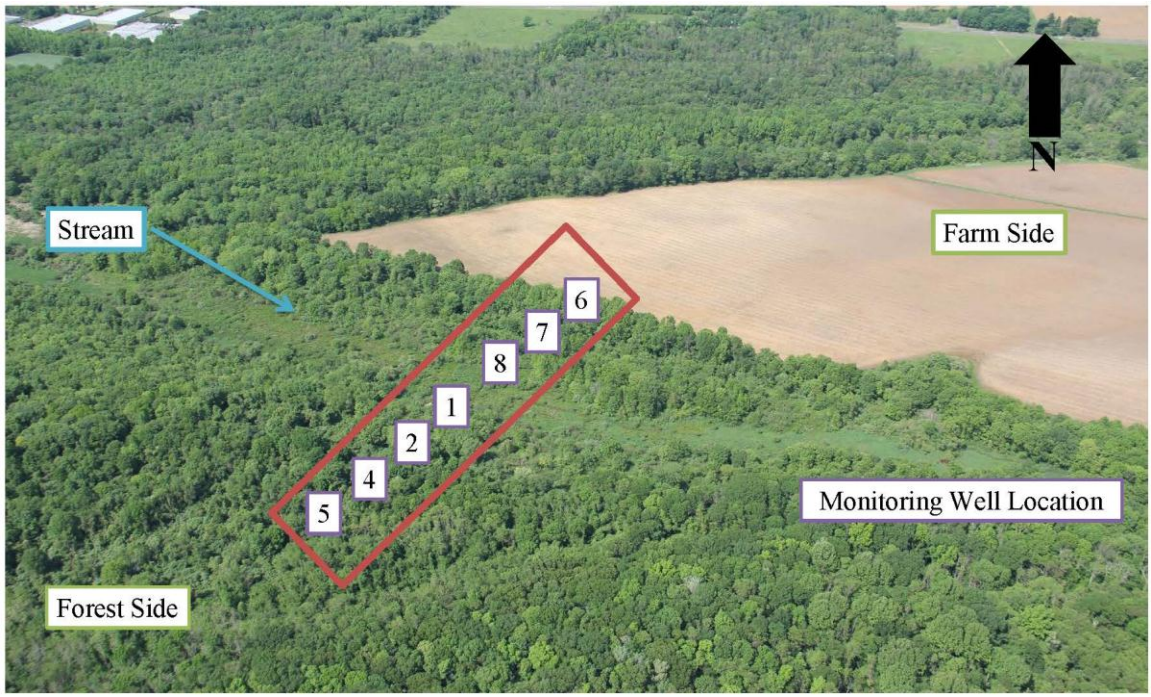

Figure 2.9 Monitoring Wells Locations along the Study Corridor.

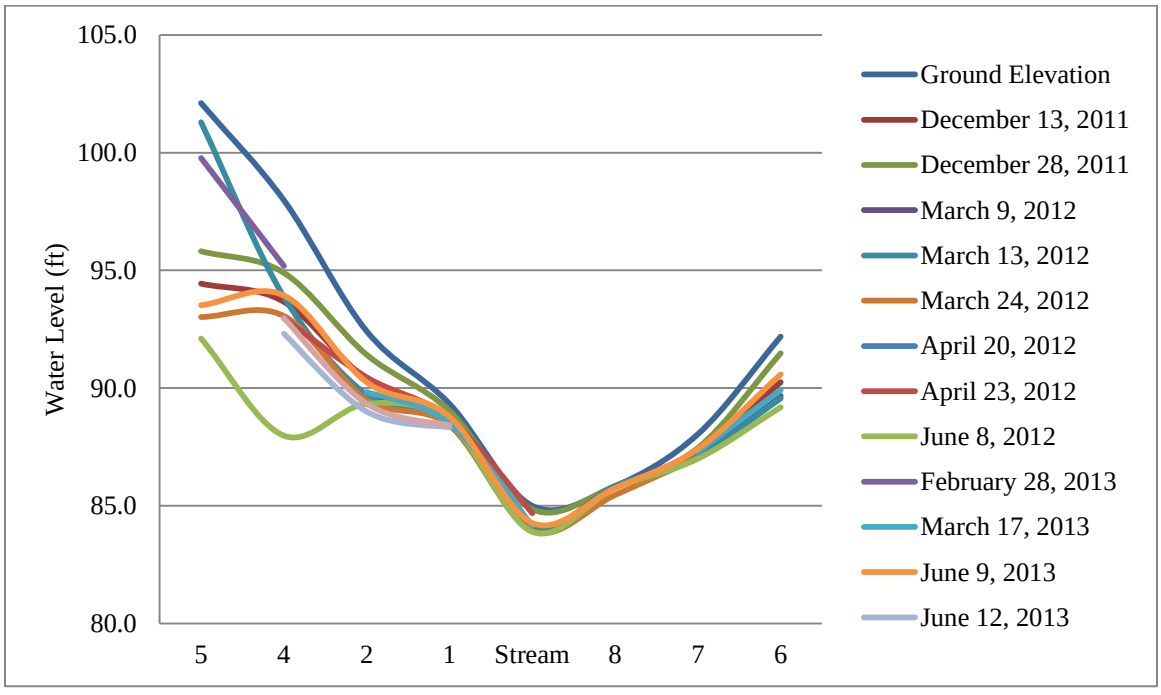

Figure 2.10 Water level readings – Stream bottom is assumed to have an elevation of 81' above ground and the other elevations are reported accordingly.

Table 2.1 Water Level Readings – Readings in Monitoring Wells (MWs) are in Inches below Ground and the Stream Readings are Based on the Installed Gauge in the Stream

Date	MW 1	MW 2	MW 3	MW 4	MW 4-5	MW 5	Stream	MW 6	MW 6-7	MW 7	MW 7-8	MW 8	MW 9	MW 10
May 3, 2011	10.8	30.8												
May 5, 2011	10	29	29.5											
May 7, 2011	11	32.5	32.75											
May 9, 2011	11.3	35	34.25											
May 16, 2011	11.3	35	35.25											
May 18, 2011	10.5	33	33.5											
June 14, 2011	13.5	44.5	44											
August 11, 2011	9.5	32.5	32.5											
September 9, 2011	6	19	19											
September 10, 2011	7	22	22											
September 11, 2011	7.5	24.5	24.5											
September 15, 2011	9	30	30											
September 17, 2011	10.5	32.5	32.5											
September 18, 2011	10.5	32.5												
September 22, 2011	10	33												
September 28, 2011	8.5	28	28											
September 30, 2011	9	29.5	29.5											
October 1, 2011		28.5												
December 13, 2011	6	24.5	25	51.75		92		23		9		0.25	11.5	
January 12, 2012	4.5	16	17.5	33		96.5								
March 9, 2012	10.5	32	32.5	Dry		Dry	28.5	30		11		0	12.5	
March 13, 2012	10.5	32.5	33.25	49.25		97.5	28.5	31.25		11.5		0	11	
March 24, 2012	11	35	35	59		109		Dry		12.5		4.5	13.5	
April 20, 2012	11.5	38	38	Dry		Dry	26			15.5		2	15.5	89.75
April 23, 2012	7.5	23.5	22.5	60		Dry								80.4
May 16, 2012										13		0.75	11	
February 28, 2013	9	0		33.5		28								
March 17, 2013	10	31	31		98		29.5	27		9.5			11	
April 12, 2013		28.5		41.5										
April 29, 2013	10	35		51.5										
May 9, 2013	10	26.5												
June 6, 2013	12	41		68				36		15		2		
June 9, 2013	6.5	26	25.75	48.5	119.5	103	31	19	26	8	20	1	9.5	
June 12, 2013	12	41		68								2	15	
July 28, 2013	11	37		60	123									

2.4.2 Land Survey

As a result of the land survey along the Study Corridor, monitoring wells relative elevations to the Stream were established. The land survey was performed only for the seven (7) monitoring well locations in the straight line (MW 1, 2, 4 & 5 at the Forest Side of the Stream and, 6, 7 & 8 at the Farm Side of the Stream). For the location of these seven (7) monitoring wells, please refer to **Figure 2.9**.

After careful review of the topographic map for Freehold, NJ (see **Figure 2.11**), which covers the Study Area, the elevation of the Stream bottom was estimated to be 81 feet above ground. At the time of the land survey, the water level was measured to be 4 feet from the Stream bottom. Therefore the elevation of the top of the Stream water was 85 feet above ground at time of land survey. Relative ground elevation of the monitoring well locations were adjusted based on the established elevation of the top of the Stream water. The results of the land survey are shown in **Figure 2.12**.

As can be seen in **Figure 2.12**, Forest Side of the Stream has a relatively higher elevation compared to the Farm Side of the Stream.

Figure 2.11 Topographic map for Freehold, NJ (U.S. Geological Survey, 2013).

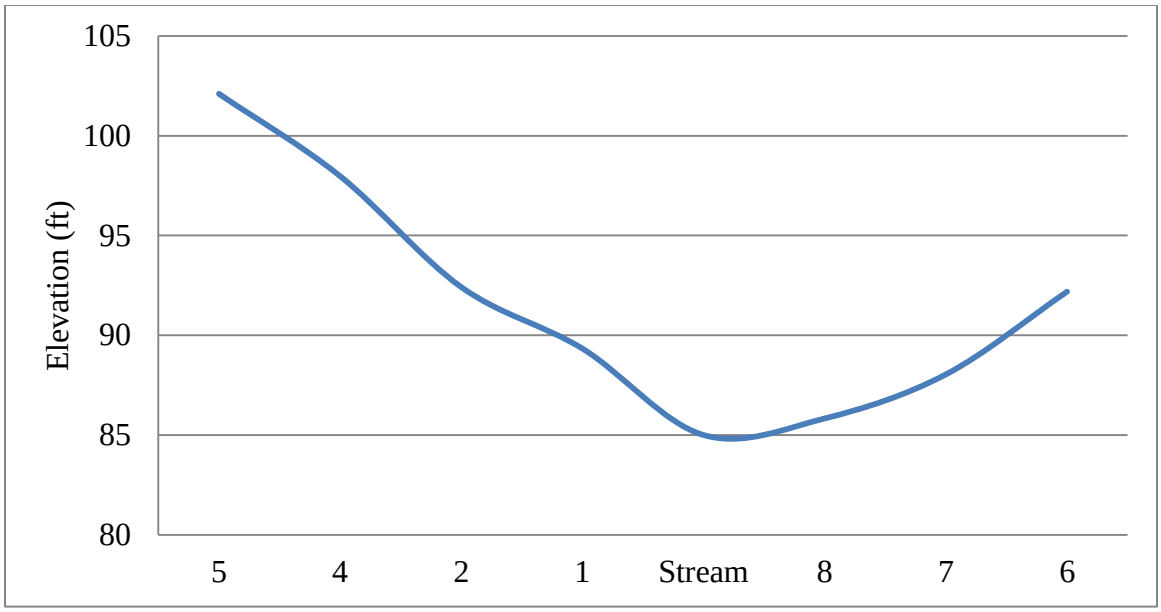

Figure 2.12 Land survey results along the Study Corridor (horizontal axis is not to scale).

2.4.3 Soil Classification

In order to classify the soil, three soil samples were collected along the Study Corridor using a hand auger. Only one soil sample (SC-1) was collected from the Farm Side of the Stream which seemed to be more uniform; and the two remaining samples (SC-2 & 3) were collected from the Forest Side of the Stream to ensure a more precise soil classification. See **Figure 2.13** for approximate locations of the soil samples.

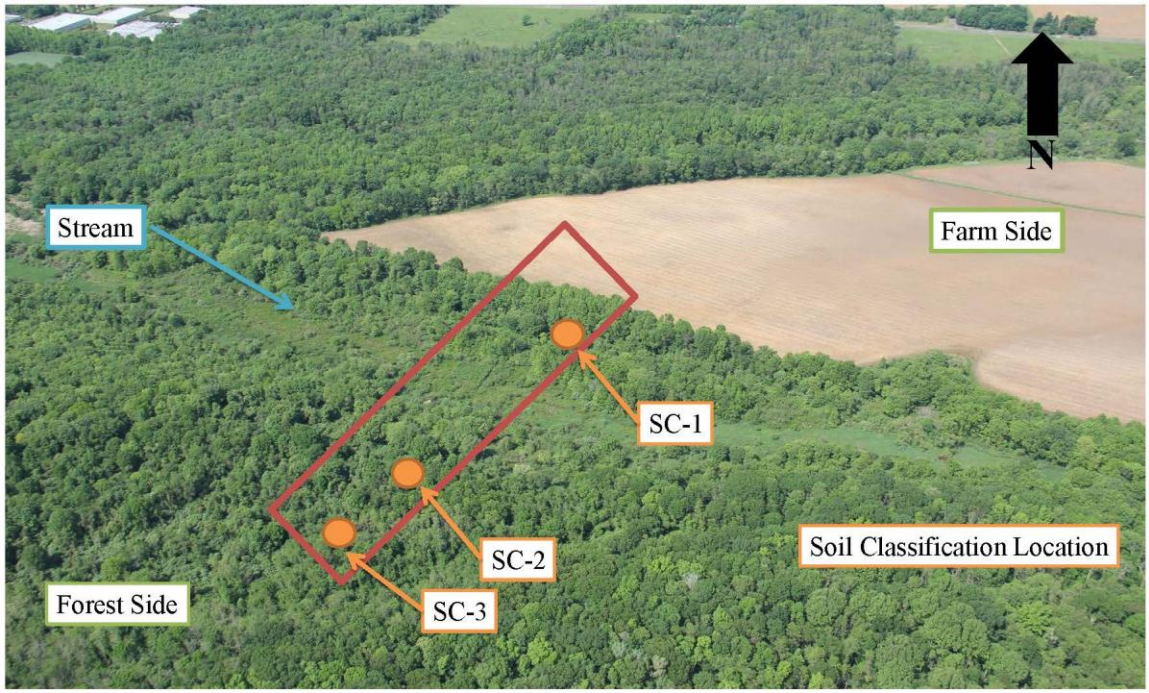

Figure 2.13 Soil classification sample location plan (SC-1, 2 & 3).

For sieve analysis set-up and a snapshot of the sampled soil after being sieved, see **Figure 2.14** and **Figure 2.15**, respectively.

Figure 2.14 Sieve analysis set-up.

Figure 2.15 A snapshot of the sampled soils after being sieved.

The cumulative particle-size plot of the sieve analysis for SC-1, 2 & 3 are presented in **Figure 2.16**, **Figure 2.17** and **Figure 2.18**, respectively.

Based on the classification, all three samples were determined to belong to the "Silty Sand" group name. Since various types of vegetation cover the Study Area, the soil is expected to contain "Organic Fines".

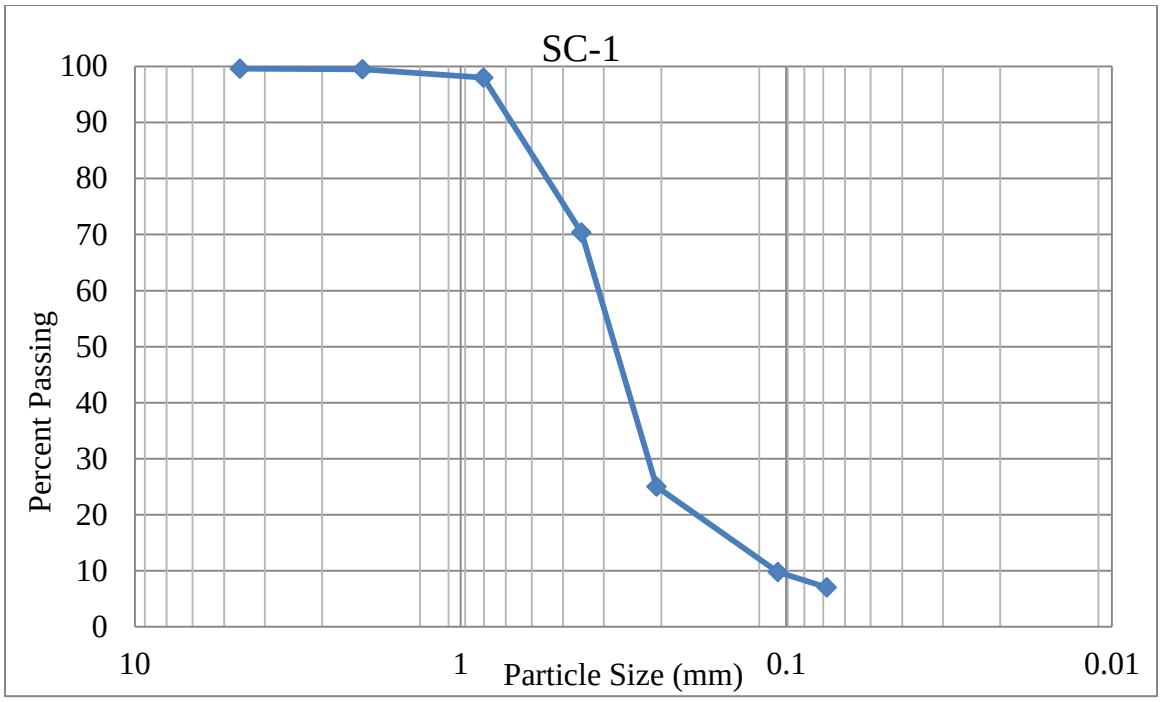

Figure 2.16 Cumulative particle-size plot of the sieve analysis for SC-1.

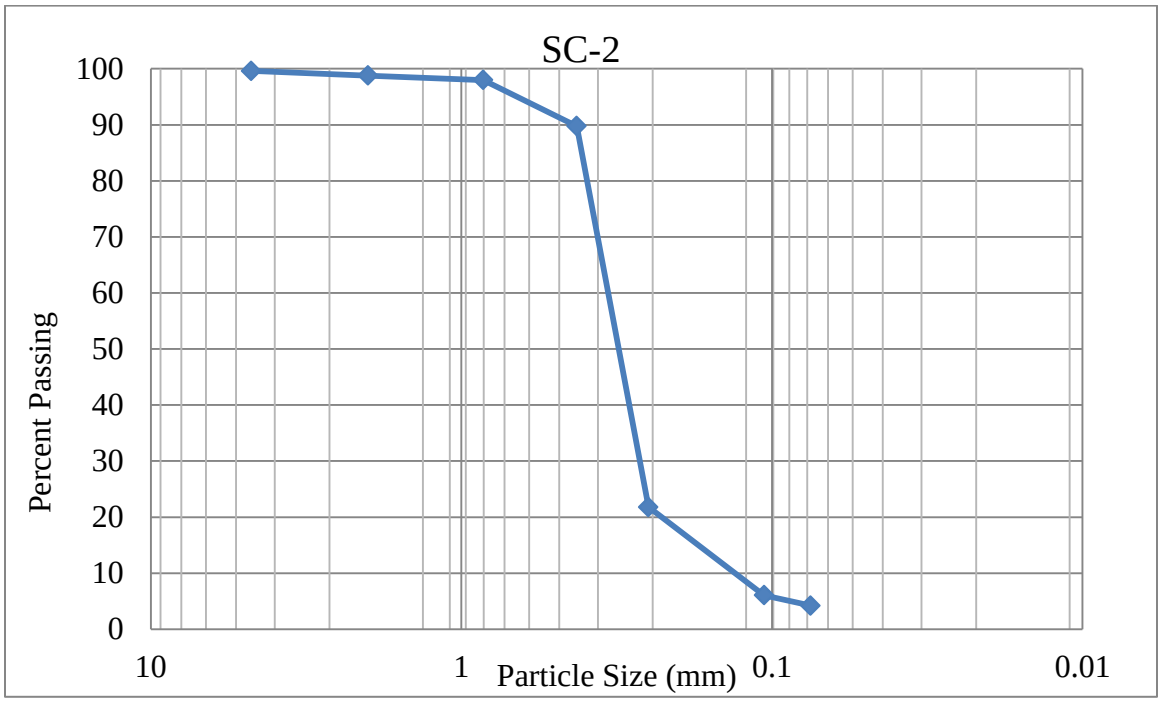

Figure 2.17 Cumulative particle-size plot of the sieve analysis for SC-2.

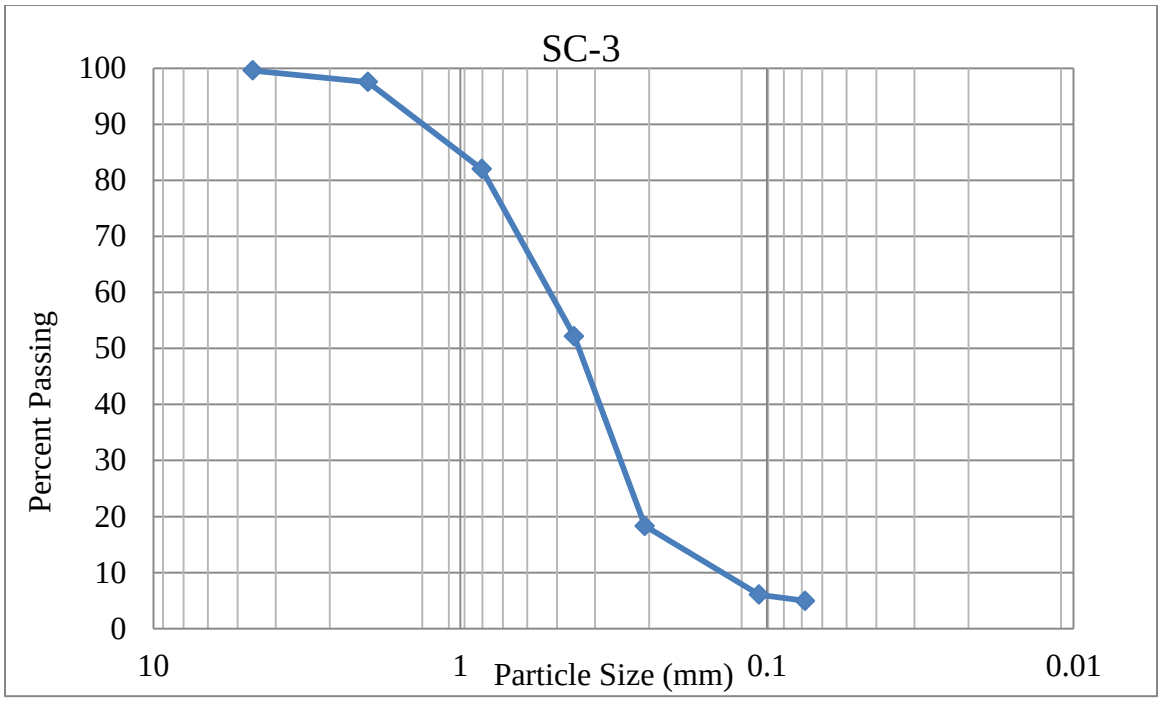

Figure 2.18 Cumulative particle-size plot of the sieve analysis for SC-3.

2.4.4 Soil Hydraulic Conductivity

Auger-hole method with a constant time interval was utilized in three locations (K-1, 2 and 3) along the Study Corridor to determine the hydraulic conductivity. Only one of the hydraulic conductivity test locations (K-1) is on the Farm Side of the Study Corridor which is expected to have a more uniform soil structure. The remaining two hydraulic conductivity tests were performed on the Forest Side of the Study Corridor (K-2 and 3).

Approximate location of the hydraulic conductivity test locations are shown in **Figure 2.19**.

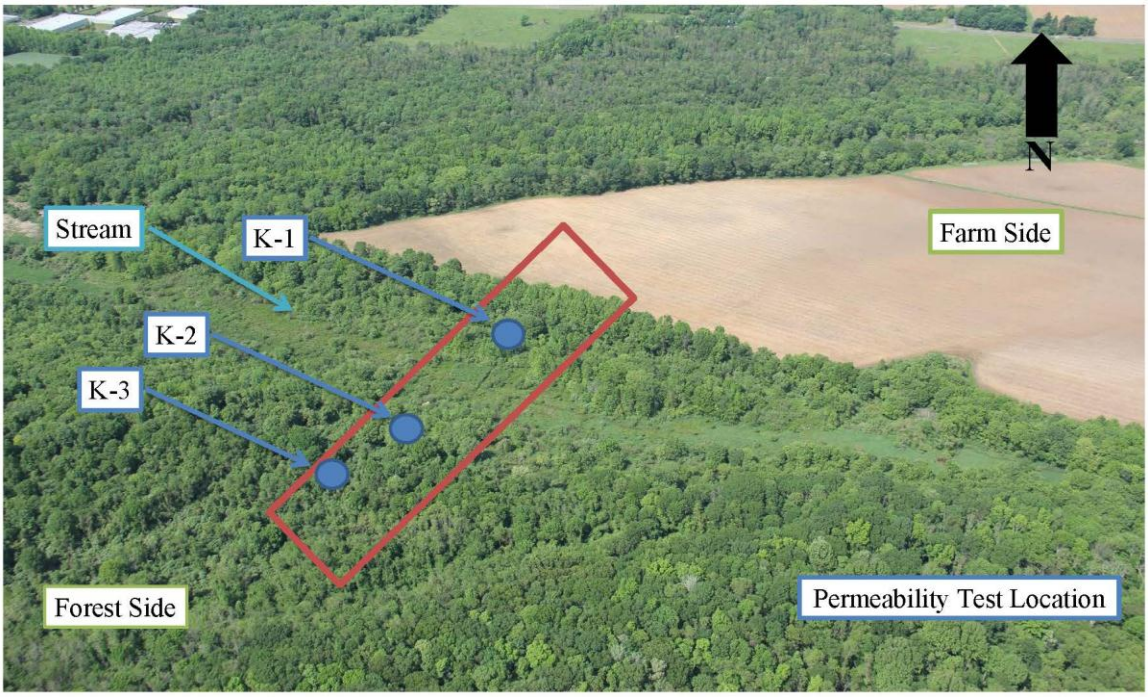

Figure 2.19 Auger-hole method hydraulic conductivity test locations along the Study Corridor.

The results of the hydraulic conductivity tests are shown in Table 2.2.

Table 2.2 Hydraulic Conductivity Test Results

Test Location Name	**Hydraulic Conductivity** $(\frac{ft}{d})$
K-1	1.1
K-2	0.1
K-3	1.0

Hydraulic conductivity of 0.1 to 1.1 $\frac{ft}{d}$ is within reasonable range for a semi-pervious soil of fine sand and silt which is consistent with the findings of Soil Classification tests performed in the Study Corridor.

The results of these hydraulic conductivity tests will be implemented in the developed model.

CHAPTER 3

MODELMUSE AND USGS MODFLOW

3.1 Introduction

In this chapter, U.S. Geological Survey (USGS) computer model, MODFLOW and a graphical user interface for USGS MODFLOW-2005 will be introduced.

The partial-differential equation governing the three-dimensional movement of groundwater flow will be discussed and discretized into a finite-difference form. Iterative methods utilized to obtain the solution of finite-difference equations for each time step will be visited.

Finally, a few simulation studies that used USGS MODFLOW will be presented.

3.2 ModelMuse

ModelMuse is a graphical user interface (GUI) for the U.S. Geological Survey model MODFLOW- 2005 (Harbaugh A. , 2005).

It simulates steady and non-steady flow in an irregularly shaped flow system in which aquifer layers can be confined, unconfined, or a combination of confined and unconfined.

ModelMuse allows the user to define the spatial input for the models by drawing points, lines, or polygons on top, front, and side views of the Model Domain. These objects can have up to two associated formulas that define their extent perpendicular to the view plane, allowing the objects to be three-dimensional. Formulas are also used to specify the values of spatial data (data sets) both globally and for individual objects. Objects can be used to specify the values of data sets independent of the spatial and

temporal discretization of the model. Thus, the grid and simulation periods for the model can be changed without specifying spatial data pertaining to the hydro-geologic framework and boundary conditions. The points, lines, and polygons can assign data set properties at locations that are enclosed or intersected by them or by interpolation among objects using several interpolation algorithms. Data for the model can be imported from a variety of data sources and model results can be viewed in ModelMuse (Winston, 2009).

As mentioned above, ModelMuse is the GUI for the USGS MODFLOW-2005; therefore, USGS MODFLOW will be introduced further.

3.3 USGS MODFLOW

3.3.1 History

Prior to the development of MODFLOW, the two- and three-dimensional finite-difference models described by Trescott (1979), Trescott and Larson (1976), and Trescott, Pinder, and Larson (1976) were used extensively by the USGS and others for the computer simulation of ground-water flow. The first version of MODFLOW (McDonald & Harbaugh, 1984) was the result of the need to consolidate all the commonly used simulation capabilities into a single code that was easy to understand, use, and modify. This first version was developed between the spring of 1981 and the winter of 1983. That model code was originally called the USGS Modular Three-Dimensional Finite-Difference Ground-Water Flow Model, but the model became known as MODFLOW several years later. This was developed using the Fortran 66 computer language.

By the early 1990s, MODFLOW had become the most widely used ground-water flow model both within and outside the USGS.

MODFLOW was originally conceived solely as a ground-water flow model. The authors viewed the solution of additional related equations as something to be done in separate programs.

By the late 1990s, there was a growing belief by many developers of modeling programs that combining such related capabilities into a single program promised to make development and use easier; therefore, the decision was made to broaden the scope of MODFLOW to allow capabilities such as transport and parameter estimation to be directly incorporated.

To facilitate the incorporation of related equations into MODFLOW, an expansion of the modular design was required. The result, which became MODFLOW-2000 (Harbaugh, Banta, Hill, & McDonald, 2000), was the addition of "Process," which is defined as parts of the code that solve a major equation or set of related equations. The part of the code that solves the ground-water flow equation became the Ground-Water Flow (GWF) Process. Three processes, Observation, Sensitivity and Parameter Estimation, aid calibration and model evaluation (Hill, Banta, Harbaugh, & Anderman, 2000). Solution of the transport equation is the Ground-Water Transport Process (Konikow, Goode, & Hornberger, 1996) and the management of ground-water is the Ground-Water Management Process (Ahlfeld, Barlow, & Mulligan, 2005). MODFLOW-2005 is similar in design to MODFLOW-2000. The expanded concept of processes continues as in MODFLOW-2000. The primary change in MODFLOW-2005 is the incorporation of a different approach for managing internal data.

3.3.2 Mathematical Model

The three-dimensional movement of ground water of constant density through porous earth material may be described by the partial-differential equation (3.1).

$$\frac{\partial}{\partial x}\left(K_{xx}\frac{\partial h}{\partial x}\right)+\frac{\partial}{\partial y}\left(K_{yy}\frac{\partial h}{\partial y}\right)+\frac{\partial}{\partial z}\left(K_{zz}\frac{\partial h}{\partial z}\right)+W=S_s\frac{\partial h}{\partial t} \quad (3.1)$$

Where

K_{xx}, K_{yy} and K_{zz} are values of hydraulic conductivity along the x, y, and z coordinate axes, which are assumed to be parallel to the major axes of hydraulic conductivity (L/T);

h is the potentiometric head (L);

W is a volumetric flux per unit volume representing source and/or sinks of water, with W<0.0 for flow out of the groundwater system, and W>0.0 for flow into the system (T^{-1});

S_s is the specific storage of the porous material (L^{-1}); and

t is time (T).

In general, S_s, K_{xx}, K_{yy} and K_{zz} may be functions of space ($S_s = S_s(x,y,z), K_{xx} = K_{xx}(x,y,z)$ and so forth) and W may be a function of space and time and anisotropic medium, provided the principal axes of hydraulic conductivity are aligned with the coordinate directions. Equation (3.1), together with specification of flow and/or head conditions at the boundaries of an aquifer system and specification of initial-head conditions, constitutes a mathematical representation of a ground-water flow system. A solution of Equation (3.1), in an analytical sense, is an algebraic expression giving h(x,y,z,t) such that, when the derivatives of h with respect to space and time are substituted into Equation (3.1), the equation and its initial and boundary conditions are

satisfied. A time-varying head distribution of this nature characterizes the flow system, in that it measures both the energy of flow and the volume of water in storage, and can be used to calculate directions and rates of movement. Except for very simple systems, analytical solutions of Equation (3.1) are rarely possible, so various numerical methods must be employed to obtain approximate solutions. One such approach is the finite-difference method, wherein the continuous system described by Equation (3.1) is replaced by a finite set of discrete points in space and time, and the partial derivatives are replaced by terms calculated from the differences in head values at these points. The process leads to systems of simultaneous linear algebraic difference equations; their solution yields values of head at specific points and times. These values constitute an approximation to the time-varying head distribution that would be given by an analytical solution of the partial-differential equation of flow.

3.3.3 Finite Difference Equation

Development of the ground-water flow equation in finite-difference form follows from the application of the continuity equation: the sum of all flows into and out of the cell must be equal to the rate of change in storage within the cell. Under the assumption that the density of ground water is constant, the continuity equation expressing the balance of flow for a cell is represented as Equation (3.2)

$$\sum Q_i = SS\frac{\Delta h}{\Delta t}\Delta \mathrm{V} \tag{3.2}$$

Where

Q_i is a flow rate into the cell (L^3T^{-1});

SS has been introduced as the notation for specific storage in the finite-difference formulation; its definition is equivalent to that of S_s in Equation (3.1) – that is,

SS is the volume of water that can be injected per unit volume of aquifer material per unit change in head(L^{-1});

ΔV is the volume of the cell (L^3); and

Δh is the change in head over a time interval of length Δt.

The term on the right-hand side is equivalent to the volume of water taken into storage over a time interval Δt given a change in head of Δh. Equation (3.2) is stated in terms of inflow and storage gain. Outflow and loss are represented by defining outflow as negative inflow and loss as negative gain.

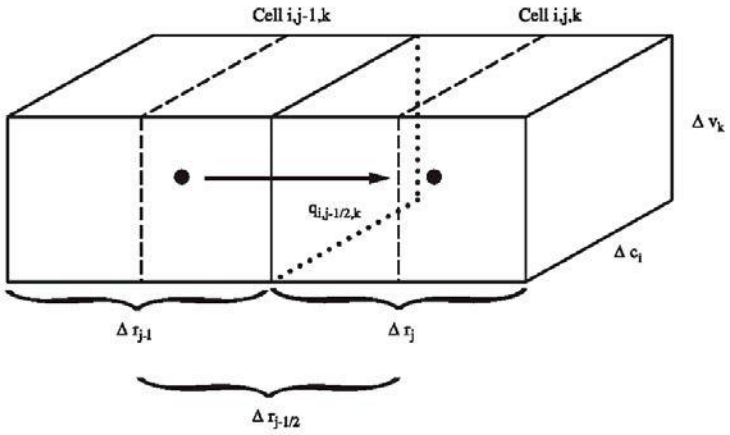

Figure 3.1 Flow into cell i,j,k from cell i,j-1,k. (McDonald & Harbaugh, 1988).

To simplify the following development, flows are considered positive if they are entering cell i,j,k; the negative sign usually incorporated in Darcy's law has been dropped from all terms. Following these conventions, flow into cell i,j,k in the row direction from cell i,j-1,k (**Figure 3.1**), is given by Darcy's law as

$$q_{i,j-1/2,k} = KR_{i,j-1/2,k}\Delta c_i \Delta v_k \frac{(h_{i,j-1,k} - h_{i,j,k})}{\Delta r_{j-1/2}} \quad (3.3)$$

Where

$h_{i,j,k}$ is the head at node i,j,k and $h_{i,j-1,k}$ is the head at node i,j-1,k;

$q_{i,j-1/2,k}$ is the volumetric flow rate through the face between cells i,j,k and i,j-1,k (L^3T^{-1});

$KR_{i,j-1/2,k}$ is the hydraulic conductivity along the row between nodes i,j,k and i,j-1,k ($L\ \ T^{-1}$);

$\Delta c_i \Delta v_k$ is the area of the cell faces normal to the row direction; and

$\Delta r_{j-1/2}$ is the distance between nodes i,j,k and i,j-1, k (L).

Equation (3.3) gives the exact flow for a one-dimensional steady-state case through a block of aquifer extending from node i,j-1,k to node i,j,k and having a cross-sectional area $\Delta c_i \Delta v_k$. $KR_{i,j-1/2,k}$ is the conductivity of the material between nodes i,j,k and i,j-1,k, which is the effective hydraulic conductivity for the entire region between the nodes.

The subscript i,j-1/2,k is used in Equation (3.3) to designate the region between nodes i,j-1,k and i,j,k.

Similar expressions can be written approximating the flow into the cell through the remaining five faces. For flow in the row direction through the face between cells i,j,k and i,j+1,k,

$$q_{i,j+1/2,k} = KR_{i,j+1/2,k} \Delta c_i \Delta v_k \frac{(h_{i,j+1,k} - h_{i,j,k})}{\Delta r_{j+1/2}} \tag{3.4}$$

While for the column direction, flow into the block through the front face is

$$q_{i+1/2,j,k} = KC_{i+1/2,j,k} \Delta r_i \Delta v_k \frac{(h_{i+1,j,k} - h_{i,j,k})}{\Delta c_{i+1/2}} \tag{3.5}$$

And flow into the block through the rear face is

$$q_{i-1/2,j,k} = KC_{i-1/2,j,k}\Delta r_i \Delta v_k \frac{(h_{i-1,j,k} - h_{i,j,k})}{\Delta c_{i-1/2}} \quad (3.6)$$

For the vertical direction inflow through the bottom face is

$$q_{i,j,k+1/2} = KV_{i,j,k+1/2}\Delta r_j \Delta c_i \frac{(h_{i,j,k+1} - h_{i,j,k})}{\Delta v_{k+1/2}} \quad (3.7)$$

Whereas inflow through the upper face is given by

$$q_{i,j,k-1/2} = KR_{i,j,k-1/2}\Delta r_j \Delta c_i \frac{(h_{ij,k-1} - h_{i,j,k})}{\Delta v_{k-1/2}} \quad (3.8)$$

Each of Equations (3.3) through (3.8) expresses inflow through a face of cell i,j,k in terms of heads, grid dimensions, and hydraulic conductivity. The notation can be simplified by combining grid dimensions and hydraulic conductivity into a single constant, the "hydraulic conductance" or, more simply, the "conductance". For example,

$$CR_{i,j-1/2,k} = \frac{KR_{i,j-1/2,k}\Delta c_i \Delta v_k}{\Delta r_{j-1/2}} \quad (3.9)$$

Where

$CR_{i,j-1/2,k}$ is the conductance in row I and layer k between nodes i,j-1,k and i,j,k (L^2T^{-1}).

Thus, conductance is the product of hydraulic conductivity and cross-sectional area of flow divided by the length of the flow path (in this case, the distance between the nodes).

Substituting conductance from Equation (3.9) into Equation (3.3) yields Equation (3.10).

$$q_{i,j-1/2,k} = CR_{i,j-1/2,k}(h_{i,j-1,k} - h_{i,j,k}) \quad (3.10)$$

Similarly, Equations (3.4) through (3.8) can be rewritten to yield Equation (3.11).

$$q_{i,j+\frac{1}{2},k} = CR_{i,j+\frac{1}{2},k}\left(h_{i,j+1,k} - h_{i,j,k}\right) \tag{3.11}$$

$$q_{i-\frac{1}{2},j,k} = CC_{i-\frac{1}{2},j,k}\left(h_{i-1,j,k} - h_{i,j,k}\right) \tag{3.12}$$

$$q_{i+\frac{1}{2},j,k} = CC_{i+\frac{1}{2},j,k}\left(h_{i+1,j,k} - h_{i,j,k}\right) \tag{3.13}$$

$$q_{i,j,k-\frac{1}{2}} = CV_{i,j,k-\frac{1}{2}}\left(h_{i,j,k-1} - h_{i,j,k}\right) \tag{3.14}$$

$$q_{i,j,k+\frac{1}{2}} = CV_{i,j,k+\frac{1}{2}}\left(h_{i,j,k+1} - h_{i,j,k}\right) \tag{3.15}$$

Where the conductances are defined analogously to CR in Equation (3.9).

Equations (3.10) through (3.15) account for flow into cell i,j,k from the six adjacent cells. To account for flows into the cell from features or processes external to the aquifer, such as rivers, drains, areal recharge, evapotranspiration, or wells, additional terms are required. Those flows may be dependent on the head in the receiving cell but independent of all other heads in the aquifer, or they may be entirely independent of the head in the receiving cell. Flow from outside the aquifer may be represented by the expression

$$a_{i,j,k,n} = p_{i,j,k,n} + q_{i,j,k,n} \tag{3.16}$$

Where $a_{i,j,k,n}$ represents flow from the nth external source into cell i,j,k (L^3T^{-1}), and $p_{i,j,k,n}$ and $q_{i,j,k,n}$ are constants ((L^2T^{-1}) and (L^3T^{-1}), respectively).

In general, if there are N external sources or stresses affecting a single cell, the combined flow is expressed by

$$\sum_{n=1}^{N} a_{i,j,k,n} = \sum_{n=1}^{N} (P_{i,j,k,n} h_{i,j,k,n}) + \sum_{n=1}^{N} q_{i,j,k,n} \tag{3.17}$$

Defining $P_{i,j,k}$ and $Q_{i,j,k}$ by the expressions

$$P_{i,j,k} = \sum_{n=1}^{N} P_{i,j,k,n} \tag{3.18}$$

And

$$Q_{i,j,k} = \sum_{n=1}^{N} q_{i,j,k,n} \tag{3.19}$$

The general external flow term for cell i,j,k is

$$\sum_{n=1}^{N} a_{i,j,k,n} = P_{i,j,k} h_{i,j,k} + Q_{i,j,k} \tag{3.20}$$

Applying the continuity Equation (3.2) to cell i,j,k, taking into account the flows from the six adjacent cells, change in storage, and the external flow rate yields

$$\begin{aligned} q_{i,j-\frac{1}{2},k} + q_{i,j+\frac{1}{2},k} + q_{i-\frac{1}{2},j,k} + q_{i+\frac{1}{2},j,k} + q_{i,j,k-\frac{1}{2}} + q_{i,j,k+\frac{1}{2}} + P_{i,j,k} h_{i,j,k} \\ + Q_{i,j,k} = SS_{i,j,k} (\Delta \mathrm{r}_j \Delta \mathrm{c}_i \Delta v_k) \frac{\Delta \mathrm{h}_{i,j,k}}{\Delta \mathrm{t}} \end{aligned} \tag{3.21}$$

Where

$\frac{\Delta \mathrm{h}_{i,j,k}}{\Delta \mathrm{t}}$ is a finite-difference approximation for the derivative of head with respect to time ($\mathrm{L}T^{-1}$);

$SS_{i,j,k}$ represents the specific storage of cell i,j,k (L^{-1}); and

$\Delta \mathrm{r}_j \Delta \mathrm{c}_i \Delta v_k$ is the volume of cell i,j,k (L^3).

Equations (3.10) through (3.15) may be substituted into Equation (3.21) to give the finite-difference approximation for cell i,j,k as

$$CR_{i,j-\frac{1}{2},k}\left(h_{i,j-1,k}-h_{i,j,k}\right)+\ CR_{i,j+\frac{1}{2},k}\left(h_{i,j+1,k}-h_{i,j,k}\right)$$
$$+\ CC_{i-\frac{1}{2},j,k}\left(h_{i-1,j,k}-h_{i,j,k}\right)+CC_{i+\frac{1}{2},j,k}\left(h_{i+1,j,k}-h_{i,j,k}\right)$$
$$+CV_{i,j,k-\frac{1}{2}}\left(h_{i,j,k-1}-h_{i,j,k}\right)+CV_{i,j,k+\frac{1}{2}}\left(h_{i,j,k+1}-h_{i,j,k}\right) \quad (3.22)$$
$$+P_{i,j,k}h_{i,j,k}+Q_{i,j,k}=SS_{i,j,k}(\Delta r_j\Delta c_i\Delta v_k)\frac{\Delta h_{i,j,k}}{\Delta t}$$

The finite-difference approximation for the time derivative of head, $\frac{\Delta h_{i,j,k}}{\Delta t}$, must next be expressed in terms of specific heads and times. **Figure 3.2** shows a hydrograph of head values at node i,j,k. two values of time are shown on the horizontal axis: t^m, the time at which the flow terms of Equation (3.22) are evaluated; and t^{m-1}, a time that precedes t^m. The head values at node i,j,k associated with these times are designated by superscript as $h_{i,j,k}^m$ and $h_{i,j,k}^{m-1}$, respectively. An approximation to the time derivative of head at time t^m is obtained by dividing the head difference $h_{i,j,k}^m - h_{i,j,k}^{m-1}$ by the time interval $t^m - t^{m-1}$; that is,

$$\frac{\Delta h_{i,j,k}}{\Delta t} \cong \frac{h_{i,j,k}^m - h_{i,j,k}^{m-1}}{t^m - t^{m-1}} \quad (3.23)$$

Thus the hydrograph slope, or time derivative, is approximated using the change in head at the node over a time interval that precedes, and ends with, the time at which flow is evaluated. This is termed a backward-difference approach, in that $\frac{\Delta h}{\Delta t}$ is approximated over a time interval that extends backward in time from t^m, the time at which the flow terms are calculated.

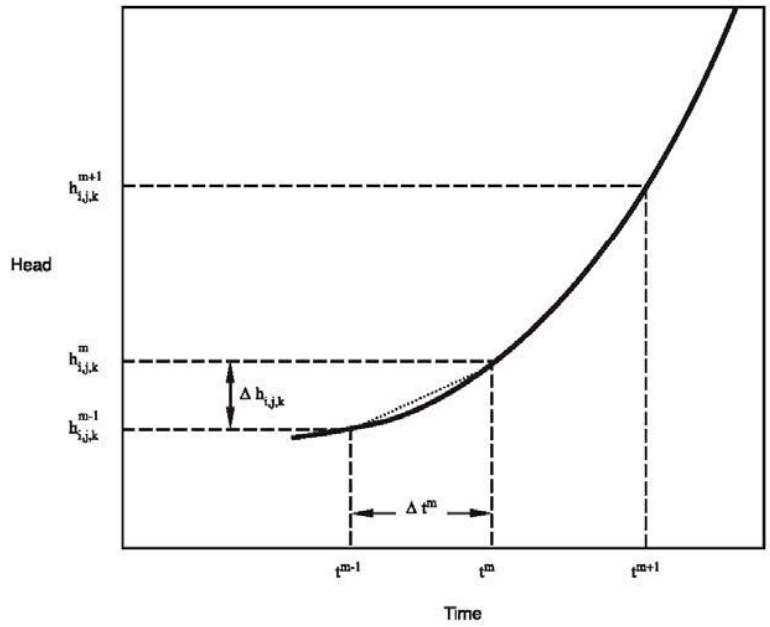

Figure 3.2 Hydrograph for cell i,j,k. Backward difference approximation to slope of hydrograph at time t^m, that is the time at the end of time step m. $h_{i,j,k}^m$ is head at node i,j,k at time t^m (McDonald & Harbaugh, 1988).

The time derivative of head could be approximated in other ways; for example, we could approximate the time derivative of head over a time interval that begins at the time of flow evaluation and extends to some later time; or over a time interval that is centered at the time of flow evaluation, extending both forward and backward from it. These alternatives, however, may cause numerical instability—that is, the growth or propagation of error during the calculation of heads at successive times in a simulation. In an unstable situation, errors that enter the calculation for any reason at a particular time will increase at each succeeding time as the calculation progresses, until finally the errors completely dominate the result. By contrast, the backward-difference approach is always numerically stable - that is, errors introduced at any time diminish progressively at succeeding times. For this reason, the backward-difference approach is preferred even

though this approach leads to large systems of equations that must be solved simultaneously for each time step.

Equation (3.22) can be rewritten in backward-difference form by specifying flow terms at t^m, the end of the time interval, and approximating the time derivative of head over the interval t^{m-1} to t^m, which is:

$$\begin{aligned} & CR_{i,j-\frac{1}{2},k}\left(h^m_{i,j-1,k} - h^m_{i,j,k}\right) + CR_{i,j+\frac{1}{2},k}\left(h^m_{i,j+1,k} - h^m_{i,j,k}\right) \\ & \quad + CC_{i-\frac{1}{2},j,k}\left(h^m_{i-1,j,k} - h^m_{i,j,k}\right) + CC_{i+\frac{1}{2},j,k}\left(h^m_{i+1,j,k} - h^m_{i,j,k}\right) \\ & \quad + CV_{i,j,k-\frac{1}{2}}\left(h^m_{i,j,k-1} - h^m_{i,j,k}\right) + CV_{i,j,k+\frac{1}{2}}\left(h^m_{i,j,k+1} - h^m_{i,j,k}\right) \\ & \quad + P_{i,j,k}h^m_{i,j,k} + Q_{i,j,k} = SS_{i,j,k}\left(\Delta r_j \Delta c_i \Delta v_k\right)\frac{h^m_{i,j,k} - h^{m-1}_{i,j,k}}{t^m - t^{m-1}} \end{aligned} \tag{3.24}$$

Equation (3.24) is a backward-difference equation that can be used as the basis for a simulation of the partial-differential equation of groundwater flow, Equation (3.1). Like the term $Q_{i,j,k}$, the coefficients of the various head terms in Equation (3.24) are all known, as is the head at the beginning of the time step, $h^{m-1}_{i,j,k}$. The seven heads at time t^m, the end of the time step, are unknown; that is, they are part of the head distribution to be predicted. Thus Equation (3.24) cannot be solved independently, because it represents a single equation in seven unknowns. An equation of this type, however, can be written for each active cell in the grid; and, because only one unknown head exists for each cell, we are left with a system of "n" equations in "n" unknowns. Such a system can be solved simultaneously.

The objective of transient simulation is generally to predict head distributions at successive times, given the initial head distribution, the boundary condition, the hydraulic parameters, and the external stresses. The initial head distribution provides a value of

$h^0_{i,j,k}$ at each point in the grid – that is, the initial head provides the values of head at the beginning of the first of the discrete time steps into which the time axis is divided in the finite-difference process. The first step in the solution process is to calculate values of $h^1_{i,j,k}$ – that is, heads at time t^1, which marks the end of the first time step. In Equation (3.24), therefore, the head superscript m is taken as 1, while the superscript m-1, which appears in only one head term, is taken as 0. Equation (3.24) then becomes

$$\begin{aligned} & CR_{i,j-\frac{1}{2},k}\left(h^1_{i,j-1,k} - h^1_{i,j,k}\right) + CR_{i,j+\frac{1}{2},k}\left(h^1_{i,j+1,k} - h^1_{i,j,k}\right) \\ & \quad + CC_{i-\frac{1}{2},j,k}\left(h^1_{i-1,j,k} - h^1_{i,j,k}\right) + CC_{i+\frac{1}{2},j,k}\left(h^1_{i+1,j,k} - h^1_{i,j,k}\right) \\ & \quad + CV_{i,j,k-\frac{1}{2}}\left(h^1_{i,j,k-1} - h^1_{i,j,k}\right) + CV_{i,j,k+\frac{1}{2}}\left(h^m_{i,j,k+1} - h^m_{i,j,k}\right) \\ & \quad + P_{i,j,k}h^m_{i,j,k} + Q_{i,j,k} = SS_{i,j,k}\left(\Delta r_j \Delta c_i \Delta v_k\right)\frac{h^1_{i,j,k} - h^0_{i,j,k}}{t^1 - t^0} \end{aligned} \tag{3.25}$$

Where again, the superscripts 0 and 1 refer to the time at which the heads are taken and should not be interpreted as exponents.

An equation of this form is written for every cell in the grid in which head is free to vary with time (variable-head cells), and the system of equations is solved simultaneously for the heads at time t^1. When these have been obtained, the process is repeated to obtain heads at time t^2, the end of the second time step. To do this, Equation (3.24) is reapplied, now using 1 as time superscript m-1 and 2 as time superscript m. again, a system of equations is formulated, where the unknowns are now the heads at time t^2; and this set of equations is solved simultaneously to obtain the head distribution at time t^2. This process is continued for as many time steps as necessary to cover the time range of interest.

The set of finite-difference equations is reformulated at each time step; that is, at each time step there is a new system of simultaneous equations to be solved. The heads at the end of the time step make up the unknowns for which this system must be solved; the heads at the beginning of the step are among the known terms in the equations. The solution process is repeated at each time step yielding a new array of heads for the end of the step.

The finite-difference flow equation for a cell is a representation of the volumetric flow from all sources in units of L^3/T, where L is a length unit and T is a time unit.

3.3.4 Iteration

MODFLOW utilizes iterative methods to obtain the solution to the system of finite-difference equations for each time step. In these methods, the calculation of head values for the end of a given time step is started by arbitrarily assigning a trial value, or estimate, for the head at each node at the end of that step. A procedure of calculation is then initiated that alters these estimated values, producing a new set of head values that are in closer agreement with the system of equations. These new, or interim, head values then take the place of the initially assumed heads, and the procedure of calculation is repeated, producing a third set of head values. This procedure is repeated successively at each stage, producing a new set of interim heads that more nearly satisfies the system of equations. Each repetition of the calculation is termed an ”iteration." Ultimately, as the interim heads approach values that would exactly satisfy the set of equations, the changes produced by succeeding stages of calculation become very small. This behavior is utilized in determining when to stop iteration.

Thus, during the calculations for a time step, arrays of interim head values are generated in succession, each array containing one interim head value for each active node in the grid. In **Figure 3.3**, these arrays are represented as three-dimensional lattices, each identified by an array symbol, h, bearing two superscripts. The first superscript indicates the time step for which the heads in the array are calculated, whereas the second indicates the number, or level, of the iteration that produced the head array. Thus $h^{m,1}$ represents the array of values computed in the first iteration for time step m; $h^{m,2}$ would represent the array of values computed in the second iteration, and so on. The head values that were initially assumed for time step m, to begin the process of iteration, appear in the array designated $h^{m,0}$. In the example of **Figure 3.3**, a total of n iterations is required to achieve closure for the heads at the end of time step m; thus the array of final head values for the time step is designated $h^{m,n}$. **Figure 3.3** also shows the array of final head values for the end of the preceding time step $h^{m-1,n}$ (where again it is assumed that n iterations were required for closure). The head values in this array appear in the storage term of Equation (3.24) that is, they are used in the term $h_{i,j,k}^{m-1}-$ on the right side of equation (3.24) - in the calculation of heads for time step m. Because they represent heads for the preceding time step, for which computations have already been completed, they appear as predetermined constants in the equation for time step m; thus they retain the same value in each iteration of the time step. Similarly, the final values of head for time step m are used as constants in the storage term during calculations for time step m+1.

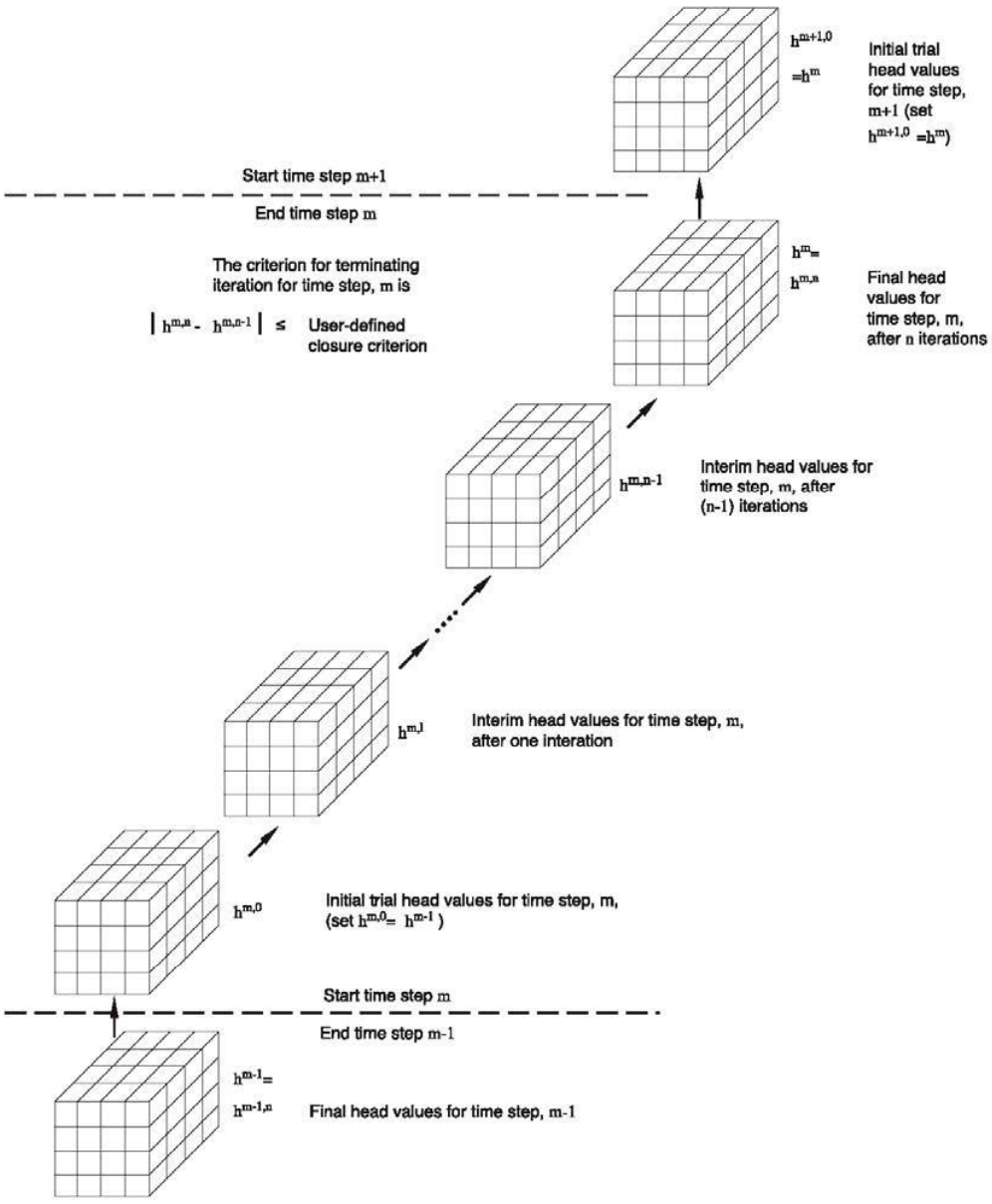

Figure 3.3 Iterative calculation of head distribution. (McDonald & Harbaugh, 1988).

Ideally, one would like to specify that iteration stop when the calculated heads are suitably close to the exact solution. Because the actual solution is unknown, however, an indirect method of specifying when to stop iterating must be used. The method most commonly employed is to specify that the changes in computed heads occurring from one iteration level to the next must be less than a certain quantity, termed the "closure

criterion" or "convergence criterion," which is specified by the user. After each iteration, absolute values of computed head change in that iteration are examined for all nodes in the grid. The largest of these absolute head-change values is compared with the closure criterion. If this largest value exceeds the closure criterion, iteration continues; if this value is less than the closure criterion, iteration is said to have "closed" or "converged," and the process is terminated for that time step. Normally, this method of determining when to stop iteration is adequate. Note that the closure criterion refers to change in computed head, and that values of head are not themselves necessarily calculated to a level of accuracy comparable to the closure criterion. As a rule of thumb, it is wise to use a value of closure criterion that is an order of magnitude smaller than the level of accuracy desired in the head results.

MODFLOW also incorporates a maximum permissible number of iterations per time step. If closure is not achieved within this maximum number of iterations, then the iterative process is terminated and a corresponding message is printed in the output.

The initial estimates of head for time step m, in array $h^{m,0}$ of **Figure 3.3**, could be assigned arbitrarily, or they could be chosen according to a number of different conventions. Theoretically, the iterative process would eventually converge to the same result regardless of the choice of initial head values, although the work required would be much greater for some choices than for others. In MODFLOW, the heads computed for the end of each time step are used as the initial trial values of head for the succeeding time step. Thus in **Figure 3.3**, the array $h^{m-1,n}$ contains the final estimates of head, obtained after n iterations, for the end of time step m-1. When the calculations for step m-1 are complete, these same values of head are transferred to the array $h^{m,0}$, and used as

the initial estimates, or trial values, for the heads of time step m. Head values for the first time step in the simulation are assumed initially to be equal to the heads specified by the user for the beginning of the simulation.

Discussions of the mathematical basis of various iterative methods can be found in many standard references, including Peaceman (1977), Crichlow (1977) and Remson, Hornberger and Molz (1971).

An iterative procedure yields only an approximation to the solution of the system of finite-difference equations for each time step; the accuracy of this approximation depends upon several factors, including the closure criterion that is employed. Even if exact solutions to the set of finite-difference equations were obtained at each step, these solutions would themselves be only an approximation to the solution of the differential equation of flow (Equation (3.1)). The discrepancy between the head, $h_{i,j,k}^{m}$, given by the solution to the system of difference equations for a given node and time and the head h(x,y,z,t), which would be given by the formal solution of the differential equation for the corresponding point and time, is termed the truncation error. In general, this error tends to become greater as the grid spacing and time-step length are increased.

3.3.5 Formulation of Equations for Solution

MODFLOW incorporates several different options for iterative solution of the set of finite-difference equations, and is organized so that alternative schemes of solution may be added without disruption of the program structure. Whatever scheme of solution is employed, it is convenient to rearrange Equation (3.24) so that all terms containing heads at the end of the current time step are grouped on the left-hand side of the equation, and all terms that are independent of head at the end of the current time step are on the right-

hand side. All coefficients of $h_{i,j,k}^{m}$ that do not include conductance between nodes are combined into a single term, HCOF, and all right-hand-side terms are combined into the term RHS. Further, the complexity can be reduced by assuming that the time superscript is m unless otherwise shown. The resulting equation is

$$CV_{i,j,k-\frac{1}{2}}h_{i,j,k-1} + CC_{i-\frac{1}{2},j,k}h_{i-1,j,k} + CR_{i,j-\frac{1}{2},k}h_{i,j-1,k} + \left(-CV_{i,j,k-\frac{1}{2}} - CC_{i-\frac{1}{2},j,k} - CR_{i,j-\frac{1}{2},k} - CR_{i,j+\frac{1}{2},k} - CC_{i+\frac{1}{2},j,k} - CV_{i,j,k+\frac{1}{2}} + HCOF_{i,j,k}\right)h_{i,j,k} + CR_{i,j+\frac{1}{2},k}h_{i,j+1,k} + CC_{i+\frac{1}{2},j,k}h_{i+1,j,k} + CV_{i,j,k+\frac{1}{2}}h_{i,j,k+1} = RHS_{i,j,k} \quad (3.26)$$

Where

$$HCOF_{i,j,k} = P_{i,j,k} - \frac{SS_{i,j,k}\Delta r_j \Delta c_i \Delta v_k}{t - t^{m-1}} \quad L^2T^{-1} \text{ and;} \quad (3.27)$$

$$RHS_{i,j,k} = -Q_{i,j,k} - SS_{i,j,k}\Delta r_j \Delta c_i \Delta v_k \frac{h_{i,j,k}^{m-1}}{t - t^{m-1}} \quad L^3T^{-1} \quad (3.28)$$

The entire system of equations of the form of Equation (3.26), which includes one equation for each variable head cell in the grid, may be written in matrix form as

$$[A]\{h\} = \{q\} \quad (3.29)$$

Where

[A} is a matrix of the coefficients of head, from the left side of Equation (3.26), for all active nodes in the grid;

{h} is a vector of head values at the end of time step m for all nodes in the grid; and

{q} is a vector of the constant terms, RHS, for all nodes of the grid.

MODFLOW assembles the vector {q} and the terms that comprise [A] through a series of subroutines. The vector {q} and the terms comprising [A] are then transferred to subroutines that actually solve the matrix equations for the vector {h}.

3.4 Examples of Large Scale Groundwater Modeling

In a study by Zhou and Li (2011), a review of modeling the regional groundwater flow is presented. The Death Valley region of southeastern California is chosen as an example of a large scale groundwater modeling. Groundwater flow in this area includes interconnected, complex groundwater flow systems. Schematic diagram of Death Valley is shown in **Figure 3.4**.

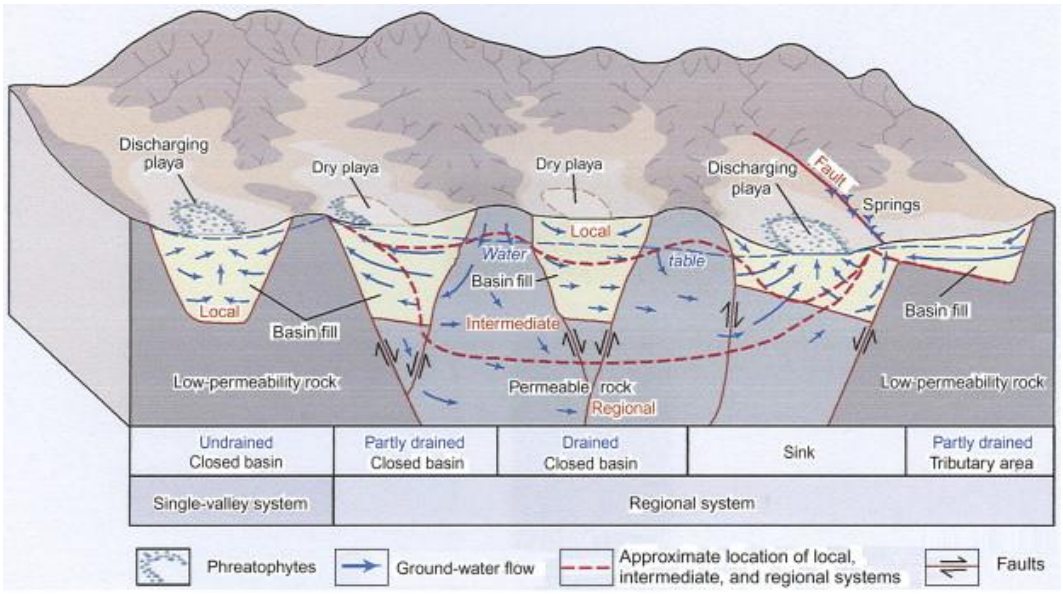

Figure 3.4 Schematic diagram of Death Valley (Faunt, D'Agnese, & O'Brien, 2004).

MODFLOW-2000 is utilized in order to construct the groundwater flow model. In this finite difference model, there are 194 rows, 160 columns and 16 layers. Grid cells are uniformly sized 1.5 km and in order to cover the whole 69,840 km² area, model consists

of 496,640 cells. Final calibrated model is evaluated by comparing measured and computed groundwater heads and discharges. In areas of flat hydraulic gradients, a good fit to observed groundwater heads occurred while in areas with steep hydraulic gradient, poor fit to the observed groundwater heads was noticed (Zhou & Li, 2011).

The Great Artesian Basin (GAB) is a confined groundwater basin that occupies 1.7 million km^2 — this area is equal to one-fifth of the Australian continent — and includes most arid and semi-arid regions of Queensland, New South Wales, South Australia and the Northern Territory. Great Artesian Basin in shown in **Figure 3.5**.

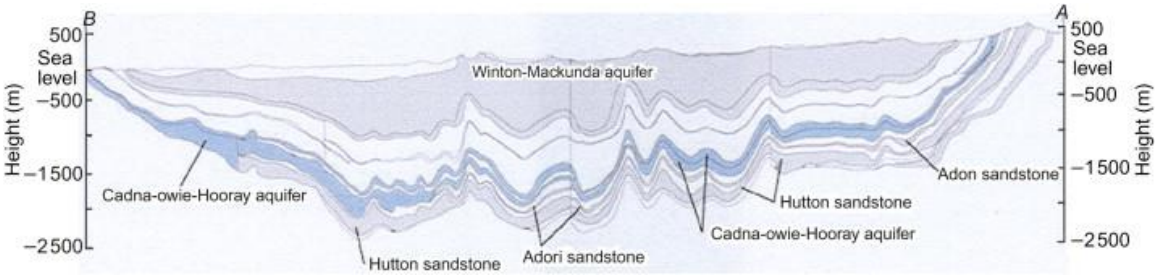

Figure 3.5 Great Artesian Basin (Radke, Ferguson, Cresswell, Ransley, & Habermehl, 2000).

To construct the groundwater flow model of the Great Artesian basin, MODFLOW-88 was used. This basin was discretized uniformly with grid size of 5 km × 5 km, and the model grid has 359 rows and 369 columns and the whole model area of 1.54 million km^2 consists of more than 60,000 cells. The grid is aligned North-South and East-West. Coastal line of the Gulf of Carpentaria is the northern boundary of the model and is simulated as a constant head boundary. Other boundaries are simulated as no flow boundaries and the modeling was carried out for steady state hydrogeological conditions. A trial-and-error method is used to calibrate the model in order to reduce the difference between the modeled and measured groundwater head surface. Hydraulic conductivities

of the modeled aquifer and recharge form precipitation were adjusted during model calibration. The accuracy of the model calibration was calculated using the Root Mean Square (RMS) error. The simulation indicated that the control of free-flowing wells with a high discharge is an effective method to save valuable groundwater from being wasted and to recover Artesian pressure (Zhou & Li, 2011).

CHAPTER 4

MODELING

In this chapter, a computer simulation of groundwater contribution to a riverine wetland, located in Monmouth Battlefield State Park (the Study Area), will be developed through comprehensive three-dimensional modeling using ModelMuse, a graphical user interface for USGS MODFLOW-2005.

Steps taken towards developing the model will be discussed. These steps include defining the Model Domain in the ModelMuse, assigning the site specific topographic elevations, defining model grid system and assigning site specific parameters (precipitation, hydraulic conductivity, etc.).

Modeling and analysis assumptions related to soil characteristics, rain data, stream levels, elevations, vegetation cover, etc. will be introduced and discussed step by step.

Collected field data will be used to validate the modeling efforts and finally the results of the modeling will be presented.

4.1 Methodology

4.1.1 Model Domain

The first step in developing a model to predict the water budget in the Monmouth Battlefield State Park is to define the Study Area in ModelMuse. The term which is used by ModelMuse for the developed area is the Model Domain. Please note that the Model Domain and the Study Area represent the same area and are interchangeable. Study Area is the more generic name which in this study is used mostly during the Field Investigation

efforts while the Model Domain is the more technical term borrowed from ModelMuse which describes the area subject to modeling efforts.

In order to define the Model Domain, the Study Area will be created first in the AutoCAD and then the results will be transferred from AutoCAD into the ModelMuse. Creating the Study Area in AutoCAD will provide a more accurate presentation of the area and consequently a more efficient simulation experience in the ModelMuse.

4.1.2 Topography

After defining the Study Area in the ModelMuse as the Model Domain, the next step would be assigning the topographical information to the Model Domain.

In order to define the topography of the Model Domain, topographic map of the area encompassing the Monmouth Battlefield State Park (U.S. Geological Survey, 2013) will be used in conjunction with the results of the land survey that was conducted during the field investigations (see Section 2.4.2). The results will be topographic contour lines along the Model Domain. Interpolation methods will be used to define the elevations in the areas in-between the topographic contour lines. These methods are:

1. Nearest - The Nearest interpolation method works by determining the object that is closest to the location where the data set in question is being evaluated. Then the formula of that object is evaluated at that location.

2. Nearest Point - The Nearest Point interpolation method is similar to the Nearest interpolation method except that only the vertices of objects are considered, rather than the lines connecting the vertices.

3. Inverse Distance Squared - With the Inverse Distance Squared interpolation method, the formula for each object is evaluated at the location under consideration. The final value is a weighted average of these values. The weights are the inverse of the distance squared from the location to the closest point on each respective object.

4. Triangle Interpolation - The Triangle Interpolation method evaluates the formula for each object at the location of each vertex on the object. It then

creates an unconstrained Delaunay triangulation of all the vertices. If a location where a value is needed is inside one of the triangles, the value assigned to that location will be calculated by fitting a plane to the three points of the triangle and determining the height of the plane at the location of interest. Other locations will be assigned the value that would have been assigned to the closest location on the convex hull of the data points.

5. Fitted Surface - The Fitted Surface interpolation method evaluates the formula for each object at the location of each vertex on the object. It then creates an unconstrained Delaunay triangulation of all the vertices (the same one as in Triangle Interp.). A piece-wise continuous function of the locations is fitted through the data values and the function is used to assign values at each location of interest.

6. Point Inverse Distance Squared - With the Point Inverse Distance Squared interpolation method, and the formula for each vertex for each object is evaluated at its own location. The final value is a weighted average of these values. The weights are the inverse of the distance squared from the location of interest to the vertex.

7. Natural Neighbor - The Natural Neighbor interpolation method uses a weighted average of some points near the location of interest. Only the vertices of objects are considered, rather than the lines connecting the vertices.

The results of the above-mentioned interpolation methods will be compared to the land survey results from the Field Investigations (refer to Section 2.4.2 Land Survey which can be found on page 37) and the best fit will be chosen to be used in the simulation efforts.

4.1.3 Model Grids

Having assigned the elevations along the Model Domain, the next step will be defining the grid system for spatial discretization.

MODFLOW uses finite-difference techniques for spatial and temporal discretization. Therefore, a grid system is required for spatial discretization.

In ModelMuse, the grid can be rotated at an angle to the global coordinate system. The coordinate system for the grid is aligned with the grid lines, but has the same origin as the global coordinate system. The coordinates of a point in the global coordinate

system are referred to as X, Y, and Z; the coordinates of a point in the grid coordinate system are referred to as X′, Y′, and Z. There is no Z′ because the grid is never rotated away from the horizontal plane. Coordinate values at the cursor location in both the global and grid coordinate system are displayed on the status bar of the main window of ModelMuse (Parkhurst, Kipp, Engesgaard, & Charlton (2004) Harbaugh (2005)).

ModelMuse can be used to create the grid; rotate it; and add, move, or remove grid lines. A variety of grid functions can be used in formulas.

The grid in MODFLOW uses block-centered nodes; the locations at which calculations are made are at the centers of blocks. In ModelMuse, groups of layers can be defined in the MODFLOW Layer Groups dialog box. Each group of layers shares a variety of common properties. If the model is to be a quasi-3-D model, some layer groups can be designated as non-simulated in the MODFLOW Layer Groups dialog box. Data sets are used to define the bottom of each layer group. An additional data set is used to define the top of the model.

4.1.4 Recharge

In the current study, water enters the system in the form of the precipitation which can be modeled in the ModelMuse using the Recharge Package. The Recharge package of the ModelMuse allows the user to specify a recharge rate over an area. The total flux entering each cell will be the rate times the horizontal area of the cell. Positive recharge rate can be used to account for precipitation. Negative recharge rates are allowed. A negative recharge rate might be used to simulate a constant evapotranspiration rate.

The user can specify where the recharge will be applied. Possible choices include:

1. the top layer,

2. A specified layer. If specified layer is selected, the user can choose whether to use the layer of the object used to assign the rates for all the stress periods or to have the layer be specified separately for each stress period.

3. The top active cells. If top active cell is specified, the location of recharge can move up or down as cells at the surface convert between dry and wet.

In the present study, the recharge will be applied to the model in form of the precipitations. There are three types of National Weather Service (NWS) precipitation monitoring stations:

1. Automated Surface Observing Systems (ASOS) - This program is a joint effort of the NWS, the Federal Aviation Administration (FAA), and the Department of Defense (DOD). The ASOS system serves as the nation's primary surface weather observing network. ASOS is designed to support weather forecast activities and aviation operations and, at the same time, support the needs of the meteorological, hydrological, and climatological research communities. These are located at airports (mostly) and there are only 12 in the state of New Jersey. All of them over twenty miles away from the Study Area;

2. Cooperative Observer Program (COOP) - COOP is the Nation's weather and climate observing network of, by and for the people. More than 11,000 volunteers take observations on farms, in urban and suburban areas, National Parks, seashores, and mountaintops. The data are representative of where people live, work and play. Observers generally record temperature and precipitation daily and electronically send those reports daily to the NWS and the National Climatic Data Center (NCDC). Many cooperative observers provide additional hydrological or meteorological data, such as evaporation or soil temperatures. Data is transmitted via telephone, computer or, in special cases, by mail. Equipment used at NWS cooperative stations may be owned by the NWS, the observer, or by a company or other government agency, as long as it meets NWS equipment standards. There are 55 in the state of New Jersey with closest one over eight miles away from the Study Area;

3. Community Collaborative Rain, Hail & Snow network (CoCoRaHS) - It is a non-profit, community-based network of volunteers of all ages and backgrounds working together to measure and map precipitation (rain, hail and snow) by using low-cost measurement tools. There are 350 of these private-citizen monitoring stations in the state of New Jersey.

Two stations, which are fairly close and within the range of 1 to 2 miles from the Study Area, are CoCoRaHS stations, US1NJMN0016 and 55. Available daily rain data (May 2012 through August 2013) from these two rain stations have been pulled from National Climatic Data Center (NCDC) of National Oceanic and Atmospheric Administration (NOAA)'s website (NOAA, 2013). Cumulative monthly precipitation for the modeling period in the Study Area, based on data from US1NJMN0016 and 55 stations is shown in **Figure 4.1**. Daily precipitation data for CoCoRaHS US1NJMN0016 and 55 stations for the time frame of May 2012 through August 2013 are presented in **Table 4.1**.

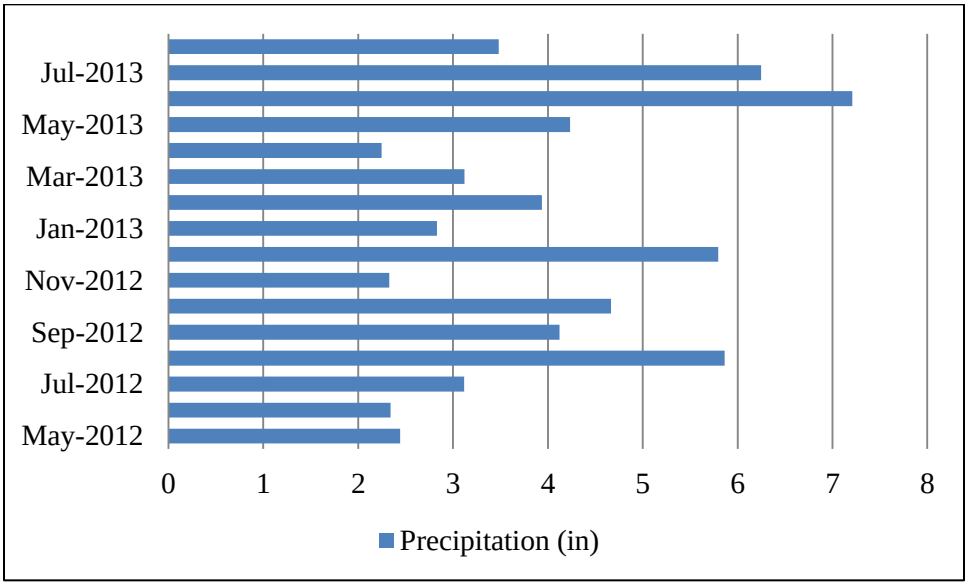

Figure 4.1 Cumulative monthly precipitation in the Study Area, based on data from CoCoRaHS US1NJMN0016 and 55 stations (May 2012 through August 2013).

Table 4.1 Daily Precipitation for CoCoRaHS US1NJMN0016 and 55 Stations, May 2012 through August 2013 (NOAA, 2013)

Date	Precipitation (in)	Date	Precipitation (in)	Date	Precipitation (in)	Date	Precipitation (in)
US1NJMN0016 Station							
5/1/2012	0.0	6/1/2012	0.0	7/1/2012	0.0	8/1/2012	N/A
5/2/2012	N/A*	6/2/2012	0.5	7/2/2012	0.0	8/2/2012	0.3
5/3/2012	N/A	6/3/2012	N/A	7/3/2012	N/A	8/3/2012	0.0
5/4/2012	0.0	6/4/2012	0.2	7/4/2012	0.0	8/4/2012	N/A
5/5/2012	0.0	6/5/2012	0.7	7/5/2012	0.2	8/5/2012	0.0
5/6/2012	N/A	6/6/2012	N/A	7/6/2012	N/A	8/6/2012	1.4
5/7/2012	0.0	6/7/2012	0.0	7/7/2012	0.0	8/7/2012	N/A
5/8/2012	N/A	6/8/2012	0.0	7/8/2012	0.3	8/8/2012	N/A
5/9/2012	N/A	6/9/2012	N/A	7/9/2012	N/A	8/9/2012	N/A
5/10/2012	0.4	6/10/2012	0.0	7/10/2012	0.0	8/10/2012	0.0
5/11/2012	N/A	6/11/2012	N/A	7/11/2012	0.0	8/11/2012	0.5
5/12/2012	N/A	6/12/2012	N/A	7/12/2012	N/A	8/12/2012	N/A
5/13/2012	N/A	6/13/2012	N/A	7/13/2012	0.0	8/13/2012	0.0
5/14/2012	0.0	6/14/2012	N/A	7/14/2012	0.1	8/14/2012	N/A
5/15/2012	N/A	6/15/2012	N/A	7/15/2012	N/A	8/15/2012	0.8
5/16/2012	N/A	6/16/2012	N/A	7/16/2012	N/A	8/16/2012	1.1
5/17/2012	N/A	6/17/2012	N/A	7/17/2012	N/A	8/17/2012	0.0
5/18/2012	N/A	6/18/2012	N/A	7/18/2012	0.0	8/18/2012	0.3
5/19/2012	N/A	6/19/2012	N/A	7/19/2012	0.1	8/19/2012	0.0
5/20/2012	0.0	6/20/2012	N/A	7/20/2012	0.1	8/20/2012	N/A
5/21/2012	0.4	6/21/2012	N/A	7/21/2012	N/A	8/21/2012	0.0
5/22/2012	N/A	6/22/2012	0.0	7/22/2012	N/A	8/22/2012	0.0
5/23/2012	0.8	6/23/2012	N/A	7/23/2012	N/A	8/23/2012	0.0
5/24/2012	0.0	6/24/2012	0.0	7/24/2012	N/A	8/24/2012	0.0
5/25/2012	0.0	6/25/2012	0.0	7/25/2012	N/A	8/25/2012	N/A
5/26/2012	0.0	6/26/2012	0.8	7/26/2012	0.0	8/26/2012	N/A
5/27/2012	0.0	6/27/2012	N/A	7/27/2012	0.6	8/27/2012	0.0
5/28/2012	0.4	6/28/2012	N/A	7/28/2012	N/A	8/28/2012	1.4
5/29/2012	0.0	6/29/2012	N/A	7/29/2012	1.7	8/29/2012	N/A
5/30/2012	0.2	6/30/2012	0.1	7/30/2012	N/A	8/30/2012	N/A
5/31/2012	N/A	-	-	7/31/2012	0.0	8/31/2012	0.0

*N/A: No data was recorded on these days.

Table 4.1 (Continued) Daily Precipitation for CoCoRaHS US1NJMN0016 and 55 Stations, May 2012 through August 2013 (NOAA, 2013)

Date	Precipitation (in)	Date	Precipitation (in)	Date	Precipitation (in)	Date	Precipitation (in)
	US1NJMN0016 Station				**US1NJMN0055 Station**		
9/1/2012	N/A*	10/1/2012	N/A	11/1/2012	N/A	12/1/2012	N/A
9/2/2012	N/A	10/2/2012	0.0	11/2/2012	N/A	12/2/2012	N/A
9/3/2012	0.1	10/3/2012	0.2	11/3/2012	N/A	12/3/2012	0.1
9/4/2012	0.4	10/4/2012	0.0	11/4/2012	N/A	12/4/2012	N/A
9/5/2012	1.1	10/5/2012	N/A	11/5/2012	N/A	12/5/2012	N/A
9/6/2012	0.8	10/6/2012	N/A	11/6/2012	N/A	12/6/2012	N/A
9/7/2012	N/A	10/7/2012	0.0	11/7/2012	N/A	12/7/2012	N/A
9/8/2012	0.0	10/8/2012	0.1	11/8/2012	1.5	12/8/2012	0.7
9/9/2012	0.4	10/9/2012	0.0	11/9/2012	N/A	12/9/2012	N/A
9/10/2012	N/A	10/10/2012	0.6	11/10/2012	N/A	12/10/2012	0.5
9/11/2012	N/A	10/11/2012	0.1	11/11/2012	N/A	12/11/2012	0.2
9/12/2012	0.0	10/12/2012	N/A	11/12/2012	N/A	12/12/2012	N/A
9/13/2012	0.0	10/13/2012	N/A	11/13/2012	0.0	12/13/2012	N/A
9/14/2012	0.0	10/14/2012	N/A	11/14/2012	0.1	12/14/2012	N/A
9/15/2012	N/A	10/15/2012	N/A	11/15/2012	N/A	12/15/2012	N/A
9/16/2012	N/A	10/16/2012	0.3	11/16/2012	N/A	12/16/2012	N/A
9/17/2012	N/A	10/17/2012	N/A	11/17/2012	N/A	12/17/2012	0.3
9/18/2012	N/A	10/18/2012	N/A	11/18/2012	N/A	12/18/2012	0.4
9/19/2012	1.2	10/19/2012	0.1	11/19/2012	N/A	12/19/2012	N/A
9/20/2012	N/A	10/20/2012	0.4	11/20/2012	N/A	12/20/2012	N/A
9/21/2012	N/A	10/21/2012	N/A	11/21/2012	N/A	12/21/2012	N/A
9/22/2012	N/A	10/22/2012	N/A	11/22/2012	N/A	12/22/2012	N/A
9/23/2012	N/A	10/23/2012	N/A	11/23/2012	N/A	12/23/2012	N/A
9/24/2012	0.0	10/24/2012	0.0	11/24/2012	0.1	12/24/2012	N/A
9/25/2012	N/A	10/25/2012	N/A	11/25/2012	N/A	12/25/2012	0.2
9/26/2012	0.0	10/26/2012	N/A	11/26/2012	N/A	12/26/2012	N/A
9/27/2012	0.0	10/27/2012	N/A	11/27/2012	N/A	12/27/2012	3.3
9/28/2012	0.1	10/28/2012	N/A	11/28/2012	0.6	12/28/2012	N/A
9/29/2012	N/A	10/29/2012	0.0	11/29/2012	N/A	12/29/2012	N/A
9/30/2012	N/A	10/30/2012	2.6	11/30/2012	N/A	12/30/2012	0.3
-	-	10/31/2012	0.1	-	-	12/31/2012	N/A

*N/A: No data was recorded on these days.

Table 4.1 (Continued) Daily Precipitation for CoCoRaHS US1NJMN0016 and 55 Stations, May 2012 through August 2013 (NOAA, 2013)

Date	Precipitation (in)	Date	Precipitation (in)	Date	Precipitation (in)	Date	Precipitation (in)
US1NJMN0055 Station							
1/1/2013	N/A*	2/1/2013	N/A	3/1/2013	N/A	4/1/2013	0.2
1/2/2013	N/A	2/2/2013	N/A	3/2/2013	N/A	4/2/2013	N/A
1/3/2013	N/A	2/3/2013	0.1	3/3/2013	N/A	4/3/2013	N/A
1/4/2013	N/A	2/4/2013	0.0	3/4/2013	N/A	4/4/2013	N/A
1/5/2013	N/A	2/5/2013	0.0	3/5/2013	N/A	4/5/2013	0.1
1/6/2013	0.1	2/6/2013	0.1	3/6/2013	N/A	4/6/2013	N/A
1/7/2013	N/A	2/7/2013	N/A	3/7/2013	0.3	4/7/2013	N/A
1/8/2013	N/A	2/8/2013	N/A	3/8/2013	0.4	4/8/2013	N/A
1/9/2013	N/A	2/9/2013	1.6	3/9/2013	0.1	4/9/2013	0.0
1/10/2013	N/A	2/10/2013	N/A	3/10/2013	N/A	4/10/2013	0.0
1/11/2013	N/A	2/11/2013	N/A	3/11/2013	N/A	4/11/2013	0.5
1/12/2013	0.7	2/12/2013	0.3	3/12/2013	N/A	4/12/2013	0.1
1/13/2013		2/13/2013	N/A	3/13/2013	0.6	4/13/2013	1.1
1/14/2013	0.0	2/14/2013	0.2	3/14/2013	N/A	4/14/2013	N/A
1/15/2013	0.3	2/15/2013	N/A	3/15/2013	N/A	4/15/2013	N/A
1/16/2013	0.9	2/16/2013	N/A	3/16/2013	N/A	4/16/2013	N/A
1/17/2013	N/A	2/17/2013	N/A	3/17/2013	0.2	4/17/2013	N/A
1/18/2013	N/A	2/18/2013	N/A	3/18/2013		4/18/2013	N/A
1/19/2013	N/A	2/19/2013	N/A	3/19/2013	0.7	4/19/2013	N/A
1/20/2013	N/A	2/20/2013	0.3	3/20/2013	0.1	4/20/2013	0.2
1/21/2013	N/A	2/21/2013	N/A	3/21/2013	N/A	4/21/2013	N/A
1/22/2013	0.1	2/22/2013	N/A	3/22/2013	N/A	4/22/2013	N/A
1/23/2013	N/A	2/23/2013	0.1	3/23/2013	N/A	4/23/2013	N/A
1/24/2013	N/A	2/24/2013	0.3	3/24/2013	N/A	4/24/2013	N/A
1/25/2013	N/A	2/25/2013	N/A	3/25/2013	N/A	4/25/2013	N/A
1/26/2013	0.1	2/26/2013	N/A	3/26/2013	0.6	4/26/2013	N/A
1/27/2013	N/A	2/27/2013	1.1	3/27/2013	N/A	4/27/2013	N/A
1/28/2013	N/A	2/28/2013	N/A	3/28/2013	N/A	4/28/2013	N/A
1/29/2013	0.1	-	-	3/29/2013	N/A	4/29/2013	N/A
1/30/2013	N/A	-	-	3/30/2013	N/A	4/30/2013	0.1
1/31/2013	0.6	-	-	3/31/2013	N/A	-	-

*N/A: No data was recorded on these days.

Table 4.1 (Continued) Daily Precipitation for CoCoRaHS US1NJMN0016 and 55 Stations, May 2012 through August 2013 (NOAA, 2013)

Date	Precipitation (in)	Date	Precipitation (in)	Date	Precipitation (in)	Date	Precipitation (in)
			US1NJMN0055 Station				
5/1/2013	N/A*	6/1/2013	N/A	7/1/2013	0.1	8/1/2013	N/A
5/2/2013	N/A	6/2/2013	N/A	7/2/2013	0.4	8/2/2013	0.9
5/3/2013	N/A	6/3/2013	N/A	7/3/2013	1.1	8/3/2013	N/A
5/4/2013	N/A	6/4/2013	0.7	7/4/2013	0.2	8/4/2013	0.1
5/5/2013	N/A	6/5/2013	N/A	7/5/2013	N/A	8/5/2013	N/A
5/6/2013	N/A	6/6/2013	N/A	7/6/2013	N/A	8/6/2013	N/A
5/7/2013	N/A	6/7/2013	N/A	7/7/2013	N/A	8/7/2013	N/A
5/8/2013	0.4	6/8/2013	3.0	7/8/2013	N/A	8/8/2013	0.6
5/9/2013	1.0	6/9/2013	N/A	7/9/2013	N/A	8/9/2013	0.0
5/10/2013	0.3	6/10/2013	N/A	7/10/2013	N/A	8/10/2013	0.1
5/11/2013	0.2	6/11/2013	1.1	7/11/2013	N/A	8/11/2013	N/A
5/12/2013	1.1	6/12/2013	N/A	7/12/2013	N/A	8/12/2013	N/A
5/13/2013	N/A	6/13/2013	N/A	7/13/2013	1.0	8/13/2013	N/A
5/14/2013	N/A	6/14/2013	1.3	7/14/2013	1.0	8/14/2013	1.3
5/15/2013	N/A	6/15/2013	N/A	7/15/2013	0.0	8/15/2013	N/A
5/16/2013	N/A	6/16/2013	N/A	7/16/2013	N/A	8/16/2013	N/A
5/17/2013	N/A	6/17/2013	N/A	7/17/2013	N/A	8/17/2013	N/A
5/18/2013	N/A	6/18/2013	0.3	7/18/2013	N/A	8/18/2013	N/A
5/19/2013	0.2	6/19/2013	N/A	7/19/2013	N/A	8/19/2013	0.0
5/20/2013	0.1	6/20/2013	N/A	7/20/2013	N/A	8/20/2013	N/A
5/21/2013	N/A	6/21/2013	N/A	7/21/2013	N/A	8/21/2013	N/A
5/22/2013	N/A	6/22/2013	N/A	7/22/2013	N/A	8/22/2013	N/A
5/23/2013	0.2	6/23/2013	N/A	7/23/2013	2.0	8/23/2013	0.3
5/24/2013	0.2	6/24/2013	0.4	7/24/2013	0.0	8/24/2013	N/A
5/25/2013	0.6	6/25/2013	N/A	7/25/2013	N/A	8/25/2013	N/A
5/26/2013	0.0	6/26/2013	N/A	7/26/2013	N/A	8/26/2013	N/A
5/27/2013	N/A	6/27/2013	0.2	7/27/2013	N/A	8/27/2013	0.1
5/28/2013	N/A	6/28/2013	0.1	7/28/2013	N/A	8/28/2013	N/A
5/29/2013	N/A	6/29/2013	0.0	7/29/2013	0.3	8/29/2013	N/A
5/30/2013	N/A	6/30/2013	N/A	7/30/2013	N/A	8/30/2013	N/A
5/31/2013	N/A	-	-	7/31/2013	N/A	8/31/2013	N/A

*N/A: No data was recorded on these days.

The NWS Multi-sensor Precipitation Estimate (MPE) program uses information from the three sources to provide reasonably accurate hourly precipitation amount estimated within four by four square miles areas or grids (the Hydrologic Rainfall Analysis Project [HRAP] spatial scale):

1. Bias-corrected Geostationary Operational Environmental Satellite (GOES) HydroEstimator rainfall estimates (an algorithm product); GOES satellites provide the kind of continuous monitoring necessary for intensive data analysis. They circle the Earth in a geosynchronous orbit, which means they orbit the equatorial plane of the Earth at a speed matching the Earth's rotation. This allows them to hover continuously over one position on the surface. Because GOES satellites stay above a fixed spot on the surface, they provide a constant vigil for the atmospheric "triggers" for severe weather conditions such as tornadoes, flash floods, hail storms, and hurricanes. When these conditions develop the GOES satellites are able to monitor storm development and track their movements. GOES satellite imagery is also used to estimate rainfall during the thunderstorms and hurricanes for flash flood warnings, as well as estimates snowfall accumulations and overall extent of snow cover (National Oceanic and Atmospheric Administration, 2013).

2. Bias-corrected WSR-88D Doppler radar rainfall estimates: NEXRAD or WSR-88D is a network of 159 high-resolution S-band Doppler weather radars operated by the NWS. NEXRAD detects precipitation and atmospheric movement or wind. It returns data which when processed can be displayed in a mosaic map which shows patterns of precipitation and its movement.

3. Near real-time automated hourly rain gauge amounts recorded from several meteorological monitoring networks located throughout the US.

From the hourly rainfall estimate data, Middle Atlantic River Forecast Center (MARFC) of NWS (NOAA's National Weather Service Middle Atlantic River Forecast Center, 2012) has created the daily rainfall estimate data for the state of New Jersey. After contacting them, daily rainfall estimates for May 2012 through August 2013 were received. Cumulative monthly precipitation for the modeling period in the Study Area, based on data from MARFC of NWS is shown in **Figure 4.2** and the daily precipitation data are presented in **Table 4.2**.

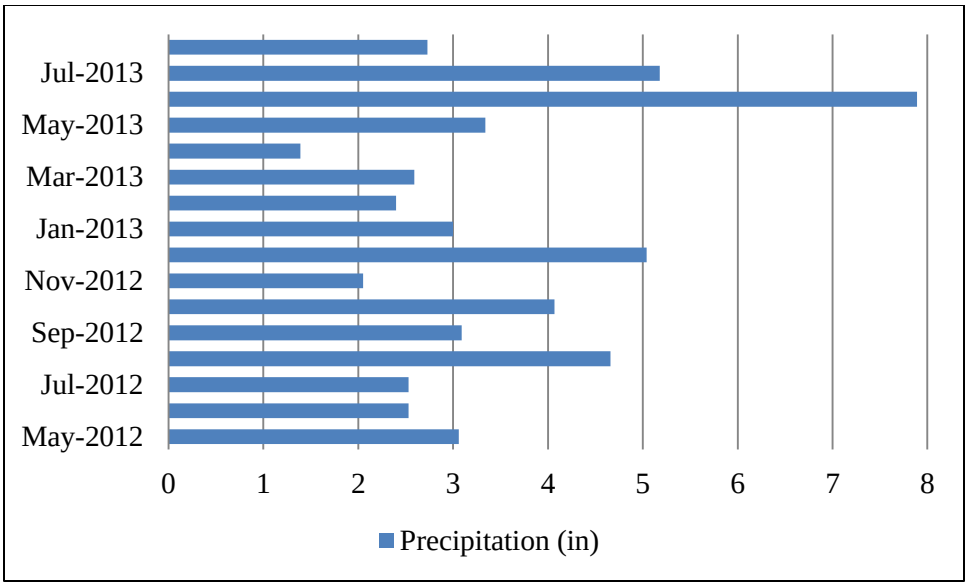

Figure 4.2 Cumulative monthly precipitation in the Study Area, based on data from MARFC of NWS.

Table 4.2 Daily Precipitation for the Study Area from MARFC of NWS, May 2012 through August 2013

Date	Precipitation (in)	Date	Precipitation (in)	Date	Precipitation (in)	Date	Precipitation (in)
5/1/2013	0.2	6/1/2013	0.0	7/1/2013	0.0	8/1/2013	0.5
5/2/2013	0.0	6/2/2013	0.3	7/2/2013	0.0	8/2/2013	0.0
5/3/2013	0.1	6/3/2013	0.1	7/3/2013	0.0	8/3/2013	0.0
5/4/2013	0.0	6/4/2013	0.4	7/4/2013	0.1	8/4/2013	0.0
5/5/2013	N/A*	6/5/2013	0.0	7/5/2013	0.0	8/5/2013	0.8
5/6/2013	N/A	6/6/2013	0.0	7/6/2013	0.0	8/6/2013	0.4
5/7/2013	0.1	6/7/2013	0.1	7/7/2013	0.1	8/7/2013	0.0
5/8/2013	0.1	6/8/2013	0.0	7/8/2013	0.0	8/8/2013	0.0
5/9/2013	0.6	6/9/2013	0.0	7/9/2013	0.0	8/9/2013	0.0
5/10/2013	0.2	6/10/2013	0.1	7/10/2013	0.0	8/10/2013	0.7
5/11/2013	0.0	6/11/2013	0.0	7/11/2013	0.0	8/11/2013	0.0
5/12/2013	0.1	6/12/2013	0.6	7/12/2013	0.0	8/12/2013	0.0
5/13/2013	0.1	6/13/2013	0.1	7/13/2013	0.0	8/13/2013	0.0
5/14/2013	0.1	6/14/2013	0.0	7/14/2013	0.1	8/14/2013	0.2
5/15/2013	0.3	6/15/2013	0.0	7/15/2013	0.2	8/15/2013	0.3
5/16/2013	0.0	6/16/2013	0.0	7/16/2013	0.0	8/16/2013	0.0
5/17/2013	0.0	6/17/2013	0.0	7/17/2013	0.0	8/17/2013	0.1
5/18/2013	0.0	6/18/2013	0.0	7/18/2013	0.2	8/18/2013	0.2
5/19/2013	0.0	6/19/2013	0.0	7/19/2013	0.0	8/19/2013	0.0
5/20/2013	0.0	6/20/2013	0.0	7/20/2013	0.4	8/20/2013	0.0
5/21/2013	0.8	6/21/2013	0.0	7/21/2013	0.0	8/21/2013	0.0
5/22/2013	0.0	6/22/2013	0.3	7/22/2013	0.0	8/22/2013	0.0
5/23/2013	0.2	6/23/2013	0.0	7/23/2013	0.0	8/23/2013	0.0
5/24/2013	0.0	6/24/2013	0.0	7/24/2013	0.0	8/24/2013	0.0
5/25/2013	0.0	6/25/2013	0.5	7/25/2013	0.0	8/25/2013	0.0
5/26/2013	0.0	6/26/2013	0.0	7/26/2013	0.4	8/26/2013	0.0
5/27/2013	0.0	6/27/2013	0.0	7/27/2013	0.0	8/27/2013	1.3
5/28/2013	0.0	6/28/2013	0.0	7/28/2013	1.1	8/28/2013	0.1
5/29/2013	0.0	6/29/2013	0.0	7/29/2013	0.0	8/29/2013	0.0
5/30/2013	0.0	6/30/2013	0.0	7/30/2013	0.0	8/30/2013	0.0
5/31/2013	0.0	-	-	7/31/2013	0.0	8/31/2013	0.0

*N/A: No data was reported on these days.

Table 4.2 (Continued) Daily Precipitation for the Study Area from MARFC of NWS, May 2012 through August 2013

Date	Precipitation (in)	Date	Precipitation (in)	Date	Precipitation (in)	Date	Precipitation (in)
9/1/2012	0.0	10/1/2012	0.0	11/1/2012	0.0	12/1/2012	0.0
9/2/2012	0.0	10/2/2012	0.2	11/2/2012	0.0	12/2/2012	0.1
9/3/2012	0.0	10/3/2012	0.0	11/3/2012	0.0	12/3/2012	0.0
9/4/2012	0.7	10/4/2012	0.1	11/4/2012	0.0	12/4/2012	0.0
9/5/2012	0.3	10/5/2012	0.0	11/5/2012	0.0	12/5/2012	0.0
9/6/2012	0.0	10/6/2012	0.0	11/6/2012	0.0	12/6/2012	0.0
9/7/2012	0.0	10/7/2012	0.1	11/7/2012	0.9	12/7/2012	0.1
9/8/2012	0.3	10/8/2012	0.0	11/8/2012	0.1	12/8/2012	0.3
9/9/2012	0.0	10/9/2012	0.1	11/9/2012	0.0	12/9/2012	0.2
9/10/2012	0.0	10/10/2012	0.4	11/10/2012	0.0	12/10/2012	0.1
9/11/2012	0.0	10/11/2012	0.0	11/11/2012	0.0	12/11/2012	0.1
9/12/2012	0.0	10/12/2012	0.0	11/12/2012	0.0	12/12/2012	0.0
9/13/2012	0.0	10/13/2012	0.0	11/13/2012	0.2	12/13/2012	0.0
9/14/2012	0.0	10/14/2012	0.0	11/14/2012	0.0	12/14/2012	0.0
9/15/2012	0.0	10/15/2012	0.1	11/15/2012	0.0	12/15/2012	0.0
9/16/2012	0.0	10/16/2012	0.0	11/16/2012	0.0	12/16/2012	0.1
9/17/2012	0.0	10/17/2012	0.0	11/17/2012	0.0	12/17/2012	0.1
9/18/2012	1.1	10/18/2012	0.0	11/18/2012	0.0	12/18/2012	0.1
9/19/2012	0.0	10/19/2012	0.7	11/19/2012	0.0	12/19/2012	0.0
9/20/2012	0.0	10/20/2012	0.0	11/20/2012	0.0	12/20/2012	0.0
9/21/2012	0.0	10/21/2012	0.0	11/21/2012	0.0	12/21/2012	1.2
9/22/2012	0.1	10/22/2012	0.0	11/22/2012	0.0	12/22/2012	0.0
9/23/2012	0.0	10/23/2012	0.1	11/23/2012	0.0	12/23/2012	0.0
9/24/2012	0.0	10/24/2012	0.0	11/24/2012	0.0	12/24/2012	0.1
9/25/2012	0.0	10/25/2012	0.0	11/25/2012	0.0	12/25/2012	0.0
9/26/2012	0.0	10/26/2012	0.0	11/26/2012	0.0	12/26/2012	1.7
9/27/2012	0.0	10/27/2012	0.0	11/27/2012	0.9	12/27/2012	0.6
9/28/2012	0.3	10/28/2012	0.0	11/28/2012	0.0	12/28/2012	0.0
9/29/2012	0.0	10/29/2012	2.0	11/29/2012	0.0	12/29/2012	0.5
9/30/2012	0.0	10/30/2012	0.3	11/30/2012	0.0	12/30/2012	0.0
-	-	10/31/2012	0.0	-	-	12/31/2012	0.0

Table 4.2 (Continued) Daily Precipitation for the Study Area from MARFC of NWS, May 2012 through August 2013

Date	Precipitation (in)	Date	Precipitation (in)	Date	Precipitation (in)	Date	Precipitation (in)
1/1/2013	0.0	2/1/2013	0.0	3/1/2013	0.0	4/1/2013	0.0
1/2/2013	0.0	2/2/2013	0.0	3/2/2013	0.0	4/2/2013	0.0
1/3/2013	0.0	2/3/2013	0.1	3/3/2013	0.0	4/3/2013	0.0
1/4/2013	0.0	2/4/2013	0.0	3/4/2013	0.0	4/4/2013	0.0
1/5/2013	0.0	2/5/2013	0.0	3/5/2013	0.0	4/5/2013	0.0
1/6/2013	0.0	2/6/2013	0.0	3/6/2013	0.2	4/6/2013	0.0
1/7/2013	0.0	2/7/2013	0.0	3/7/2013	0.2	4/7/2013	0.0
1/8/2013	0.0	2/8/2013	0.8	3/8/2013	0.4	4/8/2013	0.0
1/9/2013	0.0	2/9/2013	0.2	3/9/2013	0.0	4/9/2013	0.0
1/10/2013	0.0	2/10/2013	0.0	3/10/2013	0.0	4/10/2013	0.3
1/11/2013	0.6	2/11/2013	0.3	3/11/2013	0.0	4/11/2013	0.0
1/12/2013	0.0	2/12/2013	0.0	3/12/2013	0.6	4/12/2013	0.6
1/13/2013	0.0	2/13/2013	0.2	3/13/2013	0.0	4/13/2013	0.0
1/14/2013	0.0	2/14/2013	0.0	3/14/2013	0.0	4/14/2013	0.0
1/15/2013	0.2	2/15/2013	0.0	3/15/2013	0.0	4/15/2013	0.0
1/16/2013	0.7	2/16/2013	0.1	3/16/2013	0.1	4/16/2013	0.0
1/17/2013	0.0	2/17/2013	0.0	3/17/2013	0.0	4/17/2013	0.0
1/18/2013	0.0	2/18/2013	0.0	3/18/2013	0.2	4/18/2013	0.0
1/19/2013	0.0	2/19/2013	0.2	3/19/2013	0.2	4/19/2013	0.0
1/20/2013	0.0	2/20/2013	0.0	3/20/2013	0.0	4/20/2013	0.2
1/21/2013	0.1	2/21/2013	0.0	3/21/2013	0.0	4/21/2013	0.0
1/22/2013	0.0	2/22/2013	0.0	3/22/2013	0.0	4/22/2013	0.0
1/23/2013	0.0	2/23/2013	0.2	3/23/2013	0.0	4/23/2013	0.0
1/24/2013	0.0	2/24/2013	0.0	3/24/2013	0.0	4/24/2013	0.0
1/25/2013	0.1	2/25/2013	0.0	3/25/2013	0.4	4/25/2013	0.0
1/26/2013	0.0	2/26/2013	0.1	3/26/2013	0.0	4/26/2013	0.0
1/27/2013	0.0	2/27/2013	0.3	3/27/2013	0.0	4/27/2013	0.0
1/28/2013	0.2	2/28/2013	0.0	3/28/2013	0.0	4/28/2013	0.0
1/29/2013	0.0	-	-	3/29/2013	0.0	4/29/2013	0.2
1/30/2013	0.0	-	-	3/30/2013	0.0	4/30/2013	0.0
1/31/2013	1.1	-	-	3/31/2013	0.3	-	-

Table 4.2 (Continued) Daily Precipitation for the Study Area from MARFC of NWS, May 2012 through August 2013

Date	Precipitation (in)	Date	Precipitation (in)	Date	Precipitation (in)	Date	Precipitation (in)
5/1/2013	0.0	6/1/2013	0.0	7/1/2013	0.5	8/1/2013	0.8
5/2/2013	0.0	6/2/2013	0.1	7/2/2013	0.5	8/2/2013	0.0
5/3/2013	0.0	6/3/2013	0.6	7/3/2013	0.2	8/3/2013	0.0
5/4/2013	0.0	6/4/2013	0.0	7/4/2013	0.0	8/4/2013	0.0
5/5/2013	0.0	6/5/2013	0.0	7/5/2013	0.0	8/5/2013	0.0
5/6/2013	0.0	6/6/2013	0.1	7/6/2013	0.0	8/6/2013	0.0
5/7/2013	0.0	6/7/2013	2.7	7/7/2013	0.0	8/7/2013	0.0
5/8/2013	1.0	6/8/2013	0.1	7/8/2013	0.0	8/8/2013	0.5
5/9/2013	0.5	6/9/2013	0.0	7/9/2013	0.0	8/9/2013	0.0
5/10/2013	0.0	6/10/2013	1.4	7/10/2013	0.0	8/10/2013	0.0
5/11/2013	0.7	6/11/2013	0.0	7/11/2013	0.1	8/11/2013	0.0
5/12/2013	0.0	6/12/2013	0.0	7/12/2013	0.7	8/12/2013	0.1
5/13/2013	0.0	6/13/2013	1.0	7/13/2013	1.1	8/13/2013	0.8
5/14/2013	0.0	6/14/2013	0.1	7/14/2013	0.0	8/14/2013	0.0
5/15/2013	0.0	6/15/2013	0.0	7/15/2013	0.0	8/15/2013	0.0
5/16/2013	0.0	6/16/2013	0.0	7/16/2013	0.0	8/16/2013	0.0
5/17/2013	0.0	6/17/2013	0.2	7/17/2013	0.0	8/17/2013	0.0
5/18/2013	0.1	6/18/2013	0.6	7/18/2013	0.0	8/18/2013	0.0
5/19/2013	0.0	6/19/2013	0.0	7/19/2013	0.0	8/19/2013	0.0
5/20/2013	0.0	6/20/2013	0.0	7/20/2013	0.0	8/20/2013	0.0
5/21/2013	0.0	6/21/2013	0.0	7/21/2013	0.0	8/21/2013	0.0
5/22/2013	0.0	6/22/2013	0.0	7/22/2013	0.8	8/22/2013	0.4
5/23/2013	0.1	6/23/2013	0.3	7/23/2013	0.9	8/23/2013	0.0
5/24/2013	0.3	6/24/2013	0.1	7/24/2013	0.0	8/24/2013	0.0
5/25/2013	0.2	6/25/2013	0.0	7/25/2013	0.0	8/25/2013	0.0
5/26/2013	0.0	6/26/2013	0.2	7/26/2013	0.0	8/26/2013	0.0
5/27/2013	0.0	6/27/2013	0.4	7/27/2013	0.0	8/27/2013	0.0
5/28/2013	0.4	6/28/2013	0.0	7/28/2013	0.3	8/28/2013	0.1
5/29/2013	0.0	6/29/2013	0.0	7/29/2013	0.0	8/29/2013	0.0
5/30/2013	0.0	6/30/2013	0.1	7/30/2013	0.0	8/30/2013	0.0
5/31/2013	0.0	-	-	7/31/2013	0.0	8/31/2013	0.0

4.1.5 The Stream

River package of the ModelMuse will be used to simulate the Stream in the Study Area. ModelMuse provides this package to be used in simulating rivers or streams. The River package is assigned to boundaries in which the flow into or out of the groundwater system is a function of the head. If the head is above a threshold value the flow is a linear function of head. However, if the head in the cell falls below the threshold, the flow from the river to the model cell is set to a specified lower bound.

4.1.6 Time

The model starts at the beginning of May 2012 and ends at the end of August 2013 covering a period of sixteen (16) months with time steps of two weeks. This period is based on the fact that majority of the water level readings from monitoring wells were recorded in the above-mentioned period.

4.1.7 Hydraulic Conductivity

Hydraulic conductivity along the Model Domain will be assigned as (k_x, k_y, k_z) = $(0.0001\frac{ft}{s}, k_x, \frac{k_x}{10})$, based on results of the field investigations presented at Section 2.4.4 Soil Hydraulic Conductivity (can be found at page 43).

4.1.8 Model Calibration and Evaluation

Simulated groundwater levels will be validated against monitoring well groundwater levels that were collected during the field visits to the Study Corridor. Percent error and BIAS value will be used to evaluate the performance and accuracy of the developed model. Root mean squared deviation (RMSD) and mean absolute error (MAE) will be used to compare the accuracy of the modeling results for two sides of the Stream.

Simulated versus observed groundwater levels will be illustrated and percent error will be used to demonstrate any discrepancy between the observed and simulated groundwater level values.

BIAS measures the tendency of the simulated values to be larger or smaller than their corresponding observed values, with the positive values of BIAS indicating a tendency to overestimation, and negative values indicating a tendency to underestimation while the ideal, unachievable BIAS value is absolute zero (Yapo, Gupta, & Sorooshian, 1996).

Root mean squared deviation is a good measure for indicating goodness of fit of a model. In general RMSD values are larger than MAE values, and the degree to which RMSE exceeds MAE is an indicator of the extent to which large outliers (variance between the observed and the simulated values) exist in the model performance (Karunanithi, Grenney, Whitley, & Bovee, 1994).

These parameters are defined as follows:

$$E_P = \frac{|h_S - h_O|}{h_O} \tag{4.1}$$

$$BIAS = \frac{\sum_{i=1}^{n}(h_S - h_O)}{\sum_{i=1}^{n} h_O} \tag{4.2}$$

$$RMSD = \sqrt{\frac{\sum_{i=1}^{n}(h_S - h_O)^2}{n}} \tag{4.3}$$

$$MAE = \frac{\sum_{i=1}^{n}|h_S - h_O|}{n} \tag{4.4}$$

Where:

E_P: Percent Error;

RMSD: Root Mean Squared Deviation;

MAE: Mean Absolute Error;

n: Number of observed values.

4.2 Results

In this section, created ModelMuse in AutoCAD and imported into the ModelMuse, assigned topography to the contour lines and elevation interpolation results for the Model Domain, spatial discretization and grid lines, utilized precipitation data and finally water levels resulted from the modeling efforts will be presented.

4.2.1 Model Domain

After reviewing the topographic map of the area covering Monmouth Battlefield State Park, in order to find the no-flow boundary conditions to make the model a more accurate simulation of the study site, the Model Domain in **Figure 4.3** was proposed. This figure is a part of USGS topographic map for Freehold, NJ which can be found as **Figure 2.11** on page 38.

This Domain covers an area of approximately 13,000 feet by 11,000 feet. According to USGS National Map, US Topo Map, the highest elevation contour lines present in this area is 160 feet above sea level and the lowest contour lines present are 100 feet above sea level.

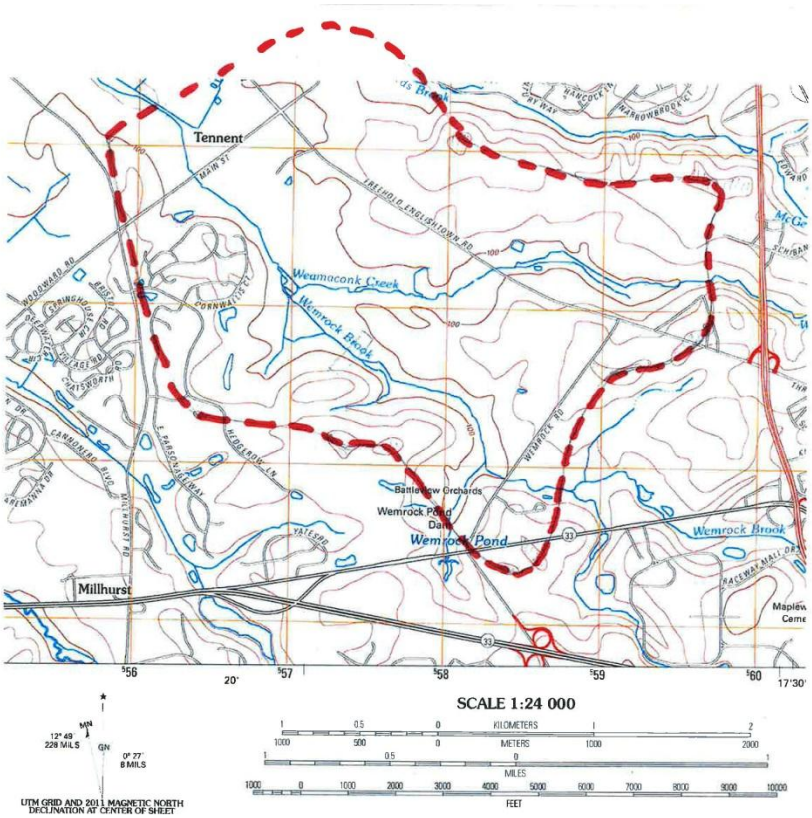

Figure 4.3 Model Domain covers the area being simulated in ModelMuse (U.S. Geological Survey, 2013).

4.2.2 Importing Model Domain into ModelMuse

Model Domain was initially created in AutoCAD assigning different colors to topographic layers with different elevations. AutoCAD files can be saved with a DXF format. DXF is an AutoCAD data file format developed by Autodesk for enabling data interoperability between AutoCAD and other programs. ModelMuse has the ability to recognize and import DXF files. Imported DXF file can be used in order to define the Model Domain and also to assign elevations to the contour lines. AutoCAD file is shown in **Figure 4.4**.

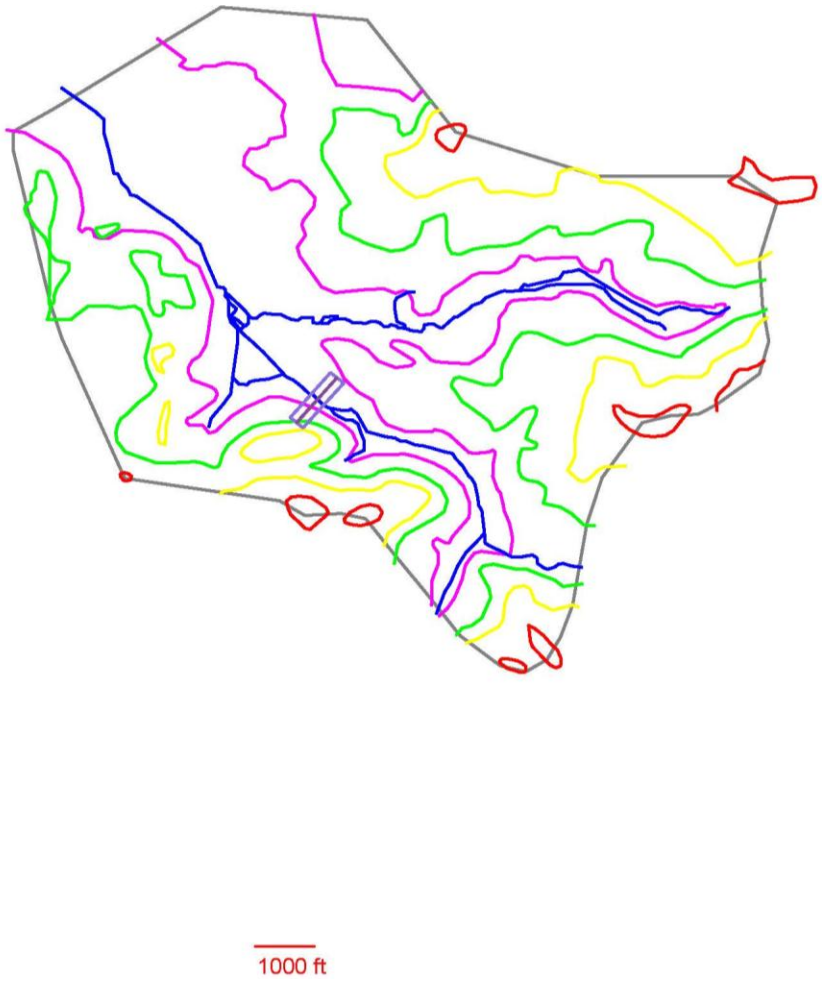

Figure 4.4 Model Domain, developed in AutoCAD - blue represents river, magenta, green, yellow and red represent elevations of 100, 120, 140 & 160 feet above sea level, respectively.

4.2.3 Assigning Topography in ModelMuse

Topography of the Model Domain was assigned using the contour lines created initially in and imported from AutoCAD. Doing so only defines the elevations along the topographic lines. Interpolation was used in order to assign elevations in the area between the contour lines. ModelMuse provides seven interpolation methods. As discussed in Section 4.1.2 Topography (on page 69), ModelMuse provides seven interpolation methods which are as follows:

1. The nearest interpolation method;
2. The nearest point interpolation method;
3. The inverse distance squared interpolation method;
4. The triangle interpolation method;
5. The fitted surface interpolation method;
6. The point inverse distance interpolation method; and,
7. The natural neighbor interpolation method.

More detailed description of these interpolation methods can be found under Section 4.1.2 Topography on page 69. The results of the interpolation methods used are shown in **Figure 4.5** through **Figure 4.11**.

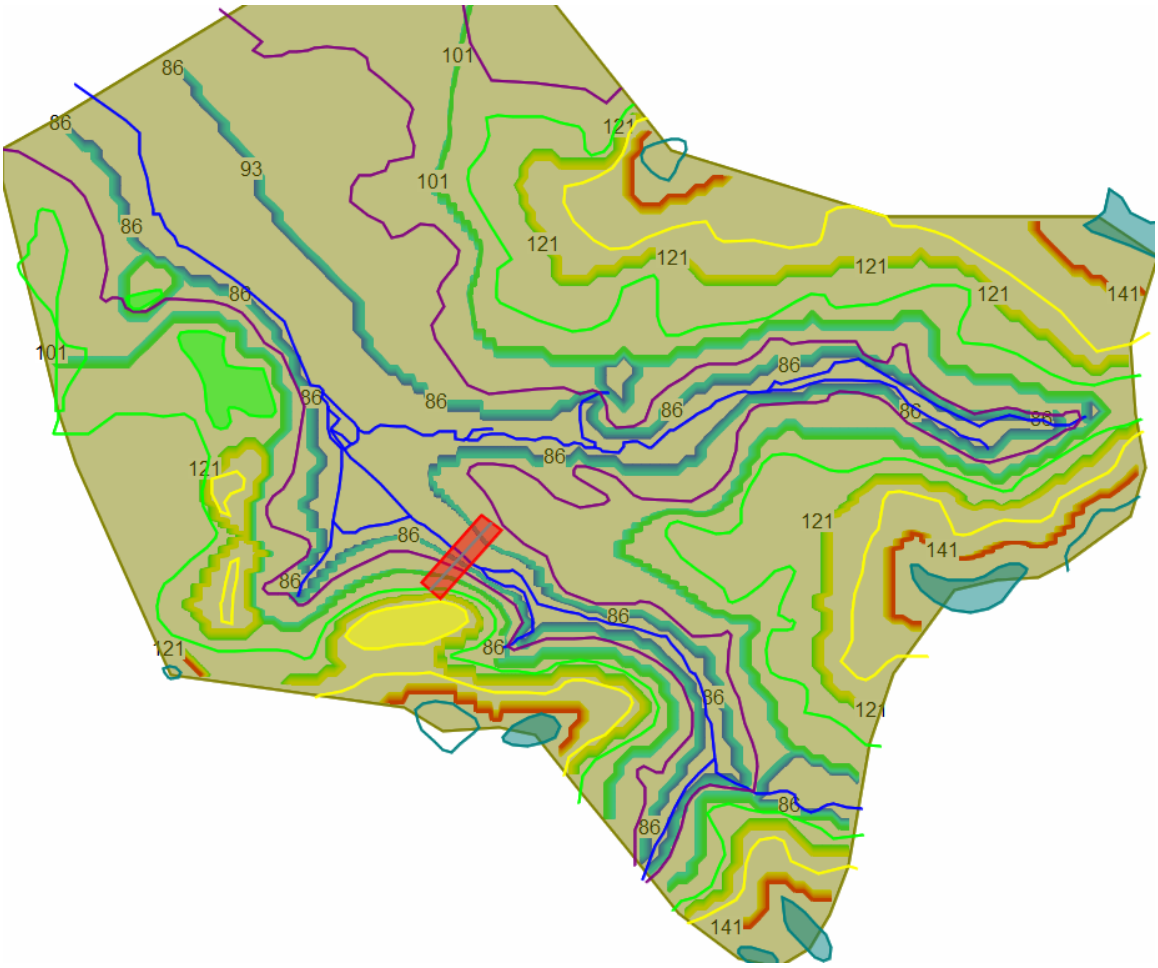

Figure 4.5 Topography of the Study Area based on the nearest interpolation method.

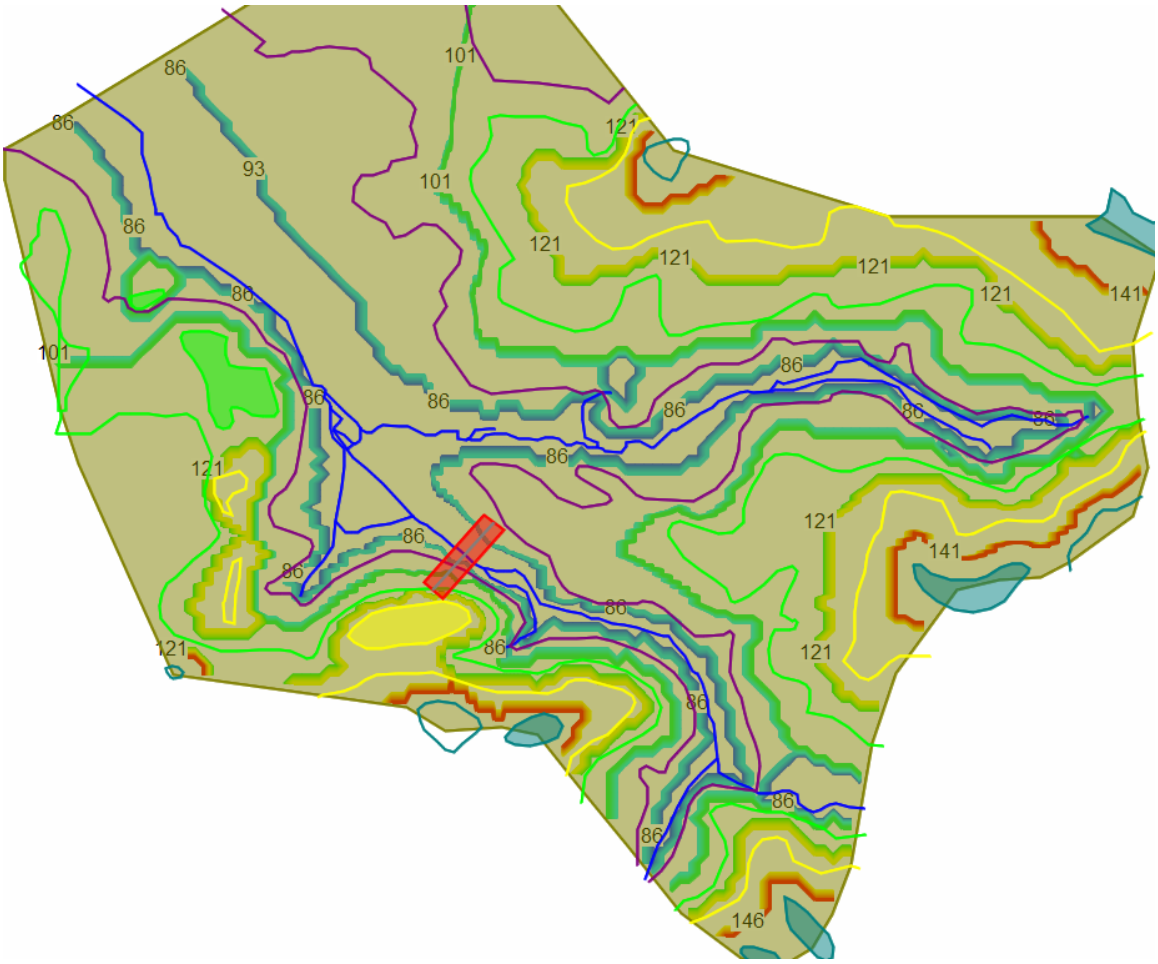

Figure 4.6 Topography of the Study Area based on the nearest point interpolation method.

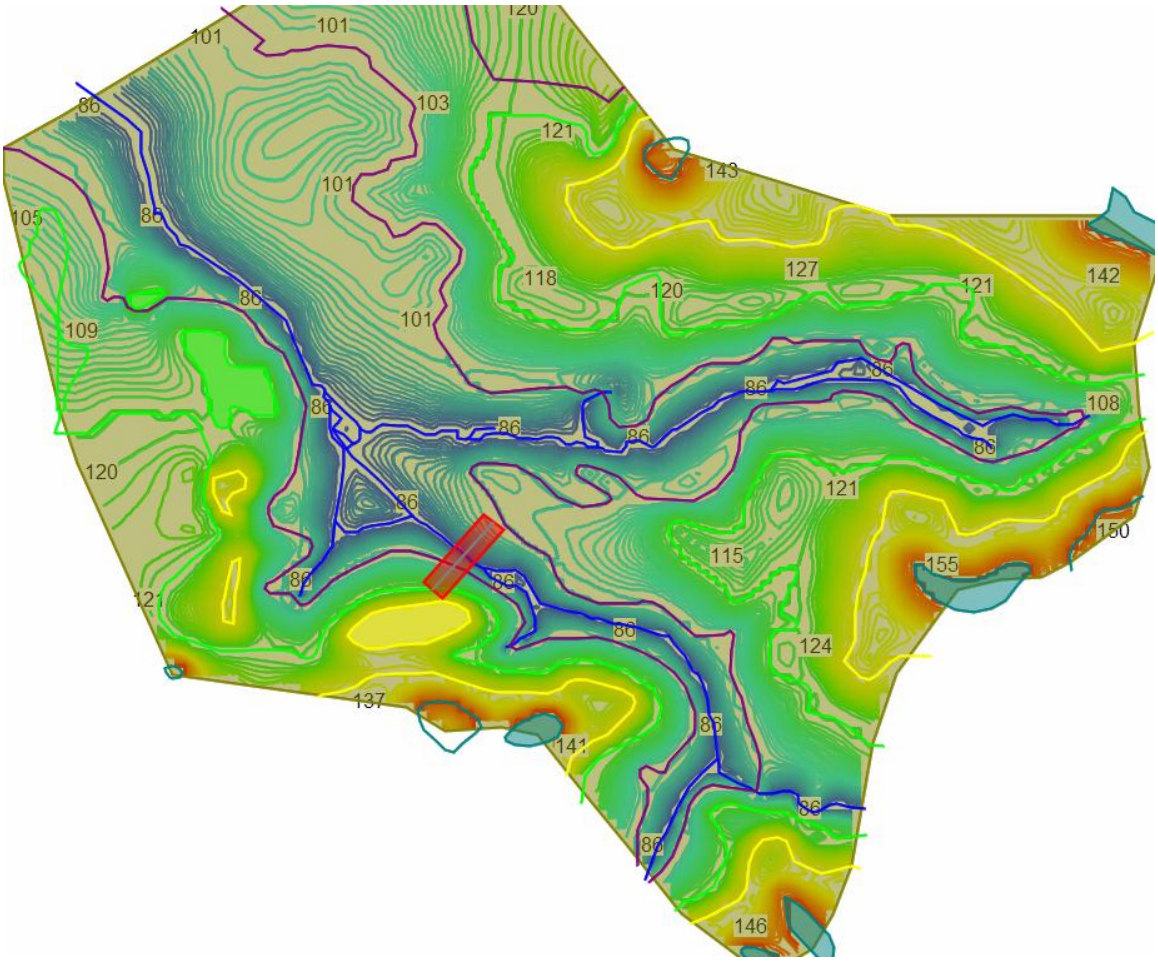

Figure 4.7 Topography of the Study Area based on the inverse distance squared interpolation method.

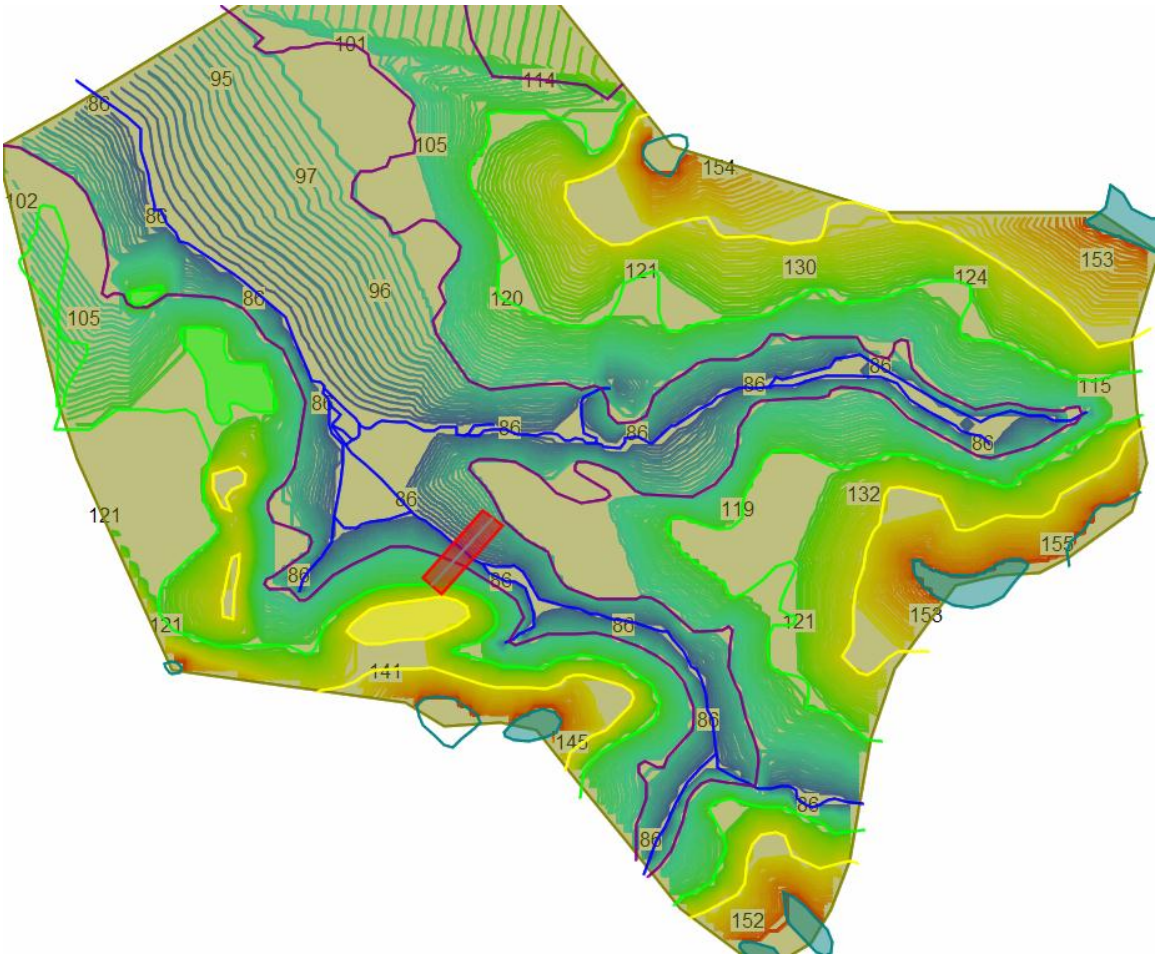

Figure 4.8 Topography of the Study Area based on the triangle interpolation method.

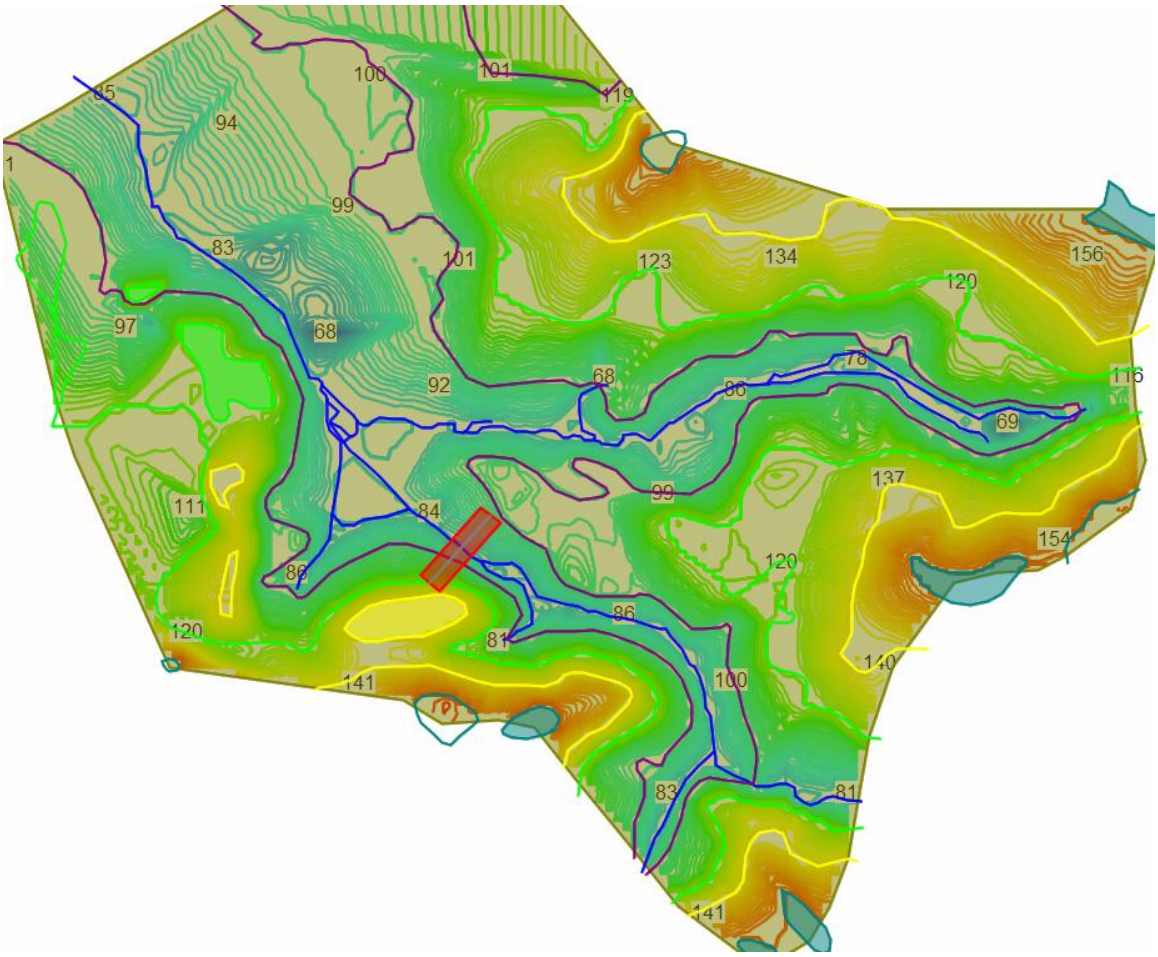

Figure 4.9 Topography of the Study Area based on the fitted surface interpolation method.

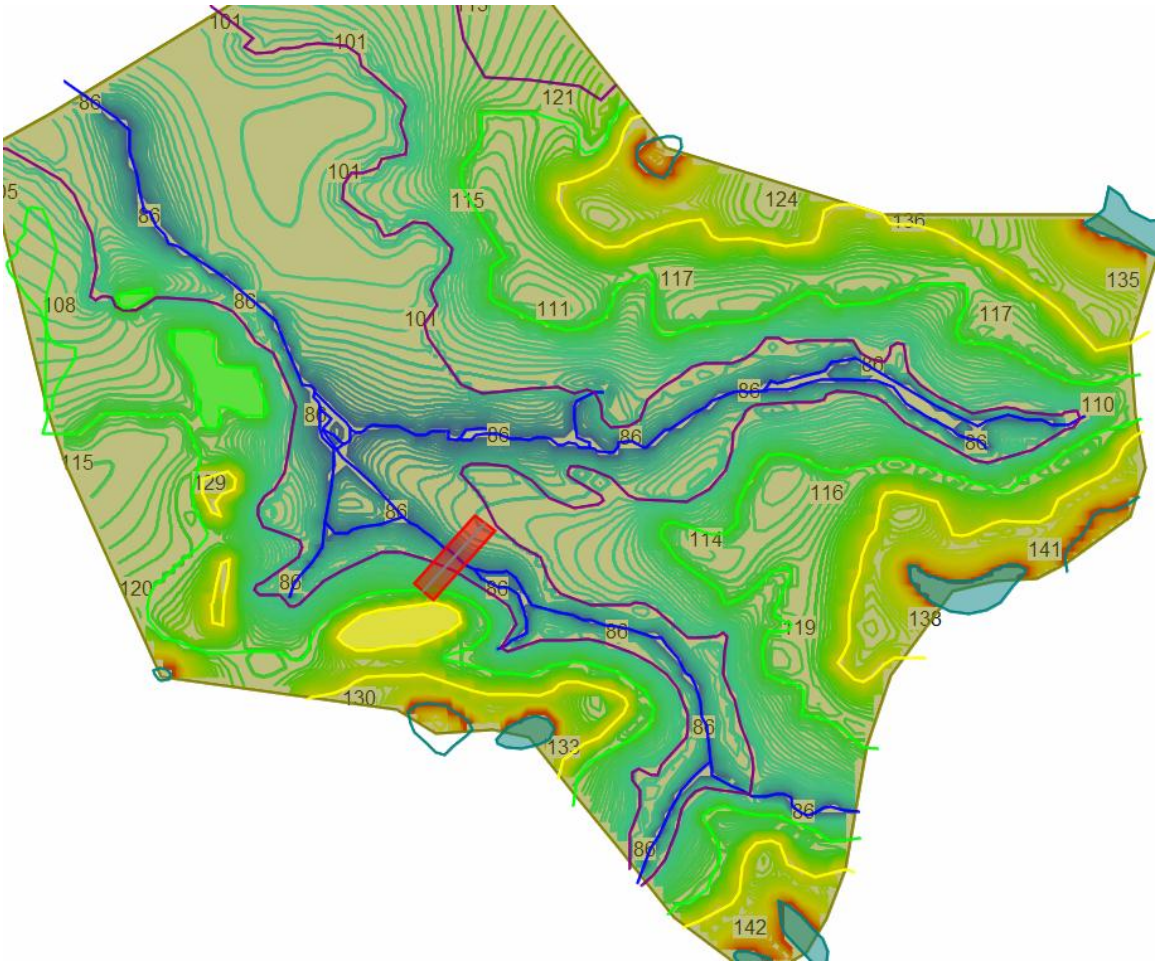

Figure 4.10 Topography of the Study Area based on the point inverse distance squared interpolation method.

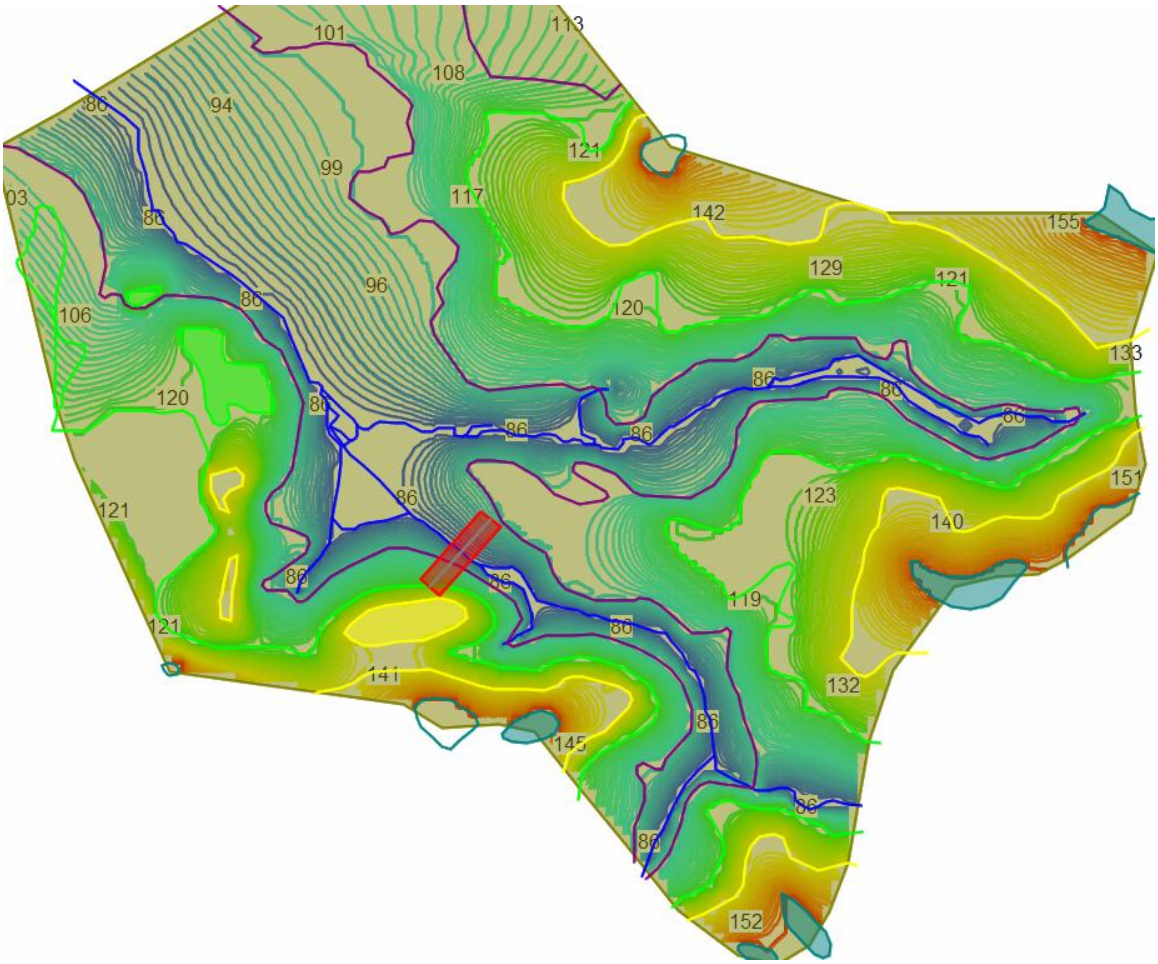

Figure 4.11 Topography of the Study Area based on the natural neighbor interpolation method.

After careful examination of the results of all the above-mentioned interpolation methods and comparing them against the surveyed elevation levels of the Study Corridor, the Triangle Interpolation method was found to provide the closest simulated elevations to the surveyed ones.

4.2.4 Defining Model Grids

In the present model, grid lines were generated at every 35 feet, which results in a grid consisting of 392 by 320 cells to cover the 13,000 by 11,300 square feet of the Model Domain. A depth of 100 feet, broken down into 5, 20-feet layers, was chosen as the third dimension of the model. 100 feet provides enough length for the third dimension of the model to account for the elevation of the area and also enough depth below ground level. Approximate number of grid cells in all layers is 627, 200. Model Domain spatial discretization is shown in **Figure 4.12**.

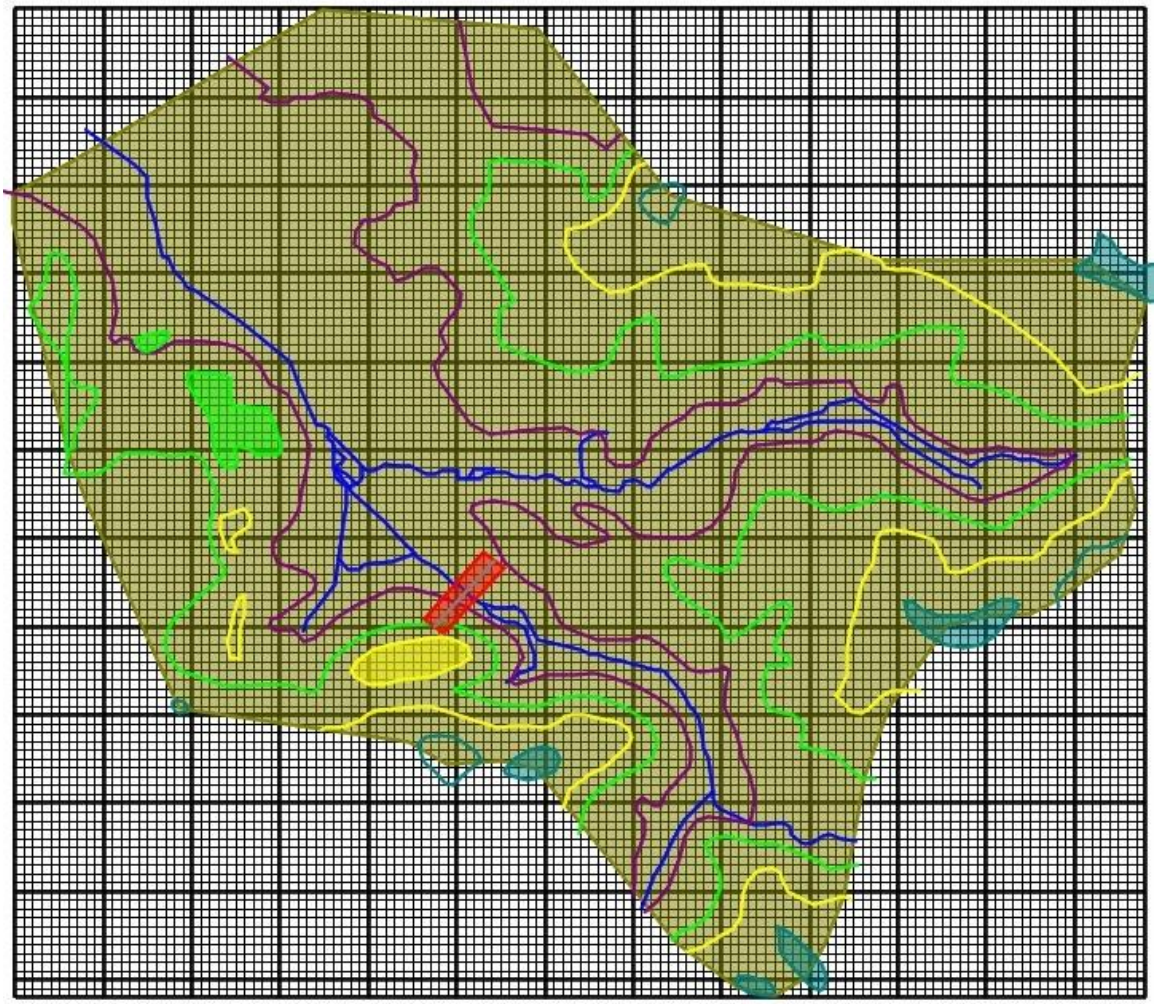

Figure 4.12 Model Domain spatial discretization (grid system).

4.2.5 Refined Grid Zone

In the Study Corridor where all the field data was collected, a more refined grid system can provide more simulation precision. A grid cell size of 10 feet by 10 feet was assigned to this area (compared to 35 feet by 35 feet in other parts of the Model Domain) and the results are shown in **Figure 4.13**. Defining Refined Grid Zone increases the total cell counts to almost 800, 000 in 5 layers.

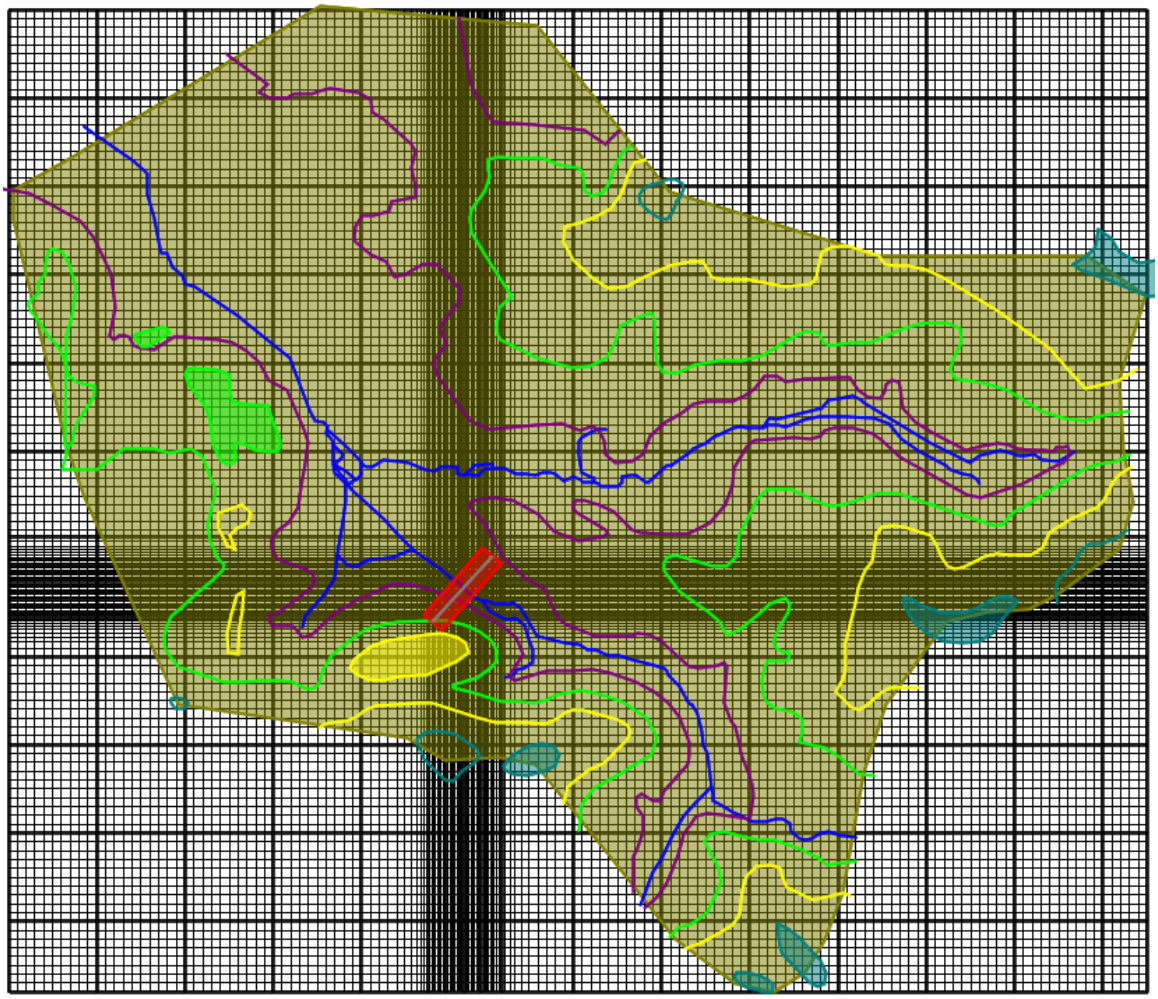

Figure 4.13 Refined grid lines at the Study Corridor will improve modeling results.

4.2.6 Recharge

Precipitation data from CoCoRaHS stations, US1NJMN0016 and 55 from NCDC of NOAA were used as the first modeling alternative (precipitation data from US1NJMN0016 – which is the closest station to the Study Area - is only available from May 2012 through October 2012. Therefore precipitation data from US1NJMN0055 – which is the second closest station to the Study Area - is used for November 2012 through August 2013). The data from the MARFC of NWS were used as the second alternative for applying recharge to the simulated model. Despite similarities between the

two sets, the precipitation data from CoCoRaHS stations showed better consistency with field readings collected from the monitoring wells at the Study Corridor. The inconsistency between the simulated results and the precipitation data from the MARFC of NWS can be related to the estimations in the process of creating the precipitation data (NWS MPE program initially creates hourly precipitation amounts based on their sources and then MARFC of NWS converts them into the daily rainfall estimates for the state of New Jersey).

4.2.7 Groundwater Levels

After developing the Study Area in the ModelMuse, implementing the topography, defining the grid and refined grid systems and assigning the recharge (precipitation), hydraulic conductivity and stream parameters in the ModelMuse, the model is ready to be executed. The modeling results were validated against monitoring well groundwater levels collected during the field visits to the Study Corridor.

The simulated versus observed groundwater levels are illustrated in **Figure 4.14**. The simulated heads are consistent with the observed heads.

Percent error was used to show the discrepancy between the observed and simulated groundwater levels. The present model shows an average percent error of 3.4 percent. The average percent error for simulated groundwater levels is 4.4 and 2.9 percent for the Forest and Farm Sides of the Stream, respectively.

BIAS measures the tendency of the simulated values to be larger or smaller than their corresponding observed values, with the positive values of BIAS indicating a tendency to overestimation, and negative values indicating a tendency to underestimation while the ideal, unachievable BIAS value is absolute zero (Yapo, Gupta, & Sorooshian,

1996). BIAS value of 0.0006 represents the tendency of the present model for overestimation. Implementing the same method, BIAS values of -0.0044 and 0.0140 suggest the tendency of the present model to underestimate and overestimate the values of groundwater levels for the Forest and Farm Sides of the Stream, respectively.

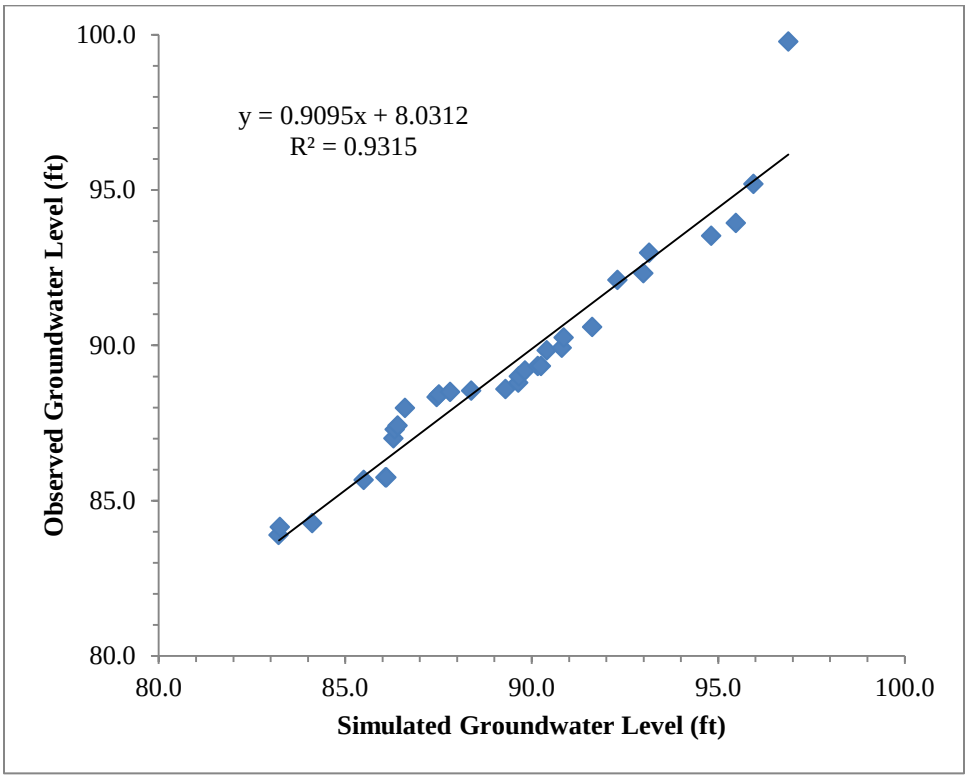

Figure 4.14 Relationship between the observed and simulated groundwater levels.

Root means squared deviation is a good measure for indicating goodness of fit of a model. RMSD vale of 2.10 was calculated for the whole model while this value was 2.39 and 2.19 for the Forest and Farm Sides of the Stream, respectively. Mean absolute error was calculated to be 1.80, 2.18 and 1.71 for the whole model, Forest and Farm Side of the Stream, respectively. RMSD and MAE values are consistent with the percent errors calculated for two sides of the Stream, showing more accurate simulation results on the Farm Side of the Stream compared to the Forest Side.

Table 4.3 Statistical Evaluation of the Developed Model

	Model	**Forest Side Only**	**Farm Side Only**
Percent Error (%)	3.1	4.0	2.6
BIAS	-0.0063	-0.0062	-0.0071
RMSD (ft)	1.27	1.60	1.11
MAE (ft)	1.18	1.46	1.07

Figure 4.15 and **Figure 4.16** present a summary of the observed and simulated groundwater levels, respectively. Observed groundwater levels were recorded at the Monitoring Wells locations and also at the Stream during the field investigations and the simulated groundwater levels are the results of the developed model.

Simulated groundwater levels and the observed groundwater levels along the Study Corridor for the period of May 2012 to July 2013 are presented in **Figure 4.17** through **Figure 4.22**.

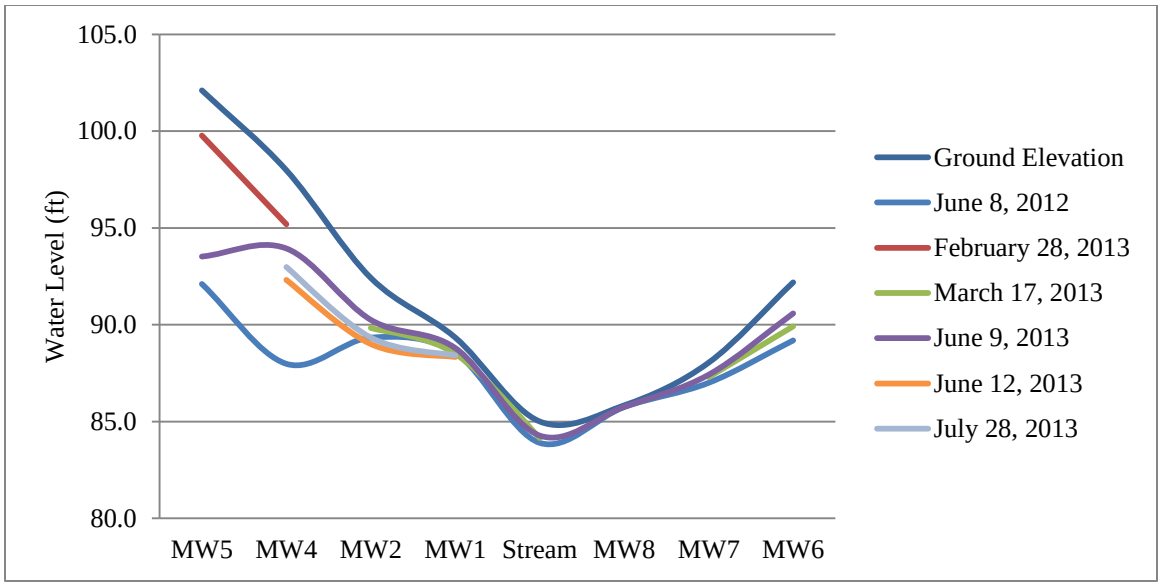

Figure 4.15 Observed groundwater levels in the Monitoring Wells along the Study Corridor.

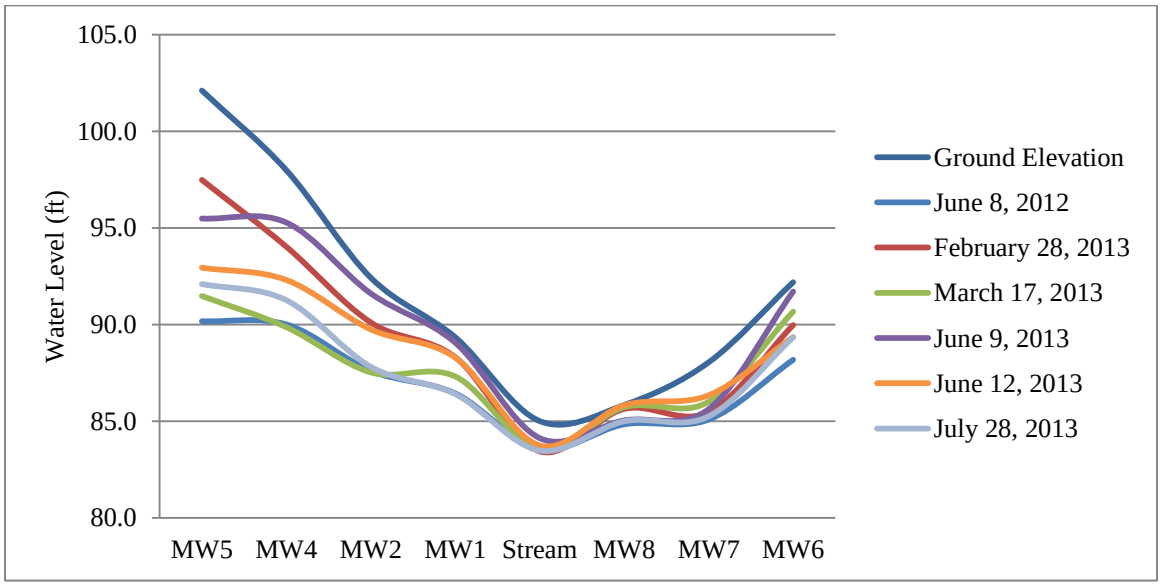

Figure 4.16 Simulated groundwater levels in the Monitoring Wells along the Study Corridor.

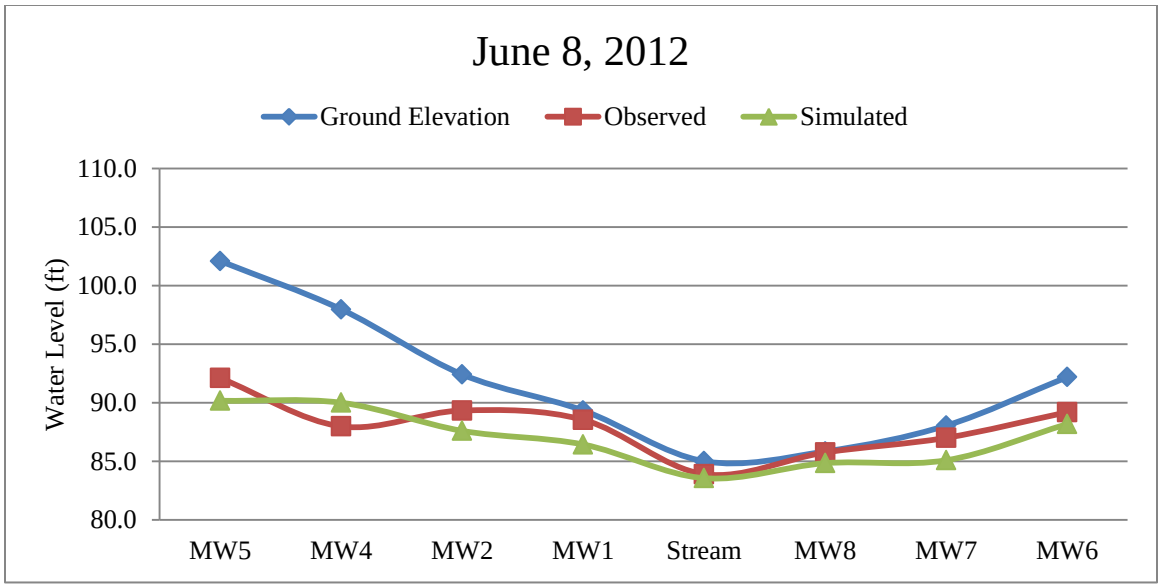

Figure 4.17 Observed and simulated groundwater levels for June 8, 2012 (horizontal axis is not to scale).

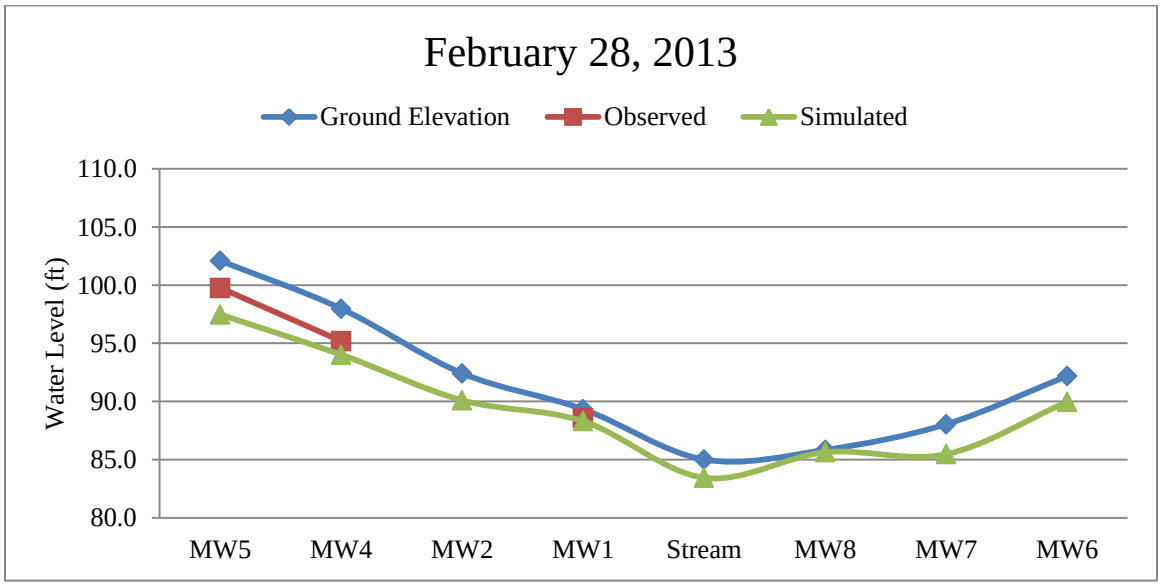

Figure 4.18 Observed and simulated groundwater levels for February 28, 2013 (horizontal axis is not to scale).

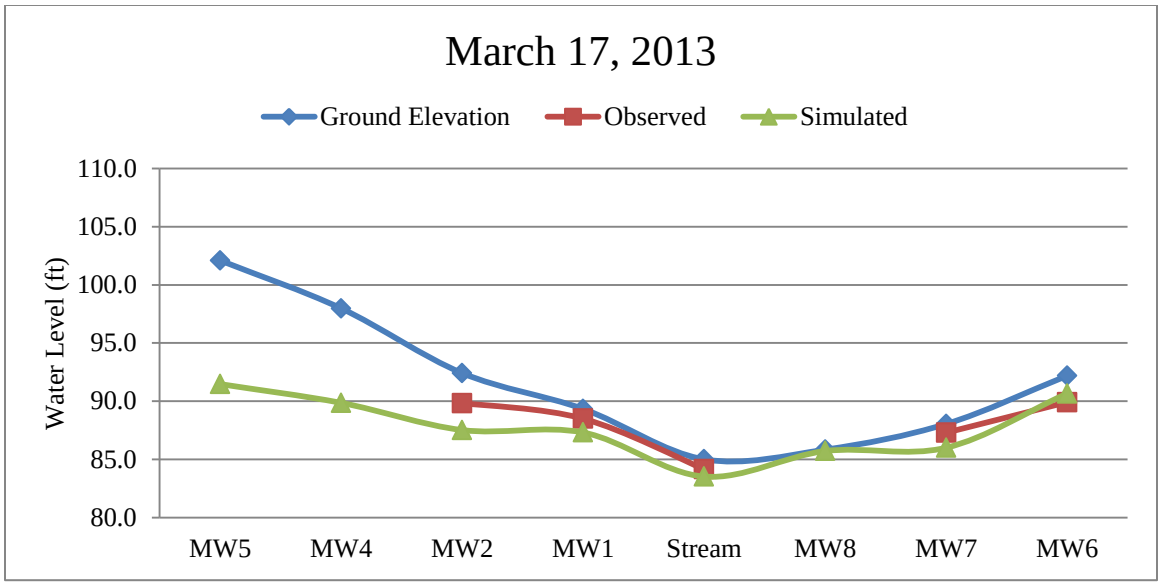

Figure 4.19 Observed and simulated groundwater levels for March 17, 2013 (horizontal axis is not to scale).

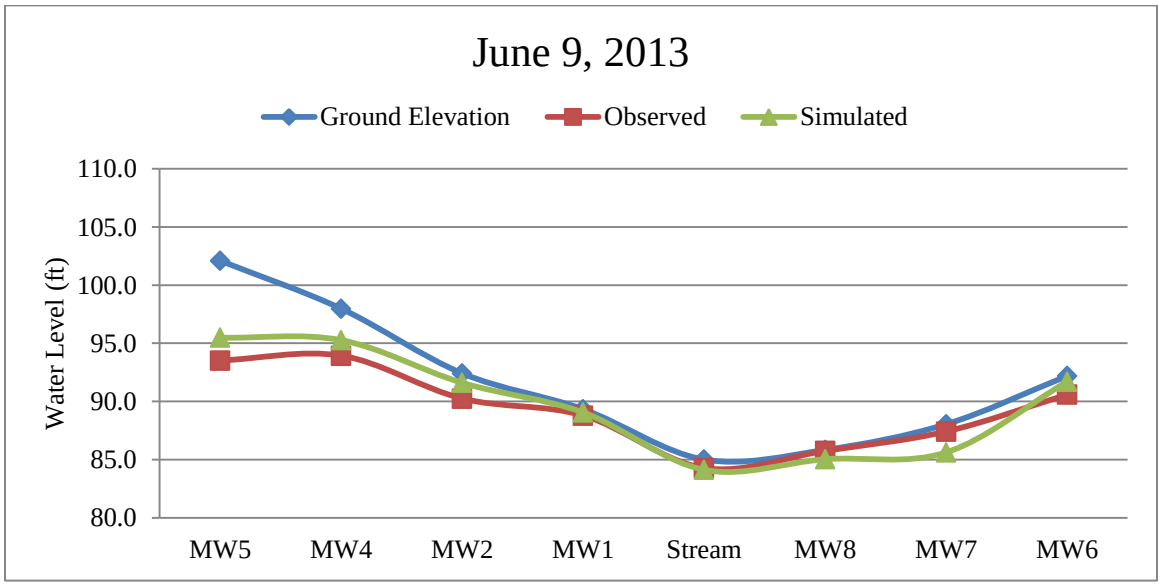

Figure 4.20 Observed and simulated groundwater levels for June 9, 2013 (horizontal axis is not to scale).

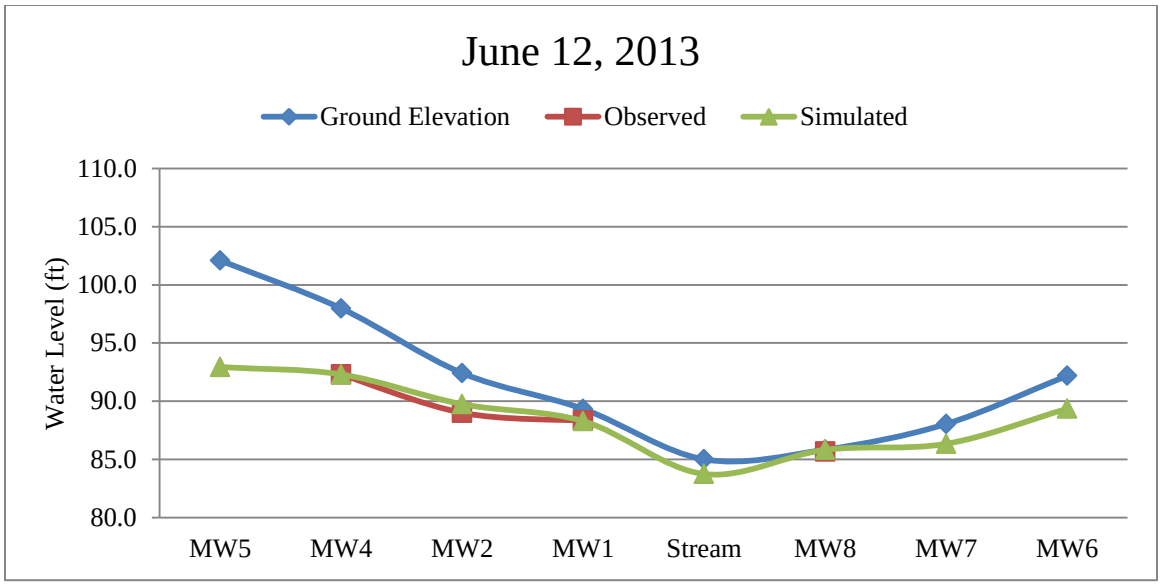

Figure 4.21 Observed and simulated groundwater levels for June 12, 2013 (horizontal axis is not to scale).

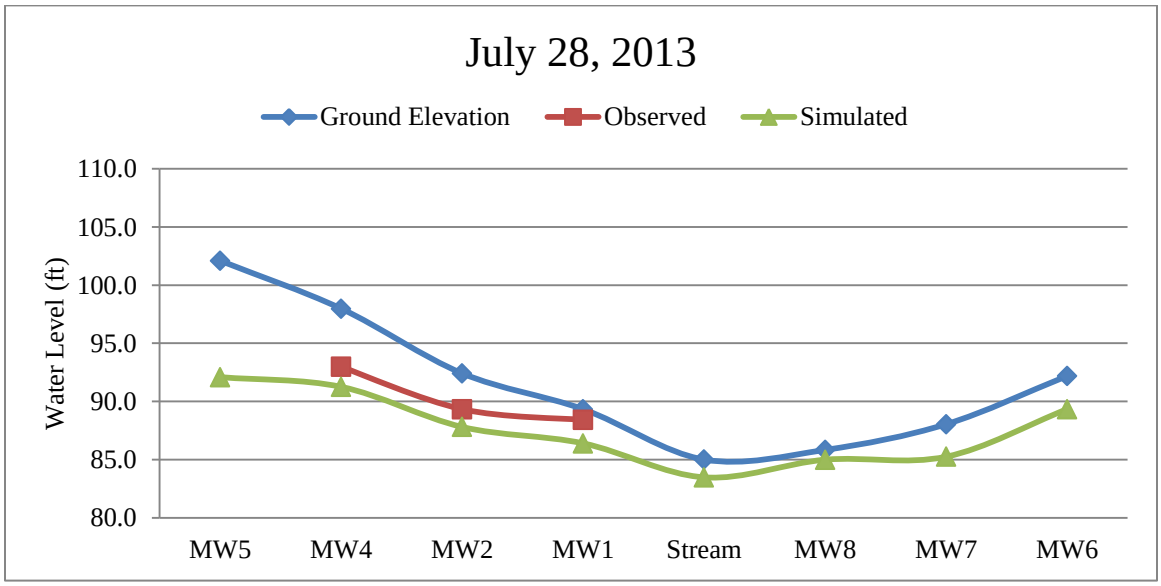

Figure 4.22 Observed and simulated groundwater levels for July 28, 2013 (horizontal axis is not to scale).

4.2.8 Evapotranspiration

Evapotranspiration is accounted for in modeling as a ratio of the precipitation data. Evapotranspiration ratios to precipitation were adjusted during the calibration process and once the simulated groundwater levels showed a reliable fit (below 5% discrepancy) to the observed ones, evapotranspiration amounts were extracted from the model.

Daily average evapotranspiration ranges from 0.1 to 5.5 and 0.0 to 4.9 millimeters per day (mm/d) for the Forest Side and Farm Side of the Stream respectively, in the Study Area from May 2012 to August 2013. For May through December 2012 daily average evapotranspiration was 1.8 and 1.5 mm/d for the Forest Side and Farm Side of the Stream, respectively. These numbers for January through August 2013 were 2.3 and 1.9 mm/d, respectively. For the whole modeling period (May 2012 through August 2013), these numbers were 2.0 and 1.7 mm/d, respectively. Average evapotranspiration on the Forest Side of the Stream are 20 and 16 percent higher than the Farm Side of the Stream for May through December 2012 and January through August 2013, respectively. The difference can be contributed to the different vegetation cover (dominant plant species and leaf area) on two sides of the Stream.

Minimum and maximum evapotranspiration occurred during November 2012 to January 2013 and June 2013 for the Forest Side of the Stream and during November 2012 to February 2013 and June 2013 for the Farm Side of the Stream.

Lowest ratio of evapotranspiration to precipitation occurred during October 2012 to February 2013 for both Forest and Farm Sides of the Stream. Highest ratio of evapotranspiration to precipitation occurred during May 2012 to July 2012 and April 2013 to July 2013 for both Forest and Farm Sides of the Stream. Higher levels of

evapotranspiration during summer can be contributed to the higher levels of solar radiation that provides energy for evapotranspiration during the growing season of the tress.

Total monthly evapotranspiration, daily average evapotranspiration for each month and the ratio of evapotranspiration to precipitation for each month during the modeling period (May 2012 through August 2013), separated for the Forest and Farm Sides of the Stream in the Study Area are presented in **Table 4.4**.

Precipitation and the amount of evapotranspiration on Forest and Farm Sides of the Stream in the Study Area are presented on a monthly basis for the modeling period (May 2012 through August 2013) in **Figure 4.23**. For the ratio of evapotranspiration to precipitation during the same period on a monthly basis refer to **Figure 4.24**.

Table 4.4 Evapotranspiration, Monthly Average Evapotranspiration and Evapotranspiration to Precipitation Ratio for Forest and Farm Sides of the Stream in the Study Area

		Forest Side of the Stream		
Date	**Precipitation (mm)**	**Evapotranspiration (mm)**	**Daily average evapotranspiration (mm/d)**	**Evapotranspiration to precipitation ratio**
May 2012	85	81	2.6	0.95
June 2012	105	95	3.2	0.9
July 2012	93	84	2.7	0.9
August 2012	135	95	3.1	0.7
September 2012	106	64	2.1	0.6
October 2012	132	13	0.4	0.1
November 2012	59	6	0.2	0.1
December 2012	147	7	0.2	0.05
January 2013	72	4	0.1	0.05
February 2013	100	10	0.4	0.1
March 2013	79	16	0.5	0.2
April 2013	57	54	1.8	0.95
May 2013	108	102	3.3	0.95
June 2013	183	165	5.5	0.9
July 2013	159	143	4.6	0.9
August 2013	88	62	2.0	0.7
		Farm Side of the Stream		
Date	**Precipitation (mm)**	**Evapotranspiration (mm)**	**Daily average evapotranspiration (mm/d)**	**Evapotranspiration to precipitation ratio**
May 2012	85	64	2.1	0.75
June 2012	105	84	2.8	0.8
July 2012	93	70	2.3	0.75
August 2012	135	81	2.6	0.6
September 2012	106	53	1.8	0.5
October 2012	132	13	0.4	0.1
November 2012	59	3	0.1	0.05
December 2012	147	1	0.0	0.01
January 2013	72	1	0.0	0.01
February 2013	100	5	0.2	0.05
March 2013	79	16	0.5	0.2
April 2013	57	43	1.4	0.75
May 2013	108	91	2.9	0.85
June 2013	183	146	4.9	0.8
July 2013	159	119	3.8	0.75
August 2013	88	44	1.4	0.5

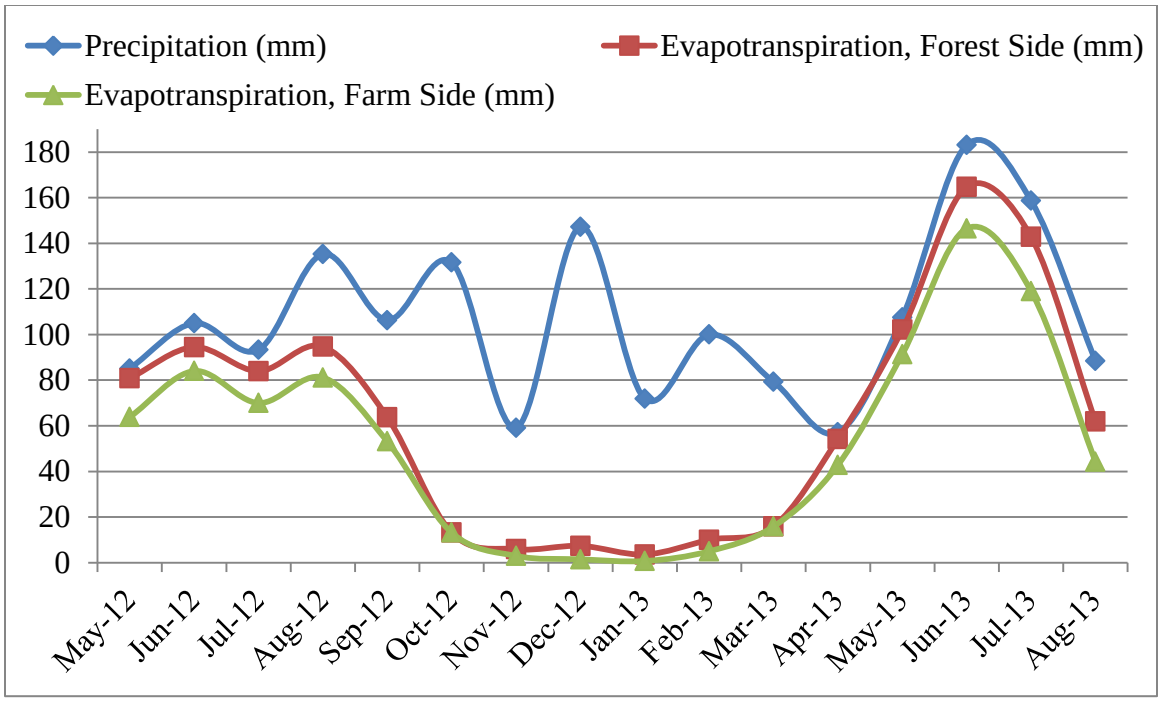

Figure 4.23 Precipitation and evapotranspiration in the Forest and Farm Sides of the Stream in the Study Area during May 2012 to August 2013.

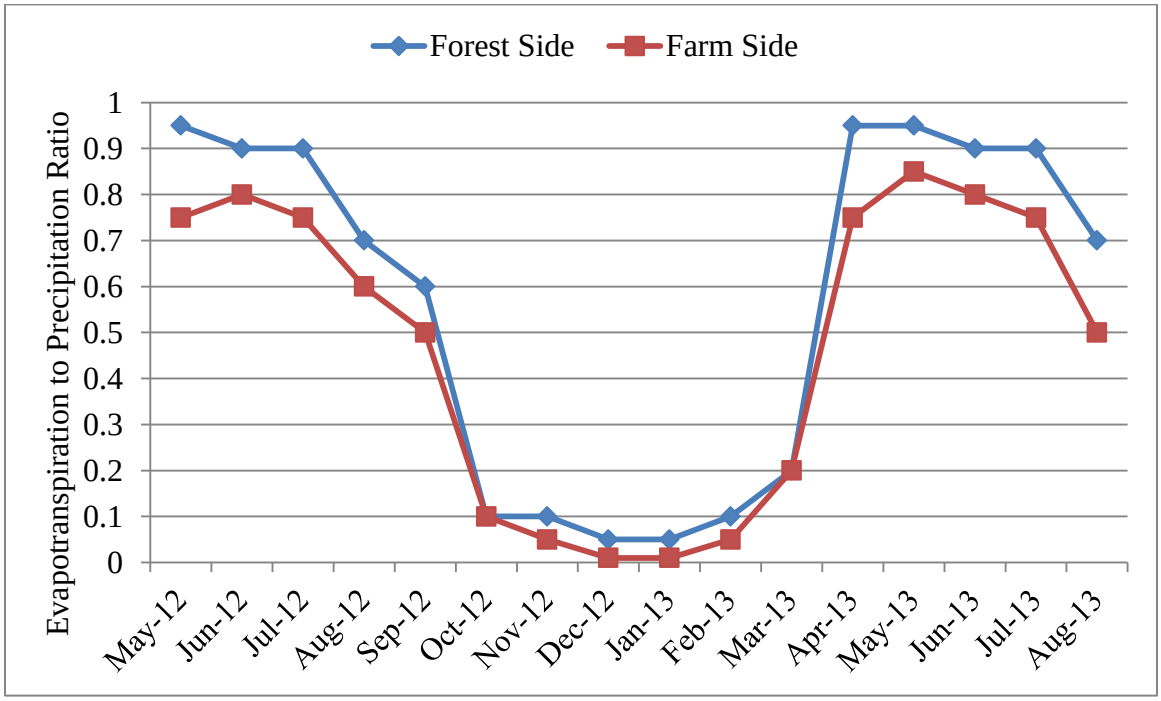

Figure 4.24 Evapotranspiration to precipitation ratio for Forest and Farm Sides of the Stream in the Study Area during May 2012 to August 2013.

CHAPTER 5

DISCUSSION AND CONCLUSION

Monmouth Battlefield State Park was chosen as the Study Area. Land survey was conducted along the Study Corridor. Soil was classified and permeability tests were conducted on Forest and Farm Sides of the Study Corridor. Groundwater levels were observed and recorded at the monitoring wells that were installed along the Study Corridor. Collected information along with the precipitation data from National Weather Service monitoring stations were utilized in adopting a groundwater model to be able to predict the groundwater table levels for the period of May 2012 to August 2013.

An illustration of the simulated groundwater levels versus observed groundwater levels ($R^2 = 0.93$) showed the consistency of the simulated results to the observed values.

The performance and accuracy of the simulated groundwater tables were evaluated by statistical parameters such as percent error and BIAS value. The model showed an average percent error of 3.4 percent. The model showed slightly less than average simulation results accuracy for the Forest Side of the Stream (percent error of 4.4) while showing higher than average simulation results accuracy on the Farm Side of the Stream (percent error of 2.9).

Water loss through evapotranspiration is a principle component of the hydrological cycle in wetlands. Simulated daily average evapotranspiration values were presented and compared for both sides of the Stream during the modeling period. Daily average evapotranspiration on the Forest Side of the Stream are higher than on the Farm Side with value ranges of 0.1 to 5.5 versus 0.0 to 4.9 mm/d, respectively. The higher

evapotranspiration on the Forest Side compared to the Farm Side of the Stream was expected due to the difference in the vegetation cover (dominant plant species and leaf area). This result is further confirmed by the fact that the average evapotranspiration on the Forest Side of the Stream are 20 and 16 percent higher than the Farm Side of the Stream for May through December 2012 and January through August 2013, respectively

Evapotranspiration demonstrates to be at high levels during May to August 2012, start to decrease in September 2012, with the lowest amounts during November 2012 to January 2013. The evapotranspiration values start to increase after that period and reaches highest levels again during June and July 2013.

Highest ratio of evapotranspiration to precipitation occurred during May 2012 to July 2012 and April 2013 to July 2013 for both Forest and Farm Sides of the Stream. This was expected since during the growing season of the plans, with higher levels of solar radiation available to provide energy for evapotranspiration, evapotranspiration increases.

Generally higher evapotranspiration levels are expected during spring and summer compared to fall and winter. Growing season accounts for highest amounts of evapotranspiration. Growing season starts in May, leaves start to mature and continue through June, July and August. Lower evapotranspiration in September can be contributed to senescence of the leaves and lower available radiation levels (Sun & Song, 2008).

Finally, a few suggestions for further studies:

- Coupling the present model with a plant growth model to improve evapotranspiration estimates
- Developing a smaller scale model focusing mainly on the Study Corridor to improve groundwater level predictions
- Compare the present estimates with results of the model for years with different crops on the Farm Side of the Stream.

REFERENCES

Acreman, M., Harding, R., Lloyd, C., & McNeil, D. (2003). Evapotranspiration characteristics of wetlands: experience from a wet grassland and a reedbed using eddy correlation measurement. *Journal of the European Geosciences Union*(7), 11-21.

Ahlfeld, D., Barlow, P., & Mulligan, A. (2005). *A ground-water management process for the U.S. Geological Survey modular ground-water model (MODFLOW–2000).* US Geological Survey.

ASTM International. (2013). *ASTM D1452 - 09*. Retrieved November 21, 2013, from ASTM International: http://www.astm.org/Standards/D1452.htm.

ASTM International. (2013). *ASTM D2487-11*. Retrieved November 21, 2013, from ASTM International: http://www.astm.org/Standards/D2487.htm.

Ballard, J. (1971). Evapotranspiration from lowland vegetation communities of the New Jersey pine barrens: New Brunswick, N.J. *Ph.D. Thesis, Rutgers University*.

Ballard, J. (1979). *Fluxes of water and energy through the Pine Barrens ecosystems.* New York: Academic Press.

Ballard, J., & Buell, M. (1975). The role of lowland vegetation communities in the evapotranspiration budget of the New Jersey Pine Barrens. *Bulletin of the New Jersey Academy of Science*(20), 26-28.

Barksdale, H. (1958). *Ground-water resources in the tri-state region adjacent to the Lower Delaware River: Special Report.* New Jersey State Water Policy Commission, State of New Jersey Department of Conservation and Economic Development, Division of Water Policy and Supply.

Buell, M. (1955). New botanical problems in the New Jersey pine barrens. *Bulletin of the Torrey Botanical Club, 82*, 237-252.

Buell, M., & Ballard, J. (1972). Evapotranspiration from lowland vegetation n the New Jersey pine barrens: New Brunswick, N.J. *New Jersey Water Resources Research Institute, Rutgers University*.

Burba, G., Verma, S., & Kim, J. (1999). Surface energy fluxes of Phragmites australis in a prairie wetland. *Agricultural and Forest Meteorologyis*(94), 31-51.

C.-Y. Xu, V. S. (2005). Evaluation of three complementary relationship evapotranspiration models by water balance approach to estimate actual regional evapotranspiration in different climatic regions. *Journal of Hydrology*(308), 105-121.

Choi, J., & Harvey, J. W. (2000). Quantifying time-varying groundwater discharge and recharge in wetlands of the northern Florida everglades. *Wetlands*, 500-511.

City of Philadelphia. (1892). *Ninth annual report of the Bureau of Water for the year ending December 31, 1891.* Philadelphia, Pa.

Clark, K., Skowronksi, N., & Hom, J. (2010). Invasive insects impact forest carbon dynamics. *Global Change Biology*(16), 88-101.

Clark, K., Skowronski, N., Gallagher, M., Schafer, K., & Renninger, H. (2011). Effects of invasive insects and fire on forest evapotranspiration and water use efficiency. *96th Annual Meeting of the Ecological Society of America, Austin, TX*.

Crichlow, H. (1977). *Modern reservoir engineering— A simulation approach.* Englewood Cliffs, N.J.: Prentice Hall Inc.

Crowe, A. S. (1985). Application of a lakewatershed. *Journal*(81), 1-26.

Disserens, E. (1934). Beitrag zur bestimmung der durchlassigkeii des Boden in natrulicher bodenlagerung. *Schweiz. Landw. Monastr*, 12.

Douglas, E. M., Jacobs, J. M., M., S. D., & Ram, R. L. (2009). A comparison of models for estimating potential evapotranspiration for Florida land cover. *Journal of Hydrology*(373), 366-376.

Ernst, L., & Westerhof, J. (1950). *A new formula for the calculation of the permeability factor with auger hole method, Translated from Dutch by H. Bouwer, Cornell University.* Ithaca, NY: Cornell University.

Faunt, C. C., D'Agnese, F. A., & O'Brien, G. M. (2004). *Chapter D of Death Valley regional groundwater flow system, Nevada and California-hydrogeological framework and transient groundwater flow model.* U.S. Geological Survey.

Gordon, A. (2004). Hydrology of the unconfined Kirkwood-Cohansey aquifer sysmte, Forked River and Cedar, Oyster, Mill, Westecunk, and Tuckerton Creek basins and adjacent basins in the southern Ocean County area, New Jersey, 1998-99. *U.S. Geological Survey Water-Resources Investigations Report*, 1-5.

Harbaugh, A. (2005). *MODFLOW–2005, the U.S. Geological Survey modular ground-water model—The ground-water flow process.* U.S. Geological Survey.

Harbaugh, A. (2005). *the U.S. Geological Survey modular ground-water model—The ground-water flow process.* U.S. Geological Survey.

Harbaugh, A., Banta, E., Hill, M., & McDonald, M. (2000). *MODFLOW–2000, the U.S. Geological Survey Modular ground-water model—user guide to modularization concepts and the Ground-Water Flow Process.* U.S. Geological Survey.

Hemond, H. F., & Benoit, J. (1988). Cumulative impacts on water quality functions of wetlands. *Environmental Management, 12*(5), 639-653.

Herbst, M., & Kappen, L. (1999). The ratio of transpiration versus evaporation in a reed belt as influenced by weather conditions. *Aquatic Botany*(63), 113-125.

Hill, M., Banta, E., Harbaugh, A., & Anderman, E. (2000). *the U.S. Geological Survey modular ground-water model—user guide to the observation, sensitivity, and parameter-estimation processes and three post-processing programs.* U.S. Geological Survey.

Hooghoudt, S. (1936). Bepaling van den doorlaatfactor van den grond met behulp van pompproeven. *Verslag Landbouwk*, 449-541.

Johnson, H., Frevert, R., & Evans, D. (1952). Simplified procedure for the measurement and computation of soil permeability below the water table. *Agricultural Engineering*, 283-286.

Johnson, M., & Watt, M. (1996). Hydrology of the unconfined aquifer system, Mullica River Basin, New Jersey 1991-92. *U.S. Geological Survey Water-Resources Investigations Report*, 1-6.

Johnsson, P., & Barringer, J. (1993). *Water quality and hydrogeochemical processes in McDonalds Branch basin, New Jersey pinelands, 1984-88.* U.S. Geological Survey.

Karunanithi, N., Grenney, W., Whitley, D., & Bovee, K. (1994). Neural networks for river flow prediction. *Journal of Computing in Civil Engineering*, 201-220.

Kirkham, D. (1945). Proposed methods for field measurements of permeability of soil below water table. *Soil Science Society*, 56-68.

Kirkham, D. (1955). *Measurement of the hydraulic conductivity of soil in place.* Philadelphia: American Society for Testing Materials.

Kirkham, D., & Van Bavel, C. (1948). Theory of seepage into auger holes. *Soil Science Society*, 75-82.

Konikow, L., Goode, D., & Hornberger, G. (1996). *A three-dimensional method-of-characteristics solute transportmodel (MOC3D): U.S. Geological Survey Water-Resources Investigations Report 96–4267, 87 p.* U.S. Geological Survey.

Lull, H., & Axley, J. (1958). Forest soil-moisture relations in the coastal plain sands of southern New Jersey. *Forest Science*(4), 2-18.

McDonald, M., & Harbaugh, A. (1984). *A modular three-dimensional finite-difference ground-water flow model.* U.S. Geological Survey .

McDonald, M., & Harbaugh, A. (1988). *A modular three-dimensional finite-difference ground-water flow model.* U.S. Geological Survey.

Mitsch, W., & Gosselink, J. (1993). *Wetlands* (2nd ed.). New York: Van Nostrand Reinhold.

Monteith, J. (1963). Gas exchange in plant communities. *Environmental Control of Plant Growth*, (pp. 95-112).

Monteith, J. (1965). Evaporation and environment. *Symposia of the Society for Experimental Biology*, 205-234.

Murphy, C. (2008, November). *Wetlands*. Retrieved November 21, 2013, from State of Rhode Island Department of Environmental Management, Office of Water Resources: http://www.dem.ri.gov/programs/benviron/water/wetlands.

National Oceanic and Atmospheric Administration. (2013). *Geostationary Operational Environmental Satellites (GOES)*. Retrieved November 21, 2013, from Office of Satellite and Product Operations: http://www.ospo.noaa.gov/Operations/GOES/index.html.

NJDEP. (2013). *Monmouth Battlefield State Park*. Retrieved November 21, 2013, from http://www.state.nj.us/dep/parksandforests/parks/monbat.html.

NOAA. (2013). *Climate data online*. Retrieved November 21, 2013, from National Oceanic and Atmospheric Administration's National Climatic Data Center: http://www.ncdc.noaa.gov/cdo-web.

NOAA's National Weather Service Middle Atlantic River Forecast Center. (2012). *National Weather Service Middle Atlantic River Forecast Center*. Retrieved November 21, 2013, from NOAA: http://www.erh.noaa.gov/marfc.

Parkhurst, D., Kipp, K., Engesgaard, P., & Charlton, S. (2004). *PHAST—A program for simulating ground-water flow, solute transport, and multicomponent geochemical reactions.* U.S. Geological Survey.

Pauliukonis, N., & Schneider, R. (2001). Temporal patterns in evapotranspiration from lysimeters with three common wetland plant species in the eastern United States. *Aquatic Botany*(71), 35-46.

Peaceman, D. (1977). *Fundamentals of numerical reservoir simulation.* New York: Elsevier Scientific Publishing Company.

Penman, H. (1948). Natural evaporation from open water, bare and grass. *Proceedings of the Royal Society,* (pp. 120-145).

Pereira, A. R. (2004). The Priestley–Taylor parameter and the decoupling factor for estimating reference evapotranspiration. *Agricultural and Forest Meteorology, 125*, 305-313.

Radke, B., Ferguson, J., Cresswell, R., Ransley, T., & Habermehl, M. (2000). *Hydrochemistry and implied hydrodynamics of the Cadna-owie-Hooray aquifer Great Artesian basin.* . Canberra, Australia: Bureau of Rural Schiences.

Remson, I., Hornberger, G., & Molz, F. (1971). *Numerical methods in subsurface hydrology.* New York: Wiley-Interscience, 389 p.

Rhodehamel, E. (1970). A hydrologic analysis of the New Jersey pine barrens region. *New Jersey Division of Water Policy Water Resources Circular*, 35.

Schafer, V. (2011). Canopy stomatal conductance following drought, disturbance, and death in an upland oak/pine forest of the New Jersey Pine Barrens, USA. *Frontiers in Plant Science*, 1-7.

Stanford, S. D., Pristas, R. S., & Hall, D. W. (2009). *Earthquake loss estimation study for Monmouth County, NJ.* New Jersey Geological Survey.

Stauffer, R. E. (1985). Use of solute tracers released by weathering. *Environmental, 19,* 405-411.

Sumner, D. M., Nicholson, R. S., & Clark, K. L. (2012). *Measurement and simulation of evapotranspiration at a wetland site in New Jersey pinelands.* USGS.

Sun, L., & Song, C. (2008). Evapotranspiration from a freshwater marsh in the Sanjiang Plain, Northeast China. *Journal of Hydrology*(352), 202-210.

The National Aeronautics and Space Administration. (2013). *The Water Cycle*. Retrieved November 21, 2013, from NASA: http://pmm.nasa.gov/education/water-cycle.

Trescott, P. (1979). *Documentation of finite-difference model for simulation of three-dimensional groundwater flow.* U.S. Geological Survey.

Trescott, P., & Larson, S. (1976). *Supplement to open-file report 75–438, documentation of finite-difference model for simulation of three-dimensional ground-water flow.* U.S. Geological Survey.

Trescott, P., Pinder, G., & Larson, S. (1976). *Finite difference model for aquifer simulation in two dimensions with results of numerical experiments.* U.S. Geological Survey.

U.S. Geological Survey. (2013, March). *Evapotranspiration*. Retrieved November 21, 2013, from USGS: http://ga.water.usgs.gov/edu/watercycleevapotranspiration.html.

U.S. Geological Survey. (2013). *The National Map, US Topo*. Retrieved November 21, 2013, from USGS: http://nationalmap.gov/ustopo.

U.S. Geological Survey. (2013, May). *The Water Cycle*. Retrieved from USGS: URL: http://ga.water.usgs.gov/edu/watercyclehi.html.

US Environmental Protection Agency. (2012, October). *Wetlands*. Retrieved November 21, 2013, from EPA: http://water.epa.gov/type/wetlands/what.cfm.

USDA. (2013). *Published soil surveys for New Jersey*. Retrieved November 27, 2013, from Natural Resources Conservation Service: http://www.nrcs.usda.gov/wps/portal/nrcs/surveylist/soils/survey/state/?stateId=NJ.

Van Beers, W. (1983). *The auger hole method.* Wageningen, the Netherlands: International Institute for Land Reclamation and Improvement.

Vermuele, C. (1894). Report on water-supply, water power, the flow of streams and attendant phenomena: Final report of the State geologist. *Geological Survey of New Jersey, III,* 352.

Vowinkel, E., & Foster, W. (1981). Hydrogeologic conditions in the coastal plain of New Jersey. *U.S. Geological Survey Open-File Report*(81), 39.

Watt, M., & Johnson, M. (1992). *Water resources of the unconfined aquifer system of the Great Egg Harbor river basin, New Jersey.* U.S. Geological Survey.

Watt, M., Johnson, M., & Lacombe, P. (1994). *Hydrology of the unconfined aquifer system, Toms River, Metedeconk River, and Kettle Creek Basins, Jew Jersey, 1987-1990.* U.S. Geological Survey.

Watt, M., Kane, A., Charles, E., & Storck, D. (2003). *Hydrology of the unconfined aquifer system, Rancocas Creek area: Rancocas, Crosswicks, Assunpink, Assiscunk, Blacks, and Crafts Creek Basins, New Jersey.* U.S. Geological Survey.

Wikimedia Foundation, Inc. (2013, October). *Evapotranspiration*. Retrieved from Wikipedia: http://en.wikipedia.org/wiki/Evapotranspiration.

Wikimedia Foundation, Inc. (2013). *Monmouth Battlefield State Park*. Retrieved from Wikipedia: http://en.wikipedia.org/wiki/Monmouth_Battlefield_State_Park.

Wikimedia Foundation, Inc. (2013, September). *Water Cycle*. Retrieved November 21, 2013, from Wikipedia: http://en.wikipedia.org/wiki/Water_cycle.

Winston, R. B. (2009). ModelMuse - A graphical user interface for MODFLOW-2005 and PHAST. In *Modeling Techniques* (p. 52). U.S. Geological Survey.

Wood, O. (1937). The interception of precipitation in an oak-pine forest. *Ecology*(18), 251-254.

Wordpress. (2011, January). *Greenconsiderations*. Retrieved November 21, 2013, from http://greenconsiderations.wordpress.com/2011/01/25/sustainability-at-rru-and-the-importance-of-wetland-restoration.

Yapo, P. D., Gupta, H. V., & Sorooshian, S. (1996). Automatic calibration of conceptual rainfall-runoff models: sensitivity to calibration data. *Journal of Hydrology*, 23-48.

Yates, D. (1997). Approaches to continental scale runoff for. *Journal of Hydrology, 201*, 289-310.

Zhou, Y., & Li, W. (2011). A review of regional groundwater flow modeling. *Geoscience Frontiers*, 205-214.